EVALUATION OF IPR CORRELATIONS FOR VERTICAL WELL

Mr. Suksan Luangwattanawilai

A Thesis Submitted in Partial Fulfillment of the Requirements
for the Degree of Master of Engineering Program in Petroleum Engineering
Department of Mining and Petroleum Engineering
Faculty of Engineering
Chulalongkorn University
Academic Year 2013

การประเมินสหสัมพันธ์การไหลเข้าหลุมผลิตแนวตั้ง

นายสุขสันต์ เหลืองวัฒนวิไล

วิทยานิพนธ์นี้เป็นส่วนหนึ่งของการศึกษาตามหลักสูตรปริญญาวิศวกรรมศาสตรมหาบัณฑิต
สาขาวิชาวิศวกรรมปิโตรเลียม ภาควิชาวิศวกรรมเหมืองแร่และปิโตรเลียม
คณะวิศวกรรมศาสตร์ จุฬาลงกรณ์มหาวิทยาลัย
ปีการศึกษา 2556

Thesis Title	EVALUATION OF IPR CORRELATIONS FOR VERTICAL WELL
By	Mr. Suksan Luangwattanawilai
Field of Study	Petroleum Engineering
Thesis Advisor	Assistant Professor Suwat Athichanagorn, Ph.D.

Accepted by the Faculty of Engineering, Chulalongkorn University in Partial Fulfillment of the Requirements for the Master's Degree

....Dean of the Faculty of Engineering

(Professor Bundhit Eua-arporn, Ph.D.)

THESIS COMMITTEE

....Chairman

(Associate Professor Sarithdej Pathanasethpong)

....Thesis Advisor

(Assistant Professor Suwat Athichanagorn, Ph.D.)

....Examiner

(Falan Srisuriyachai, Ph.D.)

....External Examiner

(Witsarut Tungsunthomkhan, Ph.D.)

สุขสันต์ เหลืองวัฒนวิไล : การประเมินสหสัมพันธ์การไหลเข้าหลุมผลิตแนวตั้ง. (EVALUATION OF IPR CORRELATIONS FOR VERTICAL WELL) อ.ที่ปรึกษาวิทยานิพนธ์หลัก: ผศ. ดร. สุวัฒน์ อธิชนากร, 113 หน้า.

ความสัมพันธ์ของสหสัมพันธ์การไหลเข้าหลุมผลิตอธิบายถึงความสัมพันธ์ระหว่างอัตราการผลิตโดยอาศัยแรงขับจากแหล่งกักเก็บปิโตรเลียมที่เกิดจากผลต่างของความดันระหว่างค่าเฉลี่ยของความดันแหล่งกักเก็บและความดันการไหลก้นหลุมผลิต วัตถุประสงค์ของการศึกษานี้คือ การประเมินสหสัมพันธ์การไหลเข้าหลุมผลิตในแนวตั้งจากสมการทั้งห้าสมการที่นำเสนอสำหรับการคาดการณ์สมรรถนะการผลิตของแต่ละหลุมผลิตน้ำมัน ได้แก่ Vogel, Fetkovich, Jones et al., Kilns & Marcher, และ Sukarno & Wisnogroho โดยการเปรียบเทียบสมรรถนะของหลุมผลิตจากผลลัพธ์ระหว่างโปรแกรมแบบจำลอง ECLIPSE100 และจากผลการคำนวณของสมการสหสัมพันธ์การไหล เพื่อศึกษาและเพิ่มความเข้าใจเกี่ยวกับความถูกต้องและความน่าเชื่อถือของแต่ละสหสัมพันธ์การไหลในแหล่งกักเก็บปิโตรเลียมที่มีแรงขับจากก๊าซที่ละลายในน้ำมัน

จากผลการศึกษาค่าเฉลี่ยของค่าความผิดพลาดร้อยละเฉลี่ยสัมบูรณ์ของแต่ละสหสัมพันธ์การไหล บ่งชี้ว่า Jones et al. มีค่าความถูกต้องและค่าความน่าเชื่อถือมากที่สุด รองลงมาคือ Fetkovich, Vogel, Sukarno & Wisnogroho, และ Kilns & Marcher ตามลำดับ โดยภาพรวมพบว่า ค่าเฉลี่ยของความผิดพลาดร้อยละเฉลี่ยสัมบูรณ์มีแนวโน้มลดลงอย่างมีนัยสำคัญในทุกๆสหสัมพันธ์การไหลเมื่อค่าความสามารถในการซึมผ่านมีค่ามากขึ้น นอกจากนี้ยังพบว่า แต่ละสหสัมพันธ์การไหลเข้าหลุมผลิตจะมีความถูกต้องและแม่นยำเฉพาะบางคุณลักษณะของหลุมกักเก็บปิโตรเลียมหนึ่ง แต่อาจจะไม่ถูกต้องและแม่นยำสำหรับคุณลักษณะของหลุมผลิตอื่นๆ

ภาควิชา	วิศวกรรมเหมืองแร่และปิโตรเลียม	ลายมือชื่อนิสิต	
สาขาวิชา	วิศวกรรมปิโตรเลียม	ลายมือชื่อ อ.ที่ปรึกษาวิทยานิพนธ์หลัก	
ปีการศึกษา	2556		

5471218021 : MAJOR PETROLEUM ENGINEERING
KEYWORDS: INFLOW PERFORMANCE RELATIONSHIP (IPR) / MEAN ABSOLUTE PERCENTAGE ERROR (MAPE) / SOLUTION GAS DRIVE RESERVOIR / VERTICAL WELL

SUKSAN LUANGWATTANAWILAI: EVALUATION OF IPR CORRELATIONS FOR VERTICAL WELL. ADVISOR: ASST. PROF. SUWAT ATHICHANAGORN, Ph.D., 113 pp.

An inflow performance relationship describes the relationship between the well production rate as a function of driving force in reservoir which is the differential pressure between average reservoir pressure and the well bottomhole flowing pressure. When there is two-phase flow in the reservoir, we need to use an empirical correlation to represent this relationship. The objective of this study is to evaluate five IPRs proposed in the literature for predicting individual oil well performance which are Vogel, Fetkovich, Jones et al., Kilns & Marcher, and Sukarno & Wisnogroho. The evaluation of IPR correlations is done by comparing the bottom-hole pressure obtained from ECLIPSE100 simulation with the calculated bottom-hole pressure from IPR correlations in order to gain an understanding of their accuracy and reliability for solution gas drive reservoirs.

As a result, the average and standard deviation of Mean Absolute Percentage Error (MAPE) between the simulated pressure (ECLIPSE100) and the calculated pressure for the five IPR correlations show that Jones et al.'s correlation gives the best value while Fetkovich, Vogel, Sukarno and Wisnogroho, and Klins and Majcher follow in less accurate order. Overall, MAPE tends to decrease significantly for every IPR correlations when the absolute permeability increases. In addition, an individual IPR correlation has more accuracy and precision at one aspect reservoir but not at the other conditions.

Department:	Mining and Petroleum Engineering	Student's Signature	....
		Advisor's Signature	....
Field of Study:	Petroleum Engineering		
Academic Year:	2013		

ACKNOWLEDGEMENTS

First of all, I would like to express my gratitude toward Asst. Prof. Suwat Athichanagorn, my thesis advisor, for giving me basic knowledge of petroleum engineering, invaluable guidance, and encouragement throughout the course of the study.

I would like to express my great appreciation to all faculty members in the Department of Mining and Petroleum Engineering who have provided petroleum knowledge and useful advice that would be beneficial for my future career. In addition, I want to thank the thesis committee members for their helpful comments and suggestions which greatly contributed many improvements.

I would like to thank Schlumberger for providing ECLIPSE reservoir simulation software to the Department of Mining and Petroleum Engineering. In addition, I would like to thank JMP for providing the trial software version for generation of cases studied. I am also indebted to Mr. Teerawat Vaccharasiritham for his valuable providing basic knowledge of using ECLIPSE reservoir simulation software and for his patient technical support throughout this study including appreciation all the supports from friends and classmates.

I would like to express my gratitude to Chevron Thailand Exploration and Production, Ltd. for providing financial support for this study.

I am grateful to my parents, Mr. Apichai and Mrs. Sanae Luangwattanawilai for their love and support for my studies.

CONTENTS

Page

Page

LIST OF TABLES

Page

Page

LIST OF FIGURES

Page

Page

Page

LIST OF ABBREVIATIONS

STB/D	Stock tank barrel per day
SCF/STB	Standard cubic foot per stock-tank barrel
mD	Millidarcy
psia	Pound per square inch absolute
rb/stb	Reservoir barrel per stock-tank barrel
cp	Centipoise
lb/cuft	Pound per cubic foot
IPR	Inflow Performance Relationship
MAPE	Mean Absolute Percentage Error

NOMENCLATURES

ρ_o	Density of oil
ρ_w	Density of water
ρ_g	Density of gas
k_h	Horizontal permeability
k_v	Vertical permeability
k	Absolute permeability of the porous media
μ_g	Viscosity of gas
μ_o	Viscosity of oil
R_s	Gas solubility
S_w	Water saturation
S_o	Oil saturation
S_g	Gas saturation
S_{wco}	Connate water saturation
k_{rog}	Oil relative permeability in presence of gas phase
k_{row}	Oil relative permeability in presence of water phase
k_{ro}	Oil relative permeability

CHAPTER I

INTRODUCTION

1.1 Background

Different oil reservoirs are composed of unique combination of rock & fluid properties and natural drive mechanism. There are no reservoirs which are identical in all characteristics. Predicting oil reservoir performance requires understanding of the well inflow performance relationship (IPR). An inflow performance relationship describes the relationship between the well production rate as a function of driving force in reservoir which is the differential pressure between average reservoir pressure and the well bottomhole flowing pressure. Having knowledge of the pressure-rate behavior enables the petroleum engineers to evaluate the precise productivity of well and determine the optimized production design and timing for doing artificial lift and make properly project planning.

For steady–state flow of a single, incompressible fluid, the inflow performance relationship can be derived from a straight-line relationship between the well bottomhole flowing pressure and production rate from Darcy's law. In contrast, when there is a presence of two-phase flow in a reservoir, the relationship should not be expected to be a straight line. The IPR is in fact nonlinear. Several of the most widely used empirical methods for predicting an IPR for a well are presented for different reservoir conditions such as Vogel's equation, Fetkovich's equation, Jones, Blount & Glaze's equation, Kilns & Marcher's equation, and Sukarno & Wisnogroho's equation. In this study, a black oil reservoir simulator ECLIPSE100 is used to evaluate the prediction of five well inflow performance correlations. The parameters which are considered in this study are solution gas-oil ratio, oil °API gravity, vertical to horizontal permeability ratio, absolute permeability, skin factor, Corey exponent for relative permeability to oil, Corey exponent for relative permeability to gas, and perforation ratio.

1.2 Objective

1. To evaluate common correlations used to estimate present inflow performance relationship of two-phase flow in vertical well for various reservoir and fluid properties.

The benefit from this evaluation will provide the oil and gas company and petroleum engineer to utilize one of the most accurate and precise IPR correlations for any reservoir conditions in overall result at the starting point of well inflow performance prediction since we don't know the conditions of the well yet when performing the well test. This also support the estimation of the ability of the well to produce, determine the optimized production design and selection of timing for doing artificial lift and make properly project planning.

1.3 Outline of methodology

1. Study various related literatures and collect required input data for reservoir simulation model.
2. Construct reservoir simulation model with a single vertical well of solution gas drive reservoir.
3. Generate cases studied by using JMP trial software version for 150 cases and vary the fluid, rock properties and completion characteristic as the following:

    a. Gas solubility (R_s) : 210, 500, 1000, 2000, *scf/STB*
    b. API gravity of oil : 23, 25, 35, 45 , *°API*
    c. Absolute permeability:100, 500, 1000, *md*
    d. k_v/k_h ratio: 0.01, 0.1, 1
    e. Skin factor: 0, 5, 10, 20
    f. Perforation ratio*:* 0.4, 0.8
    g. Corey exponent for relative permeability to oil (n_o): 2, 3
    h. Corey exponent for relative permeability to gas (n_g): 2, 3
4. Simulate each case with eight different constant oil production rates: 600, 800, 1000, 12000, 1400, 1600, 1800, and 2000 STB/D in order to obtain the bottom-hole flowing pressures.
5. Plot the well bottomhole flowing pressure against time to determine the producing time that reaches the pseudo-steady state period.
6. The bottom-hole flowing pressures obtained from ECLIPSE100 simulation and the calculated bottom-hole pressures from IPR correlations for eight different oil flow rates at the beginning of pseudo-steady state are compared.

7. Evaluate the bottom-hole flowing pressures from simulation and calculated values from IPR correlations by determination of Mean Absolute Percentage Error (MAPE) and standard deviation.
8. Discuss and summarize the accuracy and reliability of all five IPR correlations.

1.4 Thesis outline

This thesis consists of six chapters as outlined below:

Chapter I introduces the background and indicates the objective and methodology of this study.

Chapter II presents some previous works related to well inflow performance relationship which include both laboratory experiments and simulation studies.

Chapter III introduces the general concept of IPR and describes related theories.

Chapter IV provides detail of the reservoir model used in this study including reservoir dimensions, PVT data, and rock and fluid properties.

Chapter V illustrates and discusses the evaluation of results of the five IPR correlations performed under diverse reservoir conditions.

Chapter VI provides the conclusions and recommendations obtained from this study.

CHAPTER II

LITERATURE REVIEW

This chapter describes some previous studies on well inflow performance relationship correlations. Development of method, advantage, disadvantage and improvement in oil production of each method are discussed. There are several empirical methods that are designed to predict the non-linear behavior of the IPR for solution gas drive reservoirs. Most of these methods require at least one stabilized flow test in which q_o and p_{wf} are measured. The following empirical methods are designed to generate present inflow performance relationships: Vogel's equation, Fetkovich's equation, Jones et al.'s equation, Kilns & Marcher's equation, and Sukarno & Wisnogroho's equation.

2.1 Vogel's IPR correlation

Vogel [1] normalized the IPRs and expressed the calculated IPRs in dimensionless form. He plotted the IPR curve based on two dimensionless parameters which are:

$$Dimensionless\ pressure = \frac{P_{wf}}{\bar{P}_r} \quad (2.1)$$

$$Dimensionless\ flow\ rate = \frac{q_o}{(q_o)_{max}} \quad (2.2)$$

where $(q_o)_{max}$ is the oil flow rate at the condition of absolute open flow. From calculation performed at 21 reservoir conditions, he plotted the dimensionless IPR curves which resulted in a similar shape, and the equation of a curve is:

$$\frac{q_o}{(q_o)_{max}} = 1 - 0.2\left(\frac{p_{wf}}{\bar{p}_r}\right) - \left(\frac{P_{wf}}{\bar{P}_r}\right)^2 \quad (2.3)$$

where

q_o = Oil flow rate at P_{wf}

$(q_o)_{max}$ = maximum oil flow rate at absolute open flow condition

$\bar{P}_r$ = average reservoir pressure, psig

P_{wf} = well bottom-hole flowing pressure, psig

2.2 Fetkovich's IPR correlation

Fetkovich [2] observed that the non-linear flow behavior of wells has the pressure function falling into either of the two conditions as shown schematically in Figure 1. The following are two conditions of pressure function:

1. Undersaturated oil reservoir, where the pressure function *f(p)* is in the condition at $P > P_b$,then:

$$f(p) = \left(\frac{1}{\mu_o B_o}\right) \tag{2.4}$$

where

μ_o = oil viscosity at pressure *p*, cp

B_0 = oil formation volume factor at pressure *p*, bbl/STB

2. Saturated oil reservoir, where pressure function *f(p)* is in the condition at $P < P_b$. He suggested that $k_{ro}/\mu_o B_o$ changes in linear function with pressure and the straight line passes the original coordinate. The mathematical equation can be given as:

$$f(p) = \left(\frac{1}{\mu_o B_0}\right)\left(\frac{p}{p_b}\right) \tag{2.5}$$

where

μ_o = oil viscosity at bubblepoint pressure p_b, cp

B_0 = oil formation volume factor at bubblepoint pressure p_b, bb/STB

P_b = *bubblepoint pressure, psi*

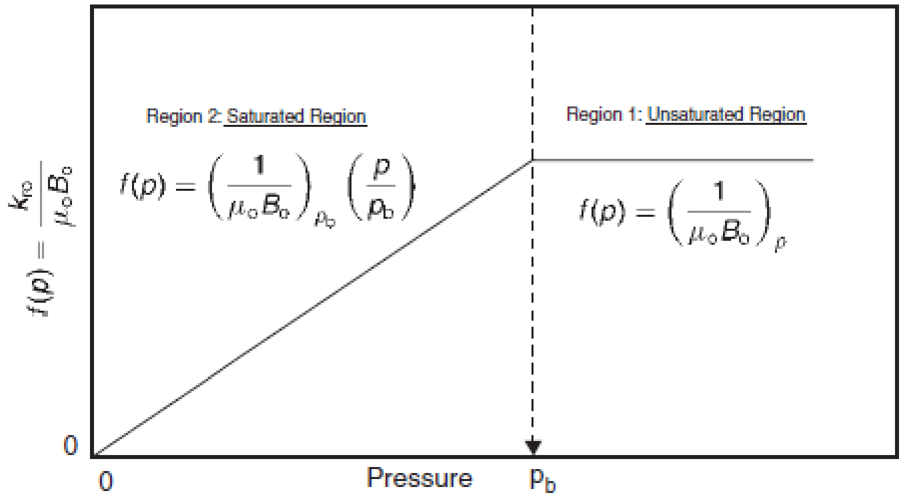

Figure 2.1 Pressure function concept, Ahmed [3]

To account for non-Darcy flow in oil wells, Fetkovich proposed the following approach to predict the well performance:

$$q_o = C(\bar{p}_r^{\,2} - p_{wf}^{\,2})^n \tag{2.6}$$

where the value of n ranges from 0.5 for highly turbulent flow to 1.0 for totally laminar flow. To determine the performance coefficient C and exponent n in Equation (2.6), this method requires at least two tests to solve for these two parameters. Plotting log-log scale of Equation (2.6) will result in a linear line providing a slope $1/n$ and intercept of Cat $\bar{p}_r^{\,2} - p_{wf}^{\,2} = 1$. Once we determine the exponent n, then C value can be calculated by using any point on linear plot, as given by:

$$C = \frac{q_o}{(\bar{p}_r^{\,2} - p_{wf}^{\,2})^n} \tag{2.7}$$

2.3 Jones et al.'s IPR correlation

Jones *et al.* [4] developed a relationship between production rate and pressure as the following expression:

$$\frac{p_r - p_{wf}}{q_o} = A + Bq_o \tag{2.8}$$

where A and B are the coefficients in which A is in the laminar flow condition and B is in the turbulent flow. In order to determine these two coefficients, a multi-rate test is required. Equation (2.8) indicates that a relationship of a ratio of pressure drawdown to flow rate versus the production rate on Cartesian yields a straight line, where A is the y-intercept and B is the slope of straight line. Once the value of A and B are determined from a plot, the flow rate at any well flowing pressure can be calculated by Equation (2.9).

$$q_o=\frac{-A+\sqrt{A^2+4B\,(p_r-p_{wf})}}{2B} \tag{2.9}$$

2.4 Klins & Marcher's IPR correlation

Klins and Majcher [5] investigated the effects of numerous reservoir and fluid properties on IPR curves. With 19,492 data points from 21 theoretical solution gas drive reservoirs, eight skin factors and seven reservoir depletion stages, Klins and Majcher simulated and generated 1344 IPR curves. They found that bubble point pressure and reservoir depletion caused a major effect on the curves. The skin and r_e/r_w had a significant influence on only the normalized curves. By nonlinear regression techniques, they proposed the following IPR.

$$\frac{q_o}{(q_o)_{max}}=1-0.295\left(\frac{P_{wf}}{\bar{P}_r}\right)-0.705\left(\frac{P_{wf}}{\bar{P}_r}\right)^n \tag{2.10}$$

in which

$$n=(0.28+0.72\frac{P_r}{P_b})(1.235+0.001P_b) \tag{2.11}$$

2.5 Sukarno & Wisnogroho's IPR correlation

Sukarno and Wisnogroho [6] developed inflow performance in perforated wells by using computer program for various sets of data. Based on simulation results that attempt to account for perforation technique and perforation geometry, the authors grouped the IPR curves obtained from model based on perforation technique and perforation radius. A nonlinear regression analysis has been run for data set in each group and yielded the following mathematical model:

$$\frac{q_o}{q_{max}}=a_0-a_1\left(\frac{P_{wf}}{\bar{P}_r}\right)-a_2\left(\frac{P_{wf}}{\bar{P}_r}\right)^2 \tag{2.12}$$

where

1. the constants a_0, a_1 and a_2 which depend on the perforation radius and perforation technique, are shown in Tables 1 and 2.
2. q_{max} is maximum production rate without perforation.

Table 2.1 Constants for Equation (2.12) of overbalance perforation, Sukarno [6]

r_p, inch	SPF	a_0	a_1	a_2
> 0.3	16	0.91995	0.08072	-0.97117
	12	0.90482	0.08881	-0.96534
	8	0.87333	0.10715	-0.983464
	4	0.77503	0.12529	-0.87781
	2	0.61710	0.26632	-0.86983
≤0.3	16	0.83925	0.12038	-0.93283
	12	0.79505	0.14935	-0.91988
	8	0.73507	0.11547	-0.82687
	4	0.57857	0.09956	-0.65332
	2	0.33247	0.20784	-0.52487

Table 2.2 Constants for Equation (2.12) of underbalance perforation, Sukarno [6]

r_p, inch	SPF	a_0	a_1	a_2
≥ 0.19	16	0.95146	0.06546	-0.98175
	12	0.93806	0.05464	-0.95875
	8	0.92006	0.05473	-0.94102
>0.3	4	0.91196	0.07855	-0.95974
	2	0.85540	0.06302	-0.88678
<0.3	4	0.79507	0.15189	-0.91899
	2	0.64374	0.22082	-0.38782

CHAPTER III

THEORY AND CONCEPT

This chapter presents fundamental principles used to describe well inflow performance relationship and also important concepts related to this principle.

3.1 Productivity index and IPR

The accurate prediction of oil well performance should be made as oil flow into a well from the reservoir. Oil flow into a well depends on reservoir characteristics and drawdown pressure. The relationship between the well flowing pressure and oil inflow rate is called the *inflow performance relationship*. The production rate at various sandface flowing pressures can be determined from plotting this relationship called IPR analysis.

Typically, the measurement of the ability of the well to produce is called *productivity index (J).*The productivity index J is described as the ratio of the total liquid flow rate to the pressure drawdown. When there is a water-free oil production, the productivity index is defined as:

$$J=\frac{q_o}{\overline{P}_r - P_{wf}}=\frac{q_o}{\Delta P} \tag{3.1}$$

where

q_o = oil flow rate, STB/day

J = productivity index, STB/day/psi

$\overline{P}_r$ = volumetric average drainage area pressure (static pressure)

P_{wf} = bottom-hole flowing pressure

ΔP = drawdown pressure, psi

Generally, the productivity index is determined from a production test on the well. The well is shut in until reaching the static reservoir pressure. Then, the well is allowed to produce at a constant flow rate and a stabilized bottom-hole flowing pressure. Observing a surface stabilized pressure does not necessarily points toward a stabilized bottom-hole flowing pressure, meaning that the bottom-hole flowing pressure is then required to be recorded continuously. With the purpose of accurately measuring the productivity index of a well, it is important to allow the well to flow at a constant flow rate for a sufficiently period of time to reach the pseudo-steady state or steady state because the productivity index is valid only if the well is flowing at these conditions.

For the pseudo-steady state laminar flow of a well in the center of a circular drainage area, the equation is given as

$$q_o = \frac{0.00708 k_o h \left(\overline{p}_r - p_{wf}\right)}{\mu_o B_o \left[ln\left(0.472 r_e / r_w\right)\right]} \tag{3.2}$$

where

q_o	= inflow rate, STB/day
k_o	= effective oil permeability, md
h	= reservoir thickness, ft
$\overline{P}_r$	= volumetric average drainage area pressure (static pressure), psi
P_{wf}	= bottom-hole flowing pressure, psi
r_e	= well's drainage radius, ft
r_w	= wellbore radius, ft
μ_o	= oil viscosity, cp and
B_0	= oil formation volume factor, Rb/STB

Equation (3.2) is combined with Equation (3.1) to give:

$$J = \frac{0.00708 k_o h}{\mu_o B_o \left[ln\left(0.472 r_e / r_w\right)\right]} \tag{3.3}$$

The inflow equation of oil flow can then be written as

$$q_o = J\left(\overline{P}_r - P_{wf}\right) \tag{3.4}$$

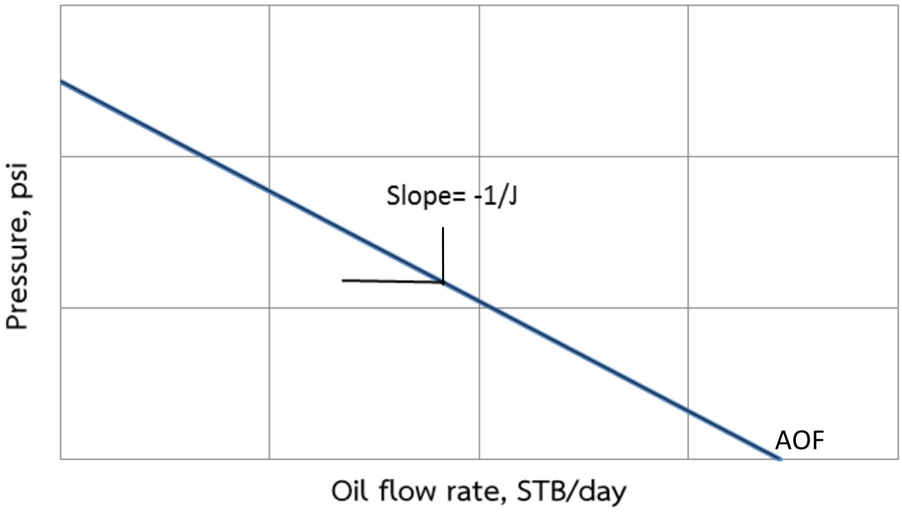

Figure 3.1 Inflow performance relationships.

From Figure 3.1, there are several important features of the straight line IPR which are

1. As p_{wf} equals the average reservoir pressure, the flow rate is zero because of the absence of any pressure drawdown.
2. As p_{wf} is zero, a point of maximum flow rate occurs. This maximum rate is called "absolute open flow (AOF)". In practice, the well cannot be produced at this condition. The AOF can be written as

$$AOF=J\,\overline{p}_r \tag{3.5}$$

3. The productivity index can be obtained from reciprocal of a slope of the straight line.
4. The intercept of $\overline{P}_r$ is at q_o being equal to zero.

This implies that the pressure function $f(P)=k_o/\mu_o B_o$ remains constant, which is unlikely the case, as will be presented later in this thesis.

The productivity index of oil well can also be expressed as Equation (3.6) when including the skin effects of both turbulence and actual formation damage as given in Equation (3.7).

$$J=\frac{0.00708h}{\left(\overline{p}_r-p_{wf}\right)\left[\ln\left(0.472\,r_e/r_w\right)+S'\right]}\int_{p_{wf}}^{\overline{p}_r}\frac{k_o}{\mu_o B_o}d \tag{3.6}$$

$$S' = S + Dq \tag{3.7}$$

where

S = skin factor due to permeability change

D = turbulence coefficient

Equation (3.6) reveals that J will not be constant except the pressure function is independent of pressure. It also can be expressed that the variables affecting the productivity index are essentially those that are dependent on the pressure, specifically, oil viscosity, oil formation volume factor and relative permeability to oil.

3.2 Factors affecting inflow performance

From the previous section, if the effects of changing conditions on some of the variables cause productivity index J to change, the slope of the IPR plot will change, and a nonlinear relationship between p_{wf} and q will exist as shown in Figure 3.2. For oil reservoirs, the primary factors affecting the IPR are (1) phase behavior in reservoir (2) relative permeability (3) oil viscosity (4) oil formation volume factor (5) skin factor (6) drive mechanism and (7) drawdown or production rate.

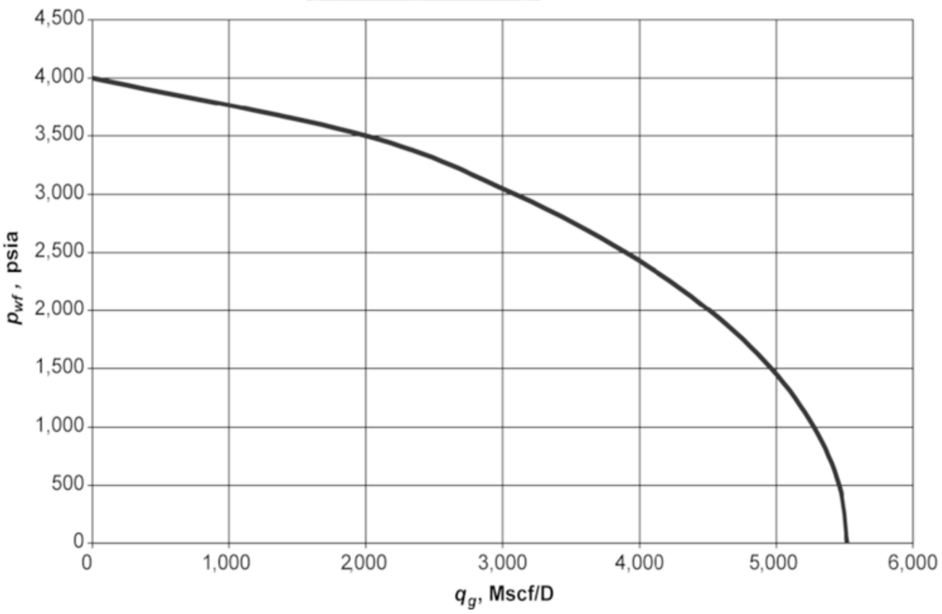

Figure 3.2 Inflow performance relationships with changing productivity index

3.2.1 Phase behavior in reservoir

Figure 3.3 represents a typical P-T phase diagram for an oil reservoir. The liquid, gas and two-phase regions are presented, and bubblepoint pressure in the reservoir can be observed at which the first free gas forms in the reservoir when the pressure is dropped while the reservoir temperature remains constant.

The reservoir fluid illustrated in Figure 4 is above the bubblepoint pressure at the initial reservoir pressure. As a result, free gas would be absent anywhere in the reservoir. Nevertheless, free gas will form and relative permeability to oil will be reduced when the reservoir pressure decreases below the bubblepoint pressure. Consequently, *J* value will decline around the wellbore if a well is produced at a rate that requires bottomhole flowing pressure be lower than the bubblepoint pressure. This state can come about even though the average reservoir pressure may be well above the bubblepoint pressure. As pressure depletion in the reservoir takes place, the average reservoir pressure will likely be below the bubblepoint pressure and free gas will be present in the reservoir.

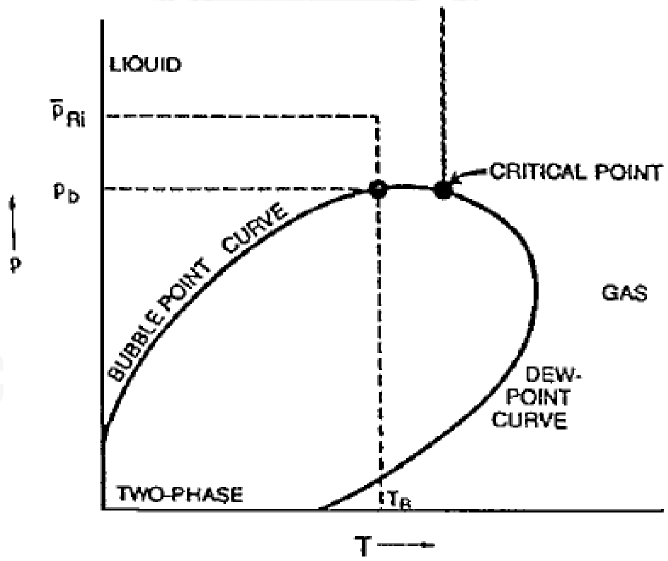

Figure 3.3 Oil reservoir phase diagram, Beggs [7]

3.2.2 Relative permeability behavior

The ability of liquid phase to flow will be lower when free gas is present in the pores of reservoir rock. Consequently, the gas saturation reduces the effective flow area of the liquids even when it is not great enough to permit gas to flow. The behavior of the gas-oil relative permeability as a function of liquid saturation is presented in Figure 3.4. The relative permeability is defined as the proportion of effective permeability to particular fluid to absolute permeability of the rock, $k_{ro}=k_o/k$. The relative permeability to gas will be increased if the gas saturation increases in the reservoir. Thus, the oil will flow less because relative permeability to oil decreases.

3.2.3 Oil viscosity behavior

At pressure below the bubblepoint, the oil viscosity is increased and the gas will vaporize out of solution as the pressure decreases. Particularly, at the constant temporary condition, the viscosity of oil saturated with gas will decrease if pressure is dropped from initial condition to bubblepoint pressure. Figure 3.5 shows graphically the behavior of oil viscosity, μ_o versus pressure at constant temperature. After the reservoir pressure falls below the bubblepoint pressure, oil viscosity increases and causes productivity index to decrease. On the other hand, the slope of Inflow Performance Relationship will increase.

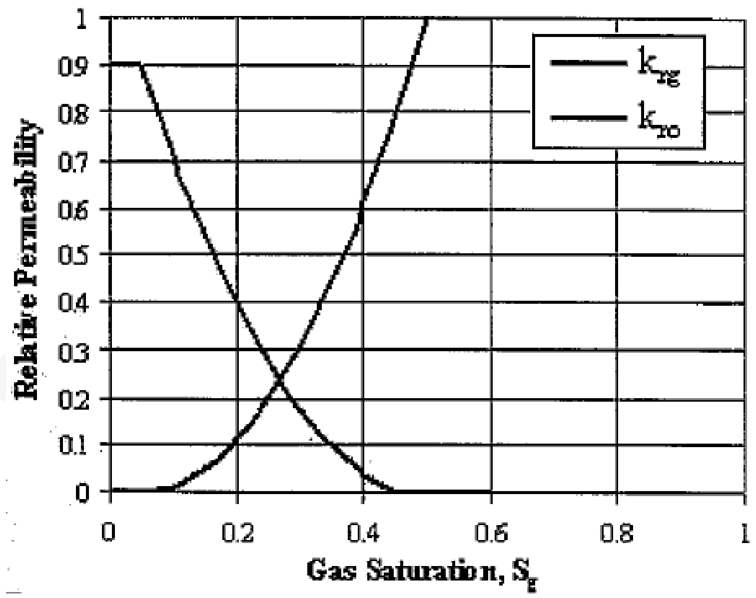

Figure 3.4 Gas-oil relative permeability, Somabutr [8].

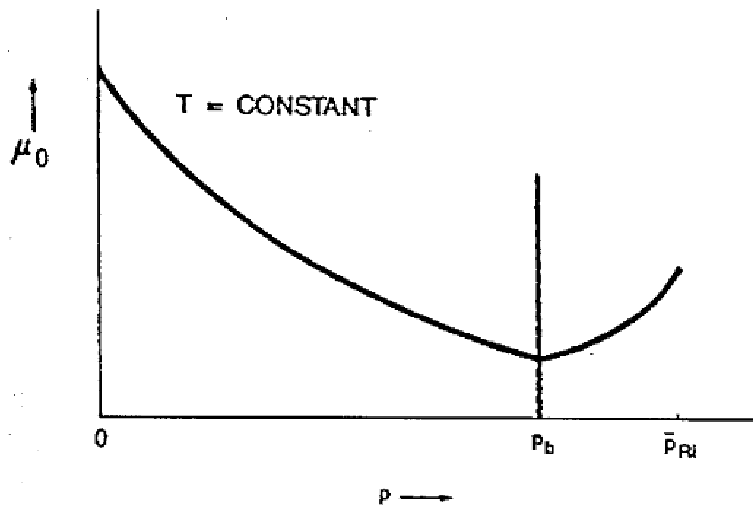

Figure 3.5 Oil viscosity behavior, Beggs [7].

3.2.4 Oil formation volume factor

The liquid will not expand unless the pressure is decreased. In the other words, when the bubblepoint pressure of oil is reached, gas will evaporate out of solution and cause the oil to shrink. Figure 3.6 illustrates the behavior of B_o versus p at constant temperature. From the plot, the curve shows that productivity index will increase as B_o decreases when the pressure is below the bubblepoint pressure, and the slope of IPR curve will decrease.

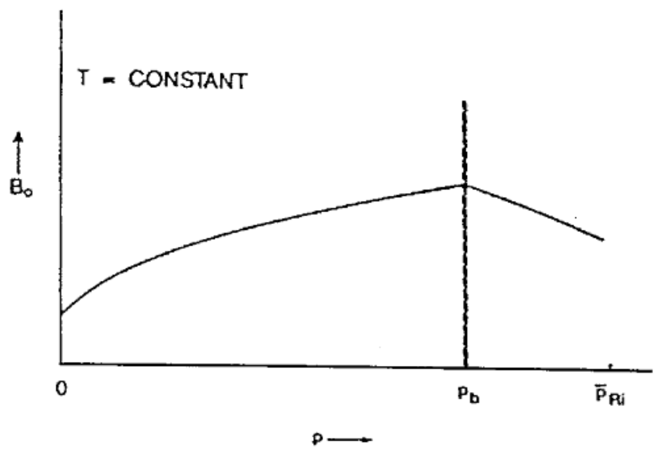

Figure 3.6 Oil formation volume factor behaviors, Beggs [7]

3.2.5 Skin factor

The skin factor *S'* is positive when there is extra pressure drop caused by damage, negative for decreased pressure drop caused by stimulation and zero for unchanged in permeability. Either well stimulation or formation damage can change the value of the absolute permeability, *k*. By performing well stimulation, the absolute permeability will be increased around the wellbore causing a negative skin. Clay swelling or pore plugging brings about a positive skin factor which decreases the absolute permeability. When the skin factor decreases, the productivity index will increase as expressed in Equation 3.6. For that reason, the slope of inflow performance will be decreased. Figure 3.7 illustrates the influence of *S'* on the pressure profile of oil well. As the permeability around the wellbore is increased by stimulation process, the wellbore flowing pressure will also increase. Then, the well stimulation causes the productivity index of oil reservoir to increase.

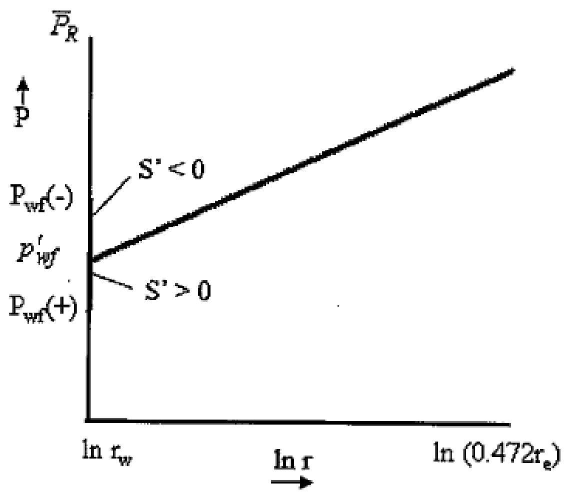

Figure 3.7 Effect of skin factor, Beggs [7]

3.2.6 Drive mechanism

The source of driving force to cause the oil and gas to flow into the wellbore has a significant effect on both the performance of oil reservoir and the total production system. Two basic types of drive mechanism which are solution gas drive and gas cap drive related in this study will be discussed. The behavior of reservoir pressure $\overline{p}_R$, the pressure function $f(\overline{p}_R)$ calculated at $p = \overline{p}_R$, and surface producing gas/oil ratio, *R*, versus cumulative recovery, *Np*, is discussed in details for each drive mechanism.

3.2.6.1 Solution gas drive

A solution gas drive reservoir is disconnected from any outside pressure of driving force such as water encroachment. The initial pressure is above the bubble point pressure, and for that reason, free gas is absent in the reservoir. Then, only the expansion of the fluids remaining in the reservoir can replace the produced fluids. Usually, we neglect the expansion of the connate water.

Before reaching $\bar{p}_R = p_b$ condition, the reservoir pressure declines quickly with production. Subsequently, it is only the oil that expands to replace the produced fluid. As long as the pressure is above the bubble point, the producing gas/oil ratio will remain constant and equal to R_{si}. Moreover, $f(p_R)$ will remain constant due to absence of free gas in the reservoir.

As soon as pressure drops below bubble point pressure, free gas will expand, and $\bar{p}_R$ will decrease less rapidly. Conversely, R will increase quickly when the gas saturation exceeds the critical gas saturation, then depleting more of the reservoir driving force. If abandonment conditions are reached, R will begin to reduce as most of the gas has been produced. Moreover, the reservoir gas volumes are more closely equal to the standard surface volumes at lower reservoir pressure condition.

Typically, recovery factor of solution gas drive reservoir at abandonment conditions ranges between 5% and 30% of original oil in place. In addition, some type of pressure maintenance may be applied to increase recovery. Figure 3.8 illustrates a typical solution gas drive performance under primary depletion. Note that when the reservoir pressure drops below the bubblepoint pressure, the slope of IPR will increase since the pressure function $f(p_R)$ quickly decreases, therefore, decreasing the productivity index.

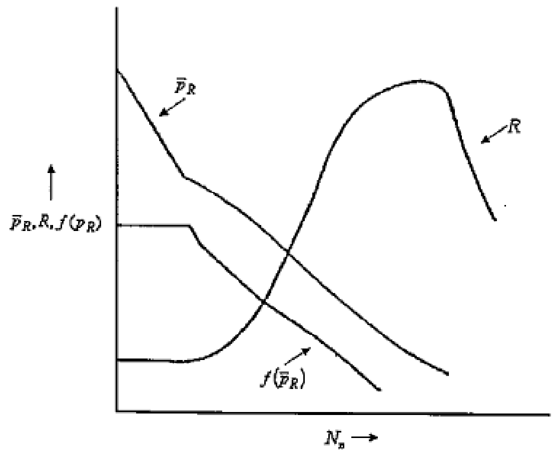

Figure 3.8 Solution gas drive performance, Beggs [7].

3.2.6.2 Gas cap drive

A gas cap drive reservoir is also closed boundary; there is no any outside pressure of driving force supported. However, at the initial pressure condition, the oil is saturated with gas. Therefore, free gas will be present. When oil is produced, the gas cap then expands and helps to preserve the reservoir pressure. Furthermore, as the reservoir pressure declines due to production, gas will evolve from the saturated oil.

Speaking of the decline of reservoir pressure, the reservoir pressure of a solution gas drive decreases faster than that of gas cap drive reservoir. Re-injecting the produced gas into the gas cap can also increase the recovery efficiency of reservoir. In addition, the effects of gravity may increase recovery. Figure 3.9 graphically shows a typical performance of a gas cap drive reservoir.

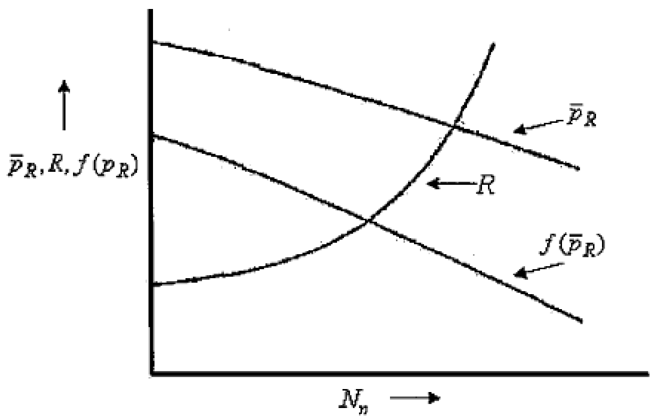

Figure 3.9 Gas cap drive performance, Beggs [7].

As the depletion proceeds below the bubble point pressure of a solution gas drive reservoir, the ability of well to produce decreases predominantly as the reservoir pressure is lower, and oil become more resistant to flow in the face of increasing gas saturation. The result is a progressive decline of the IPR's, as illustrated by the IPR curves in Figure 3.10.

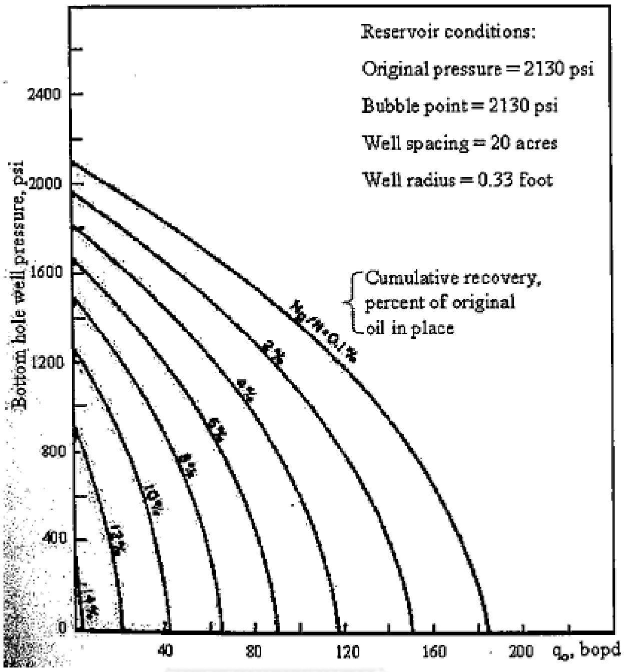

Figure 3.10 Computer-calculated inflow performance relationships for a solution-gas drive reservoir, Beggs [7].

CHAPTER IV
METHODOLOGY

The purpose of this thesis is to evaluate five IPR correlations use to estimate present inflow performance relationship of two-phase flow in vertical well. In evaluation, there are three elements to the problem that must be examined: the well bottom-hole flowing pressure, Mean Absolute Percentage Error (MAPE), and standard deviation of MAPE. In this chapter, a reservoir model, method to evaluate the IPR correlations, and example of calculation are presented.

4.1 Reservoir simulation model for base case

4.1.1 Reservoir model

A homogeneous rectangular reservoir model is constructed. The block centered geometry model consists of Cartesian grid of 25 x 25 x 5 cells in the x-, y- and z-direction, respectively. Each cell has the dimension of 150 ft. x 150 ft. x 20 ft. as shown in Figure 4.1.

The reservoir is initially saturated since the reservoir pressure is at the bubble point pressure. The depth of top face is set at 3,034.864 ft. The reservoir properties of the base case (case R001) are listed in Table 4.1.

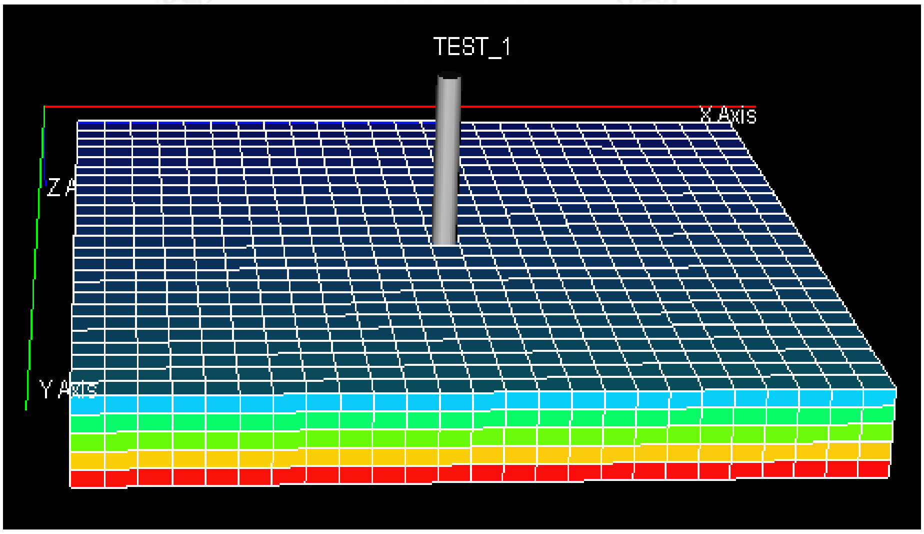

Figure 4.1 Reservoir model with well schematic of IPR.

Table 4.1 Reservoir properties (case R001).

Parameter	Value	Units
Porosity	18.0	%
Horizontal permeability	100	mD
Vertical permeability	100	mD
Datum depth	3,034.864	ft
Depth of top face	3,034.864	ft
Bubble point pressure	1,367.089	psia
Initial reservoir pressure @ datum depth	1,367.089	psia

4.1.2 PVT properties

The PVT properties of reservoir fluids used in this study are set up by using ECLIPSE correlation set 2. The input parameters are listed in Table 4.2 for correlation input. Table 4.3 shows the properties of water, and Table 4.4 demonstrates the density of each fluid. The properties of dry gas and live oil PVT obtained from the correlation are presented in Figures 4.2 and 4.3, respectively.

Table 4.2 Input data for ECLIPSE PVT correlation.

Input parameter	Value	Units
Oil gravity	23	°API
Gas gravity	0.85	-
Solution gas	210 (case R001)	scf/STB
Reference pressure	4,000	psia
Reservoir temperature	200	°F
Porosity	18.0	%
Rock type	Consolidated Sandstone	-
Rock compressibility	1.942842E-6	/psi

Table 4.3 Water PVT properties.

Property	Value	Units
Reference pressure (*Pref*)	4,000	psia
Water FVF at *Pref*	1.021734	rb/stb
Water compressibility	3.098498E-6	/psi
Water viscosity at *Pref*	0.3013227	cp
Water viscosibility	3.387726E-6	/psi

Table 4.4 Fluid density at surface condition.

Property	Value	Units
Oil density	57.11876	lb/cuft
Water density	62.42803	lb/cuft
Gas density	0.05306378	lb/cuft

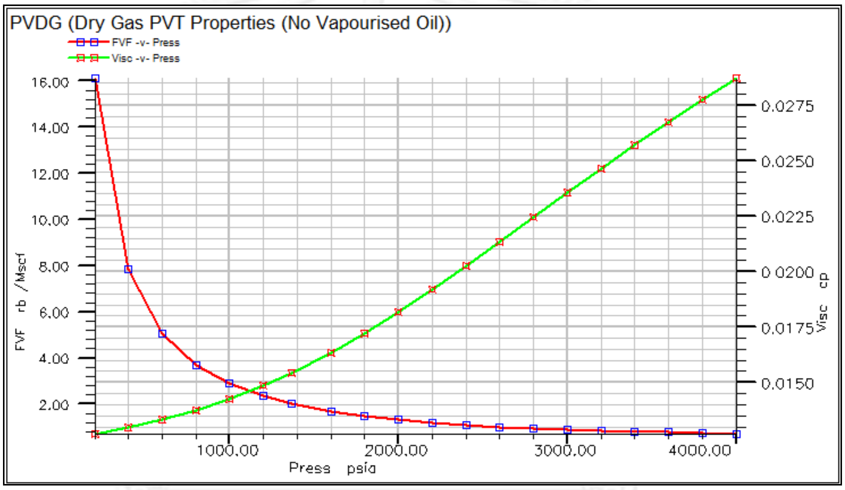

Figure 4.2 Dry gas PVT properties (no vaporized oil).

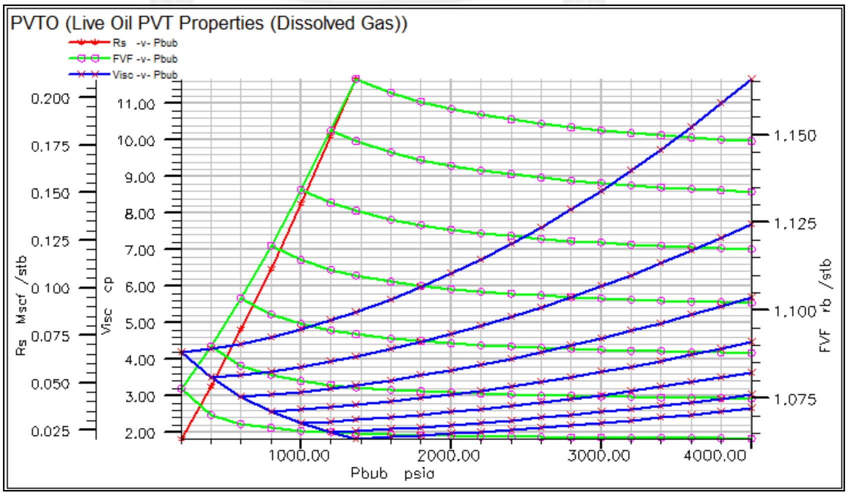

Figure 4.3 Live oil PVT properties (dissolved gas).

4.1.3 SCAL (Special Core Analysis) section

In this study, Corey's correlation is used to construct the relative permeability curves. The parameters set up in Corey's correlation are listed in Table 4.5. The values of relative permeability curves obtained from these input data are tabulated in Tables 4.6 and 4.7. Also, the plots of relative permeability are displayed in Figures 4.4 and 4.5.

Table 4.5 Input data for Corey's correlation.

Corey water	4	Corey Gas	3	Corey oil/water	3
S_{wmin}	0.2	S_{gmin}	0	Corey oil/gas	3
S_{wcr}	0.2	S_{gcr}	0.025	S_{org}	0.1
S_{wi}	0.2	S_{gi}	0	S_{orw}	0.35
S_{wmax}	1.0	$k_{rg}(S_{org})$	0.8	$k_{ro}(S_{wmin})$	0.8
$k_{rw}(S_{orw})$	0.8	$k_{rg}(S_{gmax})$	0.8	$k_{ro}(S_{gmin})$	0.8
$k_{rw}(S_{wmax})$	1.0				

Table 4.6 Water and oil relative permeability.

S_w	k_{rw}	k_{ro}
0.20	0.00	0.80
0.25	0.0001219326	0.56186557
0.30	0.001950922	0.37640604
0.35	0.009876543	0.23703704
0.40	0.031214754	0.13717421
0.45	0.076207895	0.070233196
0.50	0.15802469	0.02962963
0.55	0.29276025	0.00877915
0.60	0.49943606	0.001097394
0.65	0.80	0.00
1.00	1.00	0.00

Table 4.7 Gas and oil relative permeability.

S_g	k_{rg}	k_{ro}
0.00	0.00	0.80
0.025	0.00	0.7173105
0.109375	0.0015625	0.48054199
0.19375	0.0125	0.30261537
0.278125	0.0421875	0.17512463
0.3625	0.10	0.089663812
0.446875	0.1953125	0.037826921
0.53125	0.3375	0.011207976
0.615625	0.5359375	0.001400997
0.70	0.80	0.00
0.80	0.80	0.00

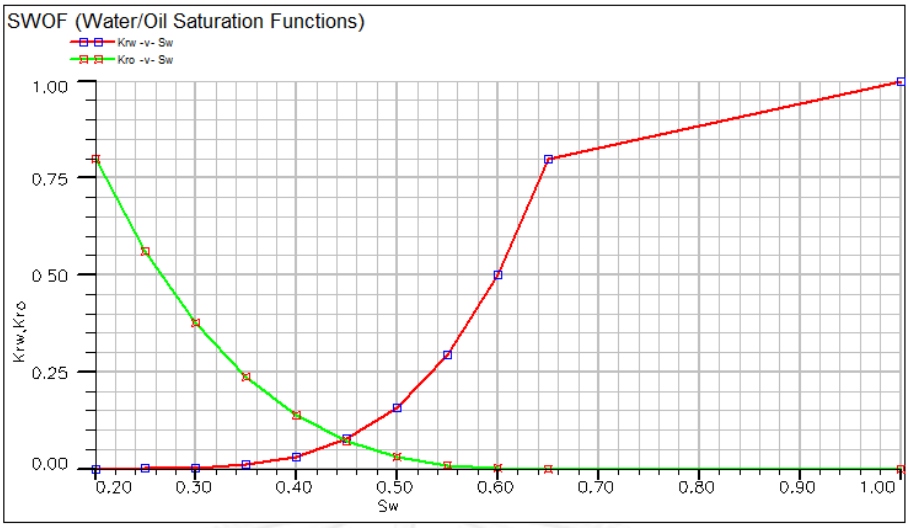

Figure 4.4 Water/ oil saturation function.

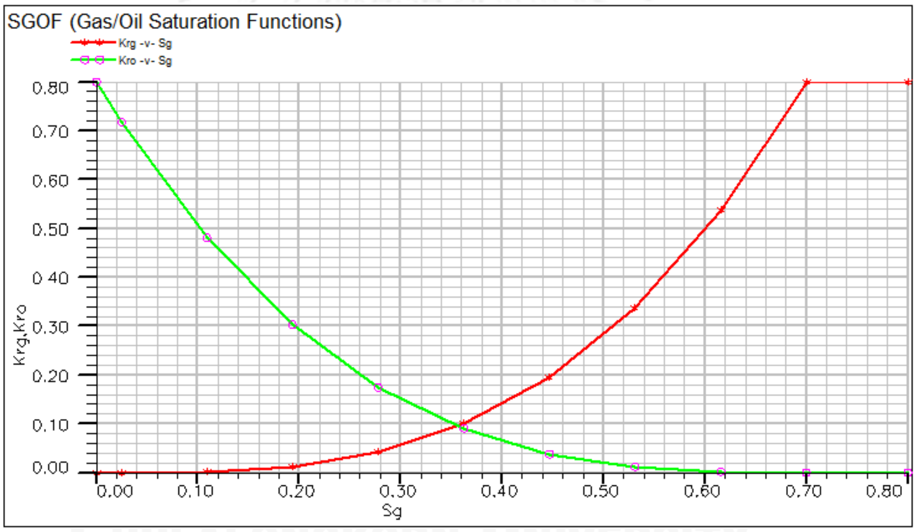

Figure 4.5 Gas/oil saturation function.

4.1.4 Well schedule

In this study, it is assumed that the wellbore diameter is 6-5/8 inches, and there is no skin for the base case (case R001). The well will be put on production at a certain maximum flow rate. The minimum bottomhole flowing pressure for the production well (tested well; TEST_1) is set at 14.7 psia.

4.2 Generation of cases studied

To obtain suitable data to construct IPR curve, numerical simulation was run using data from 150 cases to compare the ECLIPSE100 result with five equations, including Vogel, Fetkovich, Sukarno and Wisnogroho, Klins and Majcher and Jones, Blount, and Glaze. The following are the fluid, rock properties and completion characteristic use for generating the simulation cases:

a. Gas Solubility (R_s): 210, 500, 1000, 2000 , *SCF/STB*
b. API gravity of oil : 23, 25, 35, 45 , *°API*
c. Absolute permeability:100, 500, 1000 *md*
d. k_v/k_h ratio: 0.01, 0.1, 1
e. Skin factor: 0, 5, 10, 20
f. Perforation ratio: 0.4, 0.8
g. Corey exponent for relative permeability to oil (n_o): 2, 3
h. Corey exponent for relative permeability to gas (n_g): 2, 3

In this study, a trial version of JMP software is utilized in order to generate 150 cases by combining various fluid, rock properties and completion characteristic as mentioned above. Table 4.8 represents all 150 cases with different reservoir conditions generated from JMP trial software version.

Table 4.8 Detailed properties of cases studied.

Run ID.	Gas solubility R_s (scf/STB)	$^{\circ}API$	$SG.$	P_b $(psia)$	Absolute permeability (mD)	K_v (mD)	$\frac{K_v}{K_h}$	Perforation ratio	Skin factor	Corey exponent for k_{rg} (n_g)	Corey exponent for k_{ro} (n_o)
R001	210	23	0.85	1367.089	1000	10	0.01	0.4	0	3	3
R002	210	23	0.85	1367.089	1000	10	0.01	0.4	5	2	2
R003	210	23	0.85	1367.089	1000	10	0.01	0.4	5	3	3
R004	210	23	0.85	1367.089	1000	10	0.01	0.8	10	2	3
R005	210	23	0.85	1367.089	1000	100	0.1	0.4	0	2	3
R006	210	23	0.85	1367.089	1000	100	0.1	0.4	5	3	2
R007	210	23	0.85	1367.089	1000	100	0.1	0.8	5	3	3
R008	210	23	0.85	1367.089	1000	100	0.1	0.4	10	2	2
R009	210	23	0.85	1367.089	1000	100	0.1	0.4	20	2	2
R010	210	23	0.85	1367.089	1000	100	0.1	0.8	20	2	2

Table 4.8 Detailed properties of cases studied (continued)

Run ID.	Gas solubility R_s (scf/STB)	°API	$SG.$	P_b $(psia)$	Absolute permeability (mD)	K_v (mD)	$\frac{K_v}{K_h}$	Perforation ratio	Skin factor	Corey exponent for k_{rg} (n_g)	Corey exponent for k_{ro} (n_o)
R011	210	23	0.85	1367.089	1000	1000	1	0.4	0	2	3
R012	210	23	0.85	1367.089	1000	1000	1	0.8	0	2	3
R013	210	23	0.85	1367.089	1000	1000	1	0.8	10	2	2
R014	210	23	0.85	1367.089	100	1	0.01	0.4	0	2	3
R015	210	23	0.85	1367.089	100	1	0.01	0.4	0	3	3
R016	210	23	0.85	1367.089	100	1	0.01	0.8	5	3	3
R017	210	23	0.85	1367.089	100	1	0.01	0.4	10	3	3
R018	210	23	0.85	1367.089	100	1	0.01	0.8	20	2	3
R019	210	23	0.85	1367.089	100	10	0.1	0.8	5	3	2
R020	210	23	0.85	1367.089	100	100	1	0.8	0	2	3

Table 4.8 Detailed properties of cases studied (continued)

Run ID.	Gas solubility R_s (scf/STB)	$^{\circ}API$	$SG.$	P_b $(psia)$	Absolute permeability (mD)	K_v (mD)	$\frac{K_v}{K_h}$	Perforation ratio	Skin factor	Corey exponent for k_{rg} (n_g)	Corey exponent for k_{ro} (n_o)
R021	210	23	0.85	1367.089	100	100	1	0.4	0	3	2
R022	210	23	0.85	1367.089	100	100	1	0.8	0	3	3
R023	210	23	0.85	1367.089	100	100	1	0.8	10	2	3
R024	210	23	0.85	1367.089	100	100	1	0.4	20	3	2
R025	210	23	0.85	1367.089	100	100	1	0.4	20	3	3
R026	210	23	0.85	1367.089	500	5	0.01	0.8	5	2	2
R027	210	23	0.85	1367.089	500	5	0.01	0.8	20	2	2
R028	210	23	0.85	1367.089	500	5	0.01	0.8	20	2	3
R029	210	23	0.85	1367.089	500	5	0.01	0.8	20	3	3
R030	210	23	0.85	1367.089	500	50	0.1	0.4	0	3	2

Table 4.8 Detailed properties of cases studied (continued)

Run ID.	Gas solubility R_s (scf/STB)	$^{\circ}API$	$SG.$	P_b $(psia)$	Absolute permeability (mD)	K_v (mD)	$\frac{K_v}{K_h}$	Perforation ratio	Skin factor	Corey exponent for k_{rg} (n_g)	Corey exponent for k_{ro} (n_o)
R031	210	23	0.85	1367.089	500	50	0.1	0.4	0	3	2
R032	210	23	0.85	1367.089	500	50	0.1	0.8	0	3	2
R033	210	23	0.85	1367.089	500	50	0.1	0.8	0	3	3
R034	210	23	0.85	1367.089	500	50	0.1	0.8	10	2	3
R035	210	23	0.85	1367.089	500	500	1	0.8	0	3	2
R036	210	23	0.85	1367.089	500	500	1	0.4	5	3	3
R037	210	23	0.85	1367.089	500	500	1	0.4	10	2	3
R038	210	23	0.85	1367.089	500	500	1	0.8	20	2	2
R039	210	23	0.85	1367.089	500	500	1	0.8	20	3	2

Table 4.8 Detailed properties of cases studied (continued)

Run ID.	Gas solubility R_s (scf/STB)	$^{\circ}API$	$SG.$	P_b $(psia)$	Absolute permeability (mD)	K_v (mD)	$\frac{K_v}{K_h}$	Perforation ratio	Skin factor	Corey exponent for k_{rg} (n_g)	Corey exponent for k_{ro} (n_o)
R040	500	25	0.85	2651.55	1000	10	0.01	0.4	20	2	2
R041	500	25	0.85	2651.55	1000	10	0.01	0.8	0	3	2
R042	500	25	0.85	2651.55	1000	10	0.01	0.8	20	3	2
R043	500	25	0.85	2651.55	1000	100	0.1	0.8	5	2	3
R044	500	25	0.85	2651.55	1000	100	0.1	0.4	10	3	3
R045	500	25	0.85	2651.55	1000	100	0.1	0.4	10	3	3
R046	500	25	0.85	2651.55	1000	1000	1	0.8	0	2	2
R047	500	25	0.85	2651.55	1000	1000	1	0.8	0	2	3
R048	500	25	0.85	2651.55	1000	1000	1	0.8	5	3	2

Table 4.8 Detailed properties of cases studied (continued)

Run ID.	Gas solubility R_s (scf/STB)	$^{\circ}API$	$SG.$	P_b $(psia)$	Absolute permeability (mD)	K_v (mD)	$\frac{K_v}{K_h}$	Perforation ratio	Skin factor	Corey exponent for k_{rg} (n_g)	Corey exponent for k_{ro} (n_o)
R049	500	25	0.85	2651.55	1000	1000	1	0.8	20	3	3
R050	500	25	0.85	2651.55	100	1	0.01	0.4	0	2	2
R051	500	25	0.85	2651.55	100	1	0.01	0.4	0	3	3
R052	500	25	0.85	2651.55	100	1	0.01	0.8	0	2	2
R053	500	25	0.85	2651.55	100	1	0.01	0.8	5	3	3
R054	500	25	0.85	2651.55	100	10	0.1	0.4	5	3	3
R055	500	25	0.85	2651.55	100	10	0.1	0.4	20	2	3
R056	500	25	0.85	2651.55	100	100	1	0.8	0	2	2
R057	500	25	0.85	2651.55	100	100	1	0.8	5	2	3

Table 4.8 Detailed properties of cases studied (continued)

Run ID.	Gas solubility R_s (scf/STB)	$°API$	$SG.$	P_b $(psia)$	Absolute permeability (mD)	K_v (mD)	$\frac{K_v}{K_h}$	Perforation ratio	Skin factor	Corey exponent for k_{rg} (n_g)	Corey exponent for k_{ro} (n_o)
R056	500	25	0.85	2651.55	100	100	1	0.8	0	2	2
R057	500	25	0.85	2651.55	100	100	1	0.8	5	2	3
R058	500	25	0.85	2651.55	100	100	1	0.4	10	2	3
R059	500	25	0.85	2651.55	100	100	1	0.4	20	3	2
R060	500	25	0.85	2651.55	100	100	1	0.8	20	3	3
R061	500	25	0.85	2651.55	500	5	0.01	0.4	5	3	3
R062	500	25	0.85	2651.55	500	5	0.01	0.4	10	2	2
R063	500	25	0.85	2651.55	500	5	0.01	0.8	10	3	3

Table 4.8 Detailed properties of cases studied (continued)

Run ID.	Gas solubility R_s (scf/STB)	$^{\circ}API$	$SG.$	P_b $(psia)$	Absolute permeability (mD)	K_v (mD)	$\frac{K_v}{K_h}$	Perforation ratio	Skin factor	Corey exponent for k_{rg} (n_g)	Corey exponent for k_{ro} (n_o)
R064	500	25	0.85	2651.55	500	5	0.01	0.4	20	3	2
R065	500	25	0.85	2651.55	500	50	0.1	0.4	0	2	2
R066	500	25	0.85	2651.55	500	50	0.1	0.8	0	2	3
R067	500	25	0.85	2651.55	500	50	0.1	0.4	10	3	2
R068	500	25	0.85	2651.55	500	50	0.1	0.4	20	2	3
R069	500	25	0.85	2651.55	500	500	1	0.8	5	3	2
R070	500	25	0.85	2651.55	500	500	1	0.4	10	2	2
R071	500	25	0.85	2651.55	500	500	1	0.8	10	3	3
R072	1000	35	0.85	3534.718	1000	10	0.01	0.8	0	3	3

Table 4.8 Detailed properties of cases studied (continued)

Run ID.	Gas solubility R_s (scf/STB)	$^\circ API$	$SG.$	P_b $(psia)$	Absolute permeability (mD)	K_v (mD)	$\frac{K_v}{K_h}$	Perforation ratio	Skin factor	Corey exponent for k_{rg} (n_g)	Corey exponent for k_{ro} (n_o)
R073	1000	35	0.85	3534.718	1000	10	0.01	0.4	5	2	2
R074	1000	35	0.85	3534.718	1000	10	0.01	0.4	5	2	2
R075	1000	35	0.85	3534.718	1000	10	0.01	0.8	20	3	2
R076	1000	35	0.85	3534.718	1000	10	0.01	0.8	0	3	2
R077	1000	35	0.85	3534.718	1000	100	0.1	0.8	0	3	3
R078	1000	35	0.85	3534.718	1000	100	0.1	0.8	10	3	2
R079	1000	35	0.85	3534.718	1000	1000	1	0.8	0	2	2
R080	1000	35	0.85	3534.718	1000	1000	1	0.4	5	3	3
R081	1000	35	0.85	3534.718	1000	1000	1	0.4	20	2	3

Table 4.8 Detailed properties of cases studied (continued)

Run ID.	Gas solubility R_s (scf/STB)	$^\circ API$	$SG.$	P_b $(psia)$	Absolute permeability (mD)	K_v (mD)	$\frac{K_v}{K_h}$	Perforation ratio	Skin factor	Corey exponent for k_{rg} (n_g)	Corey exponent for k_{ro} (n_o)
R082	1000	35	0.85	3534.718	1000	1000	1	0.4	20	3	3
R083	1000	35	0.85	3534.718	1000	1000	1	0.4	20	3	3
R084	1000	35	0.85	3534.718	100	1	0.01	0.4	5	2	2
R085	1000	35	0.85	3534.718	100	1	0.01	0.4	0	2	2
R086	1000	35	0.85	3534.718	100	10	0.1	0.8	5	2	2
R087	1000	35	0.85	3534.718	100	10	0.1	0.8	5	3	3
R088	1000	35	0.85	3534.718	100	10	0.1	0.8	10	3	2
R089	1000	35	0.85	3534.718	100	10	0.1	0.8	0	2	3
R090	1000	35	0.85	3534.718	100	10	0.1	0.8	10	3	3

Table 4.8 Detailed properties of cases studied (continued)

Run ID.	Gas solubility R_s (scf/STB)	$^{\circ}API$	$SG.$	P_b $(psia)$	Absolute permeability (mD)	K_v (mD)	$\frac{K_v}{K_h}$	Perforation ratio	Skin factor	Corey exponent for k_{rg} (n_g)	Corey exponent for k_{ro} (n_o)
R091	1000	35	0.85	3534.718	100	10	0.1	0.4	20	2	2
R092	1000	35	0.85	3534.718	100	10	0.1	0.8	20	2	3
R093	1000	35	0.85	3534.718	100	100	1	0.8	0	2	3
R094	1000	35	0.85	3534.718	100	100	1	0.4	5	3	2
R095	1000	35	0.85	3534.718	100	100	1	0.8	10	3	2
R096	1000	35	0.85	3534.718	100	100	1	0.8	20	3	2
R097	1000	35	0.85	3534.718	500	5	0.01	0.4	0	3	3
R098	1000	35	0.85	3534.718	500	5	0.01	0.8	0	3	2
R099	1000	35	0.85	3534.718	500	5	0.01	0.4	5	2	3

Table 4.8 Detailed properties of cases studied (continued)

Run ID.	Gas solubility R_s (scf/STB)	$^\circ API$	$SG.$	P_b $(psia)$	Absolute permeability (mD)	K_v (mD)	$\frac{K_v}{K_h}$	Perforation ratio	Skin factor	Corey exponent for k_{rg} (n_g)	Corey exponent for k_{ro} (n_o)
R100	1000	35	0.85	3534.718	500	5	0.01	0.8	10	2	2
R101	1000	35	0.85	3534.718	500	5	0.01	0.8	10	2	3
R102	1000	35	0.85	3534.718	500	50	0.1	0.4	0	2	3
R103	1000	35	0.85	3534.718	500	50	0.1	0.4	20	2	2
R104	1000	35	0.85	3534.718	500	50	0.1	0.8	20	2	3
R105	1000	35	0.85	3534.718	500	500	1	0.4	0	3	2
R106	1000	35	0.85	3534.718	500	500	1	0.4	0	3	3
R107	1000	35	0.85	3534.718	500	500	1	0.4	0	2	2
R108	1000	35	0.85	3534.718	500	500	1	0.4	5	2	2

Table 4.8 Detailed properties of cases studied (continued)

Run ID.	Gas solubility R_s (scf/STB)	$°API$	$SG.$	P_b $(psia)$	Absolute permeability (mD)	K_v (mD)	$\frac{K_v}{K_h}$	Perforation ratio	Skin factor	Corey exponent for k_{rg} (n_g)	Corey exponent for k_{ro} (n_o)
R109	1000	35	0.85	3534.718	500	500	1	0.4	10	2	3
R110	2000	45	0.85	4712.048	1000	10	0.01	0.8	0	3	3
R111	2000	45	0.85	4712.048	1000	10	0.01	0.8	10	3	2
R112	2000	45	0.85	4712.048	1000	10	0.01	0.8	10	2	3
R113	2000	45	0.85	4712.048	1000	10	0.01	0.8	10	3	3
R114	2000	45	0.85	4712.048	1000	100	0.1	0.8	5	2	3
R115	2000	45	0.85	4712.048	1000	100	0.1	0.4	10	3	2
R116	2000	45	0.85	4712.048	1000	100	0.1	0.4	20	3	3
R117	2000	45	0.85	4712.048	1000	100	0.1	0.8	20	2	2

Table 4.8 Detailed properties of cases studied (continued)

Run ID.	Gas solubility R_s (scf/STB)	$^{\circ}API$	$SG.$	P_b $(psia)$	Absolute permeability (mD)	K_v (mD)	$\frac{K_v}{K_h}$	Perforation ratio	Skin factor	Corey exponent for k_{rg} (n_g)	Corey exponent for k_{ro} (n_o)
R118	2000	45	0.85	4712.048	1000	1000	1	0.4	0	3	2
R119	2000	45	0.85	4712.048	1000	1000	1	0.8	0	3	2
R124	2000	45	0.85	4712.048	100	1	0.01	0.4	0	3	2
R125	2000	45	0.85	4712.048	100	1	0.01	0.4	0	2	3
R126	2000	45	0.85	4712.048	100	1	0.01	0.8	0	2	3
R128	2000	45	0.85	4712.048	100	1	0.01	0.4	20	3	3
R129	2000	45	0.85	4712.048	100	10	0.1	0.4	0	2	2
R130	2000	45	0.85	4712.048	100	10	0.1	0.8	0	3	2
R131	2000	45	0.85	4712.048	100	10	0.1	0.4	5	2	3

Table 4.8 Detailed properties of cases studied (continued)

Run ID.	Gas solubility R_s (scf/STB)	$^{\circ}API$	$SG.$	P_b $(psia)$	Absolute permeability (mD)	K_v (mD)	$\frac{K_v}{K_h}$	Perforation ratio	Skin factor	Corey exponent for k_{rg} (n_g)	Corey exponent for k_{ro} (n_o)
R132	2000	45	0.85	4712.048	100	10	0.1	0.4	10	3	2
R133	2000	45	0.85	4712.048	100	10	0.1	0.8	20	3	2
R134	2000	45	0.85	4712.048	100	100	1	0.8	0	2	2
R135	2000	45	0.85	4712.048	100	100	1	0.4	20	2	3
R136	2000	45	0.85	4712.048	100	100	1	0.4	20	2	3
R137	2000	45	0.85	4712.048	500	5	0.01	0.8	5	3	3
R138	2000	45	0.85	4712.048	500	5	0.01	0.8	0	3	3
R139	2000	45	0.85	4712.048	500	5	0.01	0.4	0	3	3
R140	2000	45	0.85	4712.048	500	5	0.01	0.4	20	3	3

Table 4.8 Detailed properties of cases studied (continued)

Run ID.	Gas solubility R_s (scf/STB)	$^{\circ}API$	$SG.$	P_b $(psia)$	Absolute permeability (mD)	K_v (mD)	$\frac{K_v}{K_h}$	Perforation ratio	Skin factor	Corey exponent for k_{rg} (n_g)	Corey exponent for k_{ro} (n_o)
R141	2000	45	0.85	4712.048	500	50	0.1	0.4	0	3	3
R142	2000	45	0.85	4712.048	500	50	0.1	0.8	0	3	3
R143	2000	45	0.85	4712.048	500	50	0.1	0.8	5	3	2
R144	2000	45	0.85	4712.048	500	50	0.1	0.8	5	2	3
R145	2000	45	0.85	4712.048	500	500	1	0.4	5	2	2
R146	2000	45	0.85	4712.048	500	500	1	0.4	5	3	2
R147	2000	45	0.85	4712.048	500	500	1	0.8	5	2	3
R148	2000	45	0.85	4712.048	500	500	1	0.4	10	3	3
R149	2000	45	0.85	4712.048	500	500	1	0.8	0	2	2
R150	2000	45	0.85	4712.048	500	500	1	0.8	20	3	3

Refer to nonlinear convergence error case from ECLIPSE100 simulation result

4.3 Generation of data points for IPR

Firstly, the simulation is run for eight different constant oil production rates: 600, 800, 1000, 1200, 1400, 1600, 1800, and 2000 STB/D, respectively. Then, the well bottomhole flowing pressure is plotted against time on Cartesian scale in order to determine the producing time that reaches the pseudo-steady state period where the data points display a straight line as shown in Figure 4.6. From Figure 4.6, the starting of pseudo-steady state is approximately at 20 days after the production starts.

In order to select the accurate starting point of pseudo-steady state period, the derivatives of pressure respective with respect to time or the slopes of pressure curves in Figure 4.6 are plotted as illustrated in Figure 4.7. When the slope is constant, the fluid flow in the reservoir reaches pseudo-steady state conditions. Compared to Figure 4.6, the graph also shows the same trend as the slope becomes constant after 20 days onward for case R001 as an example.

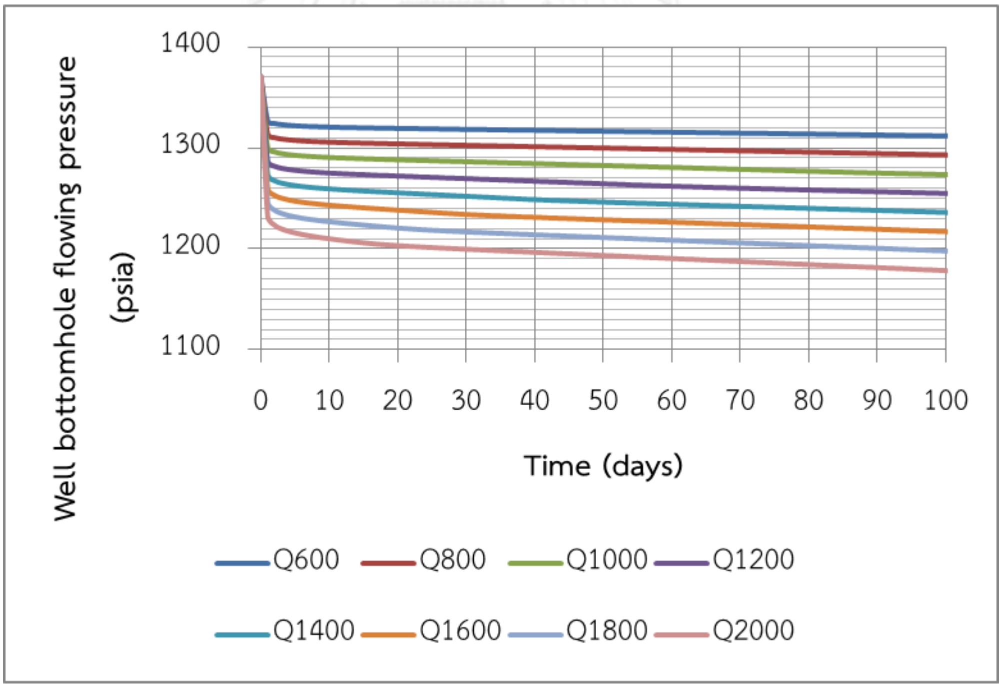

Figure 4.6 Well bottomhole pressures for different oil production rate.

The eight pairs of bottomhole flowing pressure at the beginning of pseudo-steady state flow and oil production rate will be needed to construct inflow performance relationship as shown in Figure 4.8.

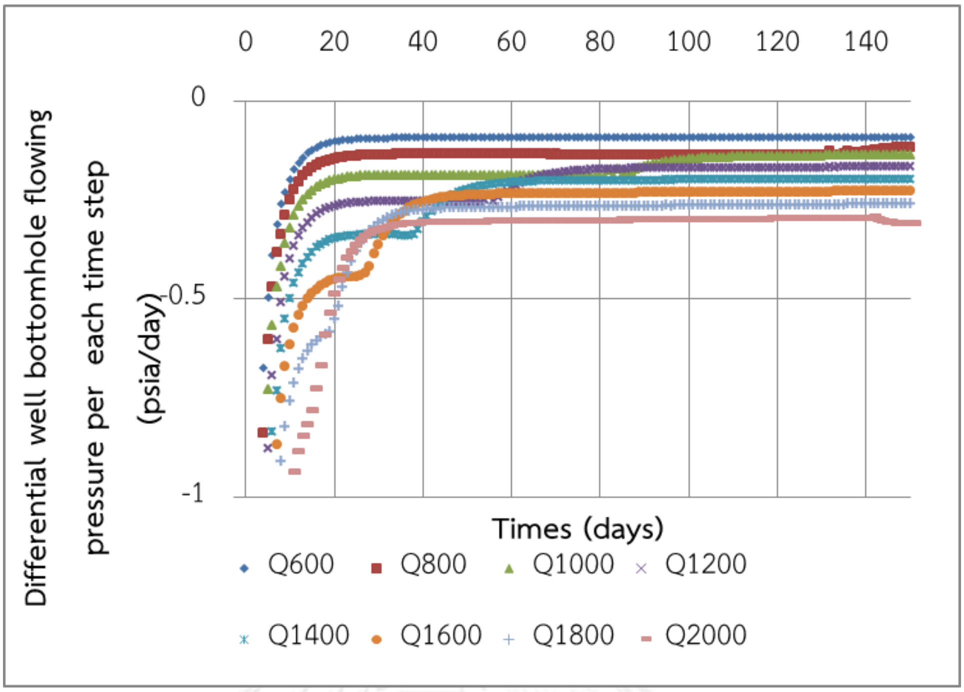

Figure 4.7 Slope of well bottomhole flowing pressure for different oil production rates

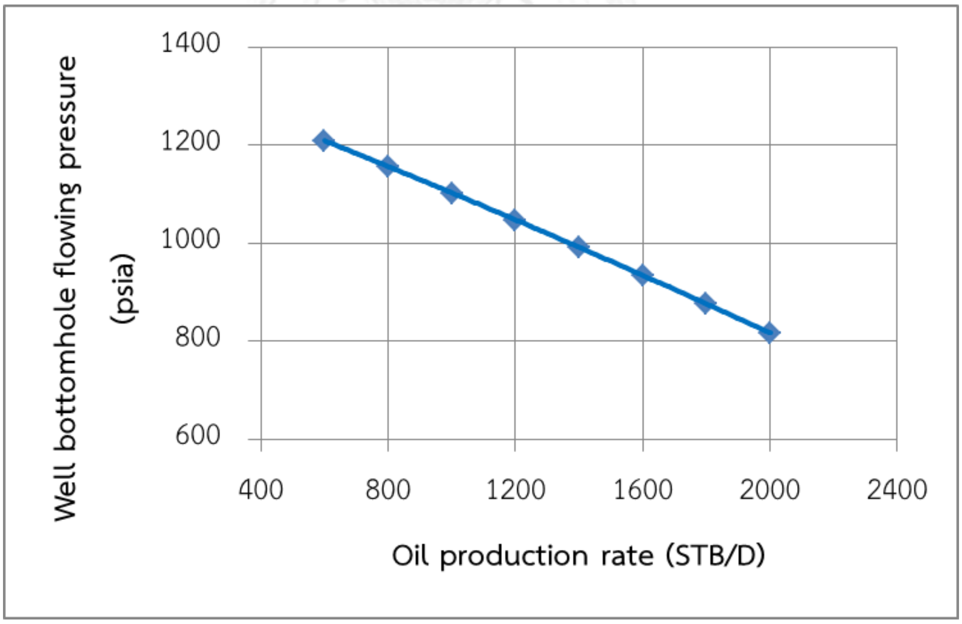

Figure 4.8 Inflow performance relationship curve.

4.4 IPR construction and evaluation method

When getting all eight corresponding well bottomhole pressures and oil production rates from ECLIPSE100, then the data are fitted into each IPR's equation to find the absolute open flow which is the maximum flow rate and determine the required coefficient of each IPR correlation in order to evaluate the common five correlations used to estimate present inflow performance relationship of two-phase flow in single vertical well in solution gas drive reservoirs. This study utilizes calculated maximum flow rate and coefficients to determine the well bottomhole flowing pressure corresponding to each oil production rate. Then, eight well bottomhole flowing pressures for eight different oil production rates are compared with well bottomhole flowing pressures from ECLIPSE100 to determine the mean absolute percentage error and standard deviation. Finally, we calculate the average of mean absolute percentage error and determine the standard deviation of MAPE of total cases studied. The proportion of cases studied which yield MAPE below 1% is observed and compared among each IPR correlations. In addition, the dispersion of MAPE value is also investigated.

4.4.1 Vogel's IPR

The Vogel IPR equation is expressed as

$$\frac{q_o}{(q_o)_{max}} = 1-0.2\left(\frac{P_{wf}}{\bar{P}_r}\right) - 0.8\left(\frac{P_{wf}}{\bar{P}_r}\right)^2$$

Thus, plotting q_o versus $1-0.2\left(\frac{P_{wf}}{\bar{P}_r}\right) - 0.8\left(\frac{P_{wf}}{\bar{P}_r}\right)^2$ will enable us to find $(q_o)_{max}$. Having done that in Figure 4.9 with $\bar{P}_R=1,370.607\ psi$, the slope of the graph which is $(q_o)_{max}$ is 9,579.03707 STB/D.

Therefore, Vogel's IPR for this case is then

$$\frac{q_o}{9,579.037\ STB/D} = 1-0.2\left(\frac{P_{wf}}{1,370.607\ psia}\right) - 0.8\left(\frac{P_{wf}}{1370.607\ psia}\right)^2$$

After obtaining the expression for Vogel's IPR, the next step is to determine the well bottomhole flowing pressure for different oil rates in order to compare with the ones generated by ECLIPSE100 reservoir simulator. For example, when the oil production rate is 600 STB/D, Vogel's IPR becomes

$$\frac{600\ STB/D}{9{,}579.037\ STB/D} = 1-0.2\left(\frac{P_{wf}}{1{,}370.607\ psia}\right)-0.8\left(\frac{P_{wf}}{1370.607\ psia}\right)^2$$

or $$0.00058368(P_{wf})^2+0.00014592(P_{wf})+1-0.062636=0$$

Thus,

$$P_{wf}=\frac{-0.00014592\pm\sqrt{0.00014592^2-(4)(0.00058368)(1-0.062636)}}{2(0.00058368)}$$

$$P_{wf}=1{,}322.151\ psia$$

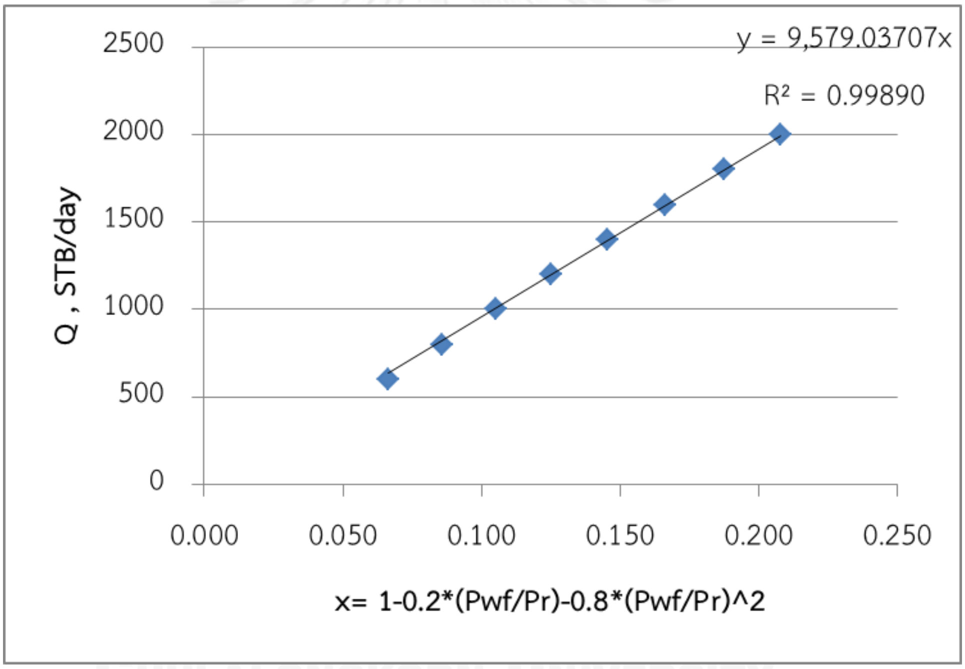

Figure 4.9 A plot to determine $(q_o)_{max}$ for Vogel's IPR

After that, the calculation for well bottomhole flowing pressure is repeated for oil production rate of 800, 1000, 1200, 1400, 1600, 1800, and 2000 in stock tank barrel per day. Table 4.9 shows the calculation result for case R001. Then, the predicted values in Table 4.9 are used to construct the IPR curve as shown in Figure 4.10.

Table 4.9 Well bottomhole flowing pressure predictions by Vogel's correlation (case R001)

Oil production rate *(STB/D)*	Well bottomhole flowing pressure *(psia)*
600.000	1,322.15105
800.000	1,305.64580
1,000.000	1,288.95401
1,200.000	1,272.06920
1,400.000	1,254.98452
1,600.000	1,237.69271
1,800.000	1,220.18603
2,000.000	1,202.45627

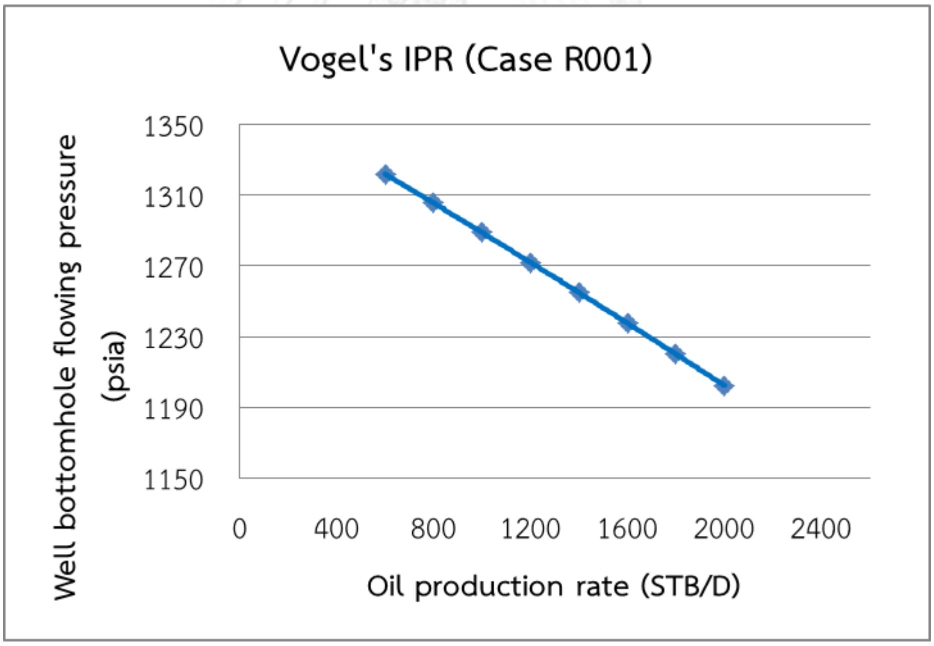

Figure 4.10 Vogel's IPR curve (case R001)

In order to compare the performance prediction of Vogel's IPR, the calculated bottomhole flowing pressures are compared with the ones obtained from simulation. The mean absolute percentage error (MAPE) is used in this study. It is defined by the formula

$$\text{MAPE} = \frac{100\%}{n} \sum_{t=1}^{n} \frac{\left| A_t - F_t \right|}{A_t} \tag{4.1}$$

Where A_t is the actual value, F_t is the forecast value and n is number of the samples. In the case of a perfect fit, MAPE is zero if the division is not zero.

Table 4.10 Calculation of the mean absolute percentage error of Vogel's IPR (case R001).

q_o (STB/D)	A_t P_{wf} (ECLIPSE)	F_t P_{wf} (Vogel)	$Abs(\frac{A_t - F_t}{A_t})$	MAPE (%)
600	1,319.3362	1,322.15105	0.00213	0.0744
800	1,303.9633	1,305.64580	0.00129	
1,000	1,288.2430	1,288.95401	0.00055	
1,200	1,272.1156	1,272.06920	0.00004	
1,400	1,255.5183	1,254.98452	0.00043	
1,600	1,238.3712	1,237.69271	0.00055	
1,800	1,220.6233	1,220.18603	0.00036	
2,000	1,203.1838	1,202.45627	0.00060	

4.4.2 Fetkovich's IPR

To analyze the performance of Fetkovich's IPR, it is necessary to solve the performance coefficient C and exponent n in the equation $q_o = C(\bar{P}^2_R - P^2_{wf})^2$. By plotting oil production rate obtained from simulation on the y-axis and the difference of squares between the average reservoir pressure and the well bottomhole flowing pressure also obtained from simulation on x-axis, regression with power model can be performed to obtain coefficient C and exponent n. From Figure 4.11, the coefficient C is 0.00236 and exponent n is equal to 1.0528. At this point, Fetkovich's IPR for this case can be expressed as

$$(q_o)_{max}=0.00236(\overline{P}_r^{\,2} - P^2_{wf})^{1.0528}$$

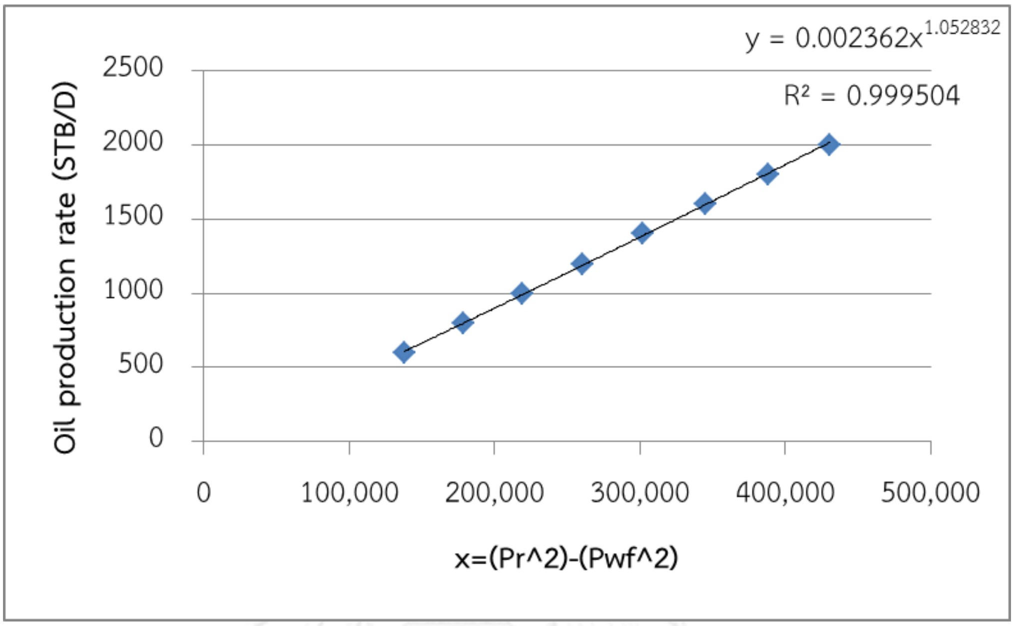

Figure 4.11 Determination of coefficient C and exponent n for Fetkovich's IPR (case R001).

The next step is to utilize the coefficient C and exponent n in the calculation of the maximum oil production rate and well bottomhole flowing pressure at different flow rates to construct the IPR curve. From Fetkovich's IPR, substituting $P_{wf}= 0$ *psia* and $\overline{P}_r=1,370.607$ *psia*, $C=0.00236$ and $n=1.0528$, we obtain

$$(q_o)_{max}=0.00236((1,370.067)^2\text{-}0)^{1.0528}$$

$$(q_o)_{max}=9,518.4147\ STB/D$$

Table 4.11 shows the results of well bottomhole flowing pressure corresponding to each oil production rate vary from 600 to 2,000 STB/D calculated from the equation:

$$P_{wf}=\sqrt{1,370.607^2\text{-}\left(\left(\frac{q_o}{0.00236}\right)^{\frac{1}{1.0528}}\right)}$$

Table 4.11 Well bottomhole flowing pressure predictions by Fetkovich's correlation (case R001)

Oil production rate (STB/D)	*Well bottomhole flowing pressure (psia)*
600.000	1,320.049
800.000	1,303.757
1000.000	1287.469
1200.000	1271.139
1400.000	1254.736
1600.000	1238.235
1800.000	1221.617
2000.000	1204.865
5747.000	849.805
9518.415	0.000

After that, we construct the IPR curve and determine MAPE in the same fashion as in the case of Vogel's method. The results are shown on Figure 4.12 and Table 4.12.

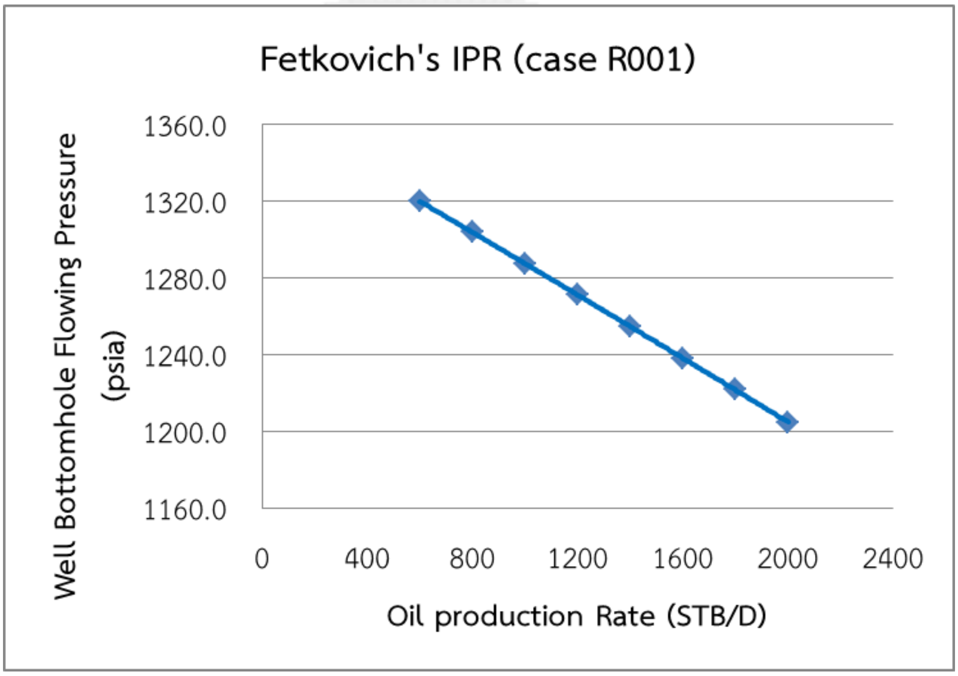

Figure 4.12 Fetkovich's IPR curve (case R001)

Table 4.12 Calculation of the mean absolute percentage error of Fetkovich's IPR (case R001).

q_o (STB/D)	A_t P_{wf} (ECLIPSE)	F_t P_{wf} (Fetkovich)	$Abs(\frac{A_t - F_t}{A_t})$	*MAPE* (%)
600	1,319.3362	1,320.049	0.00054	**0.0626**
800	1,303.9633	1,303.757	0.00016	
1,000	1,288.2430	1,287.469	0.00060	
1,200	1,272.1156	1,271.139	0.00077	
1,400	1,255.5183	1,254.736	0.00062	
1,600	1,238.3712	1,238.235	0.00011	
1,800	1,220.6233	1,221.617	0.00081	
2,000	1,203.1838	1,204.865	0.00140	

4.4.3 Sukarno and Wisnogroho's IPR

This IPR can be determined and constructed similar to Vogel's method. However, the correlation utilizes a different equation to solve for pressure-rate behavior. Likewise, MAPE and standard deviation calculation can be done in the same fashion with other correlations. The Sukarno and Wisnogroho's IPR is expressed as

$$\frac{q_o}{(q_o)_{max}} = 0.90482 - 0.08881\left(\frac{P_{wf}}{\bar{P}_r}\right) - 0.96534\left(\frac{P_{wf}}{\bar{P}_r}\right)^2$$

Thus, we need to determine $(q_o)_{max}$ first. This can be done by plotting q_o versus $0.90482 - 0.08881\left(\frac{P_{wf}}{\bar{P}_r}\right) - 0.96534\left(\frac{P_{wf}}{\bar{P}_r}\right)^2$ and fit the curve with a straight line passing through the origin. The slope of the straight line is $(q_o)_{max}$.

Figure 4.13 shows the curve fitting to the simulated results obtained in case R001. The maximum oil production rate which is the slope of the graph is 7,947.0349 STB/D.

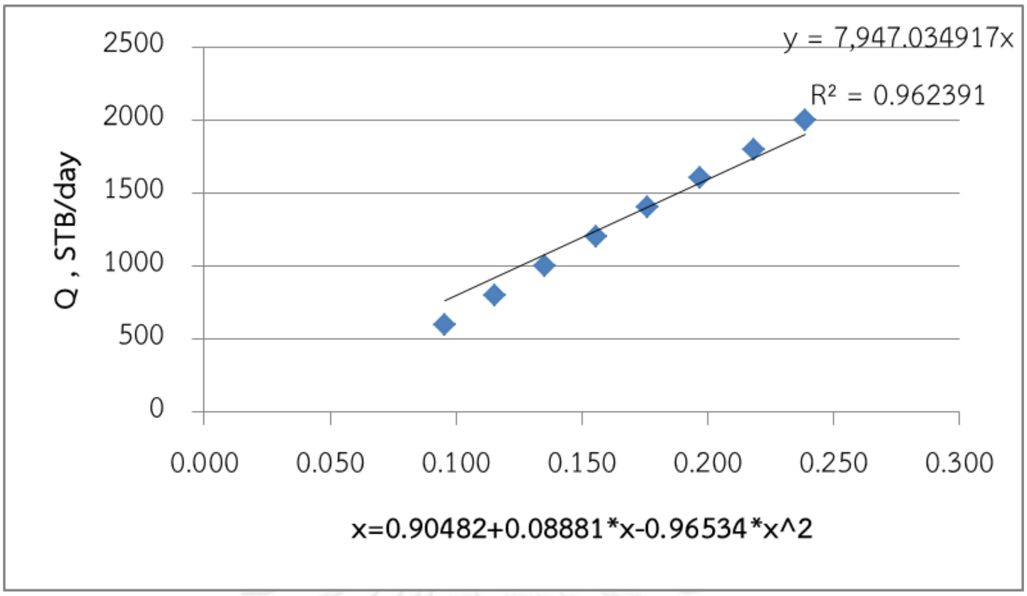

Figure 4.13 A plot to determine $(q_o)_{max}$ for Sukarno and Wisnogroho's IPR (case R001)

In order to construct IPR curve, we need to determine the well bottomhole flowing pressures for different flow rates. A sample calculation when q_o=600 STB/D is shown below:

$$\frac{600\ STB/D}{7{,}947.035\ STB/D}=0.90482-0.08881\left(\frac{P_{wf}}{1{,}370.607\ psia}\right)-0.96534\left(\frac{P_{wf}}{1{,}370.607\ psia}\right)^2$$

$$0.000704312(P_{wf})^2+0.00006479P_{wf})+1-0.0754998=0$$

$$P_{wf}=\frac{-0.00006479\pm\sqrt{0.000704312^2-(4)(0.000704312)(1-0.0754998)}}{2(0.00006479)}$$

$$P_{wf}=1{,}334.991\ psia$$

The corresponding well bottomhole flowing pressures calculated for different oil production rates for Sukarno and Wisnogroho's IPR are illustrated in Table 4.13. The IPR curve is plotted in Figure 4.14. Then, MAPE is determined for case R001 as shown in Table 4.14.

Table 4.13 Well bottomhole flowing pressure predictions by Sukarno and Wisnogroho's correlation (case R001)

Oil production rate (STB/D)	*Well bottomhole flowing pressure (psia)*
600.000	1334.991
800.000	1315.592
1000.000	1295.886
1200.000	1275.861
1400.000	1255.500
1600.000	1234.745
1800.000	1213.697
2000.000	1192.215
4768.000	835.842
7947.035	0.000

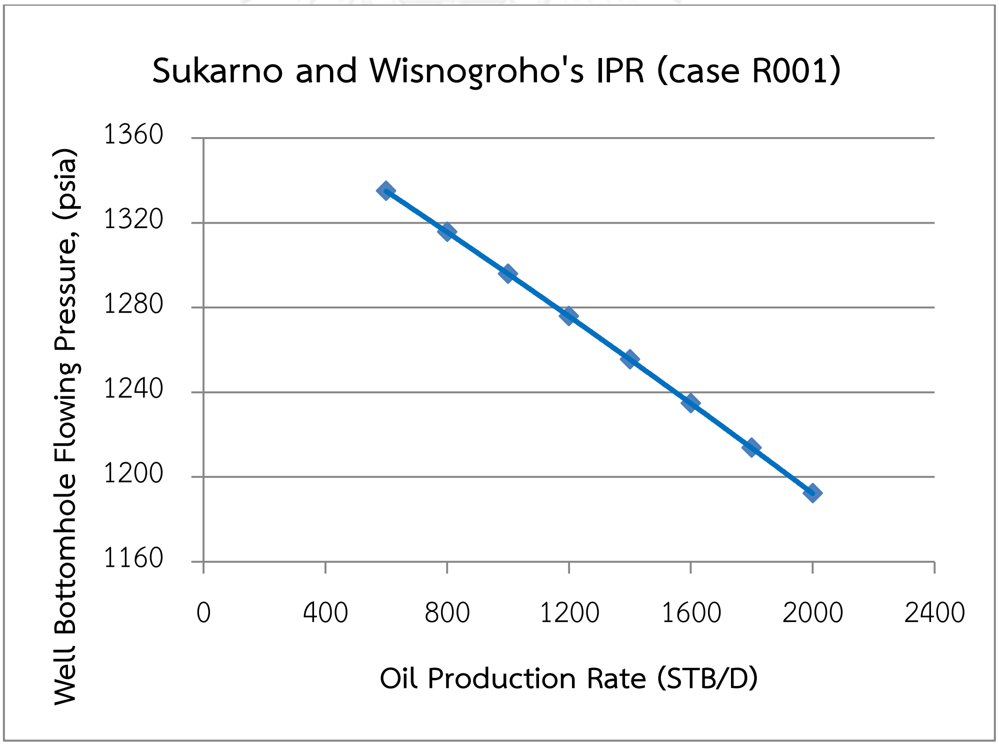

Figure 4.14 Sukarno and Wisnogroho's IPR curve (case R001)

Table 4.14 Calculation of the mean absolute percentage error of Sukarno and Wisnogroho's IPR (case R001).

q_o (STB/D)	A_t P_{wf} (ECLIPSE)	F_t P_{wf} (Sukarno and Wisnogroho)	$Abs(\frac{A_t-F_t}{A_t})$	MAPE (%)
600	1319.3362	1334.9914	0.01187	**0.59204**
800	1303.9633	1315.5916	0.00892	
1000	1288.2430	1295.8865	0.00593	
1200	1272.1156	1275.8614	0.00294	
1400	1255.5183	1255.5000	0.00001	
1600	1238.3712	1234.7849	0.00290	
1800	1220.6233	1213.6969	0.00567	
2000	1203.1838	1192.2151	0.00912	

4.4.4 Klins and Majcher's IPR

For Klins and Majcher's IPR, the methodology is similar to Vogel's method. However, the correlation uses a different equation to solve for pressure-rate behavior. Moreover, solving for pressure-rate behavior needs Newton-Raphson technique to calculate the well bottomhole flowing pressure.

The Klins and Majcher's IPR is expressed as

$$\frac{q_o}{\left(q_o\right)_{max}}=1-0.295\left(\frac{P_{wf}}{\bar{P}_r}\right)-0.705\left(\frac{P_{wf}}{\bar{P}_r}\right)^n$$

where

$$n=(0.28+0.72\frac{\bar{P_R}}{P_b})(1.235+0.001P_b)$$

In order to evaluate this IPR performance prediction, first we need getting all eight corresponding well bottomhole pressures and oil production rates. Then, these data points are feeded into Klins and Majcher' s equation to find absolute open flow. Figure 4.15 shows the plot to find Klins and Majcher's IPR maximum oil production rate for case R001 which is 8,280.567 STB/day.

Then, we calculate n value from the above equation. After that, we determine the well bottomhole flowing pressure by utilizing Newton-Raphson technique.

As an example, for case R001, q_o=600 STB/D, $(q_o)_{max}$=8,280.567 STB/D, $\bar{P}_r$=1,370.607 psia and $\bar{P}_r$=1,370.607 psia

Then substitute into equation (2.11),

$$n=(0.28+0.72\frac{1,370.607}{1,370.607})(1.235+0.001(1,370.607))$$

$$n=2.6056$$

Next, we use Newton-Rapshon's method to find the only real root of the equation below correct to 5 decimal places.

Newton-Rapshon's formula is

$$x_{t+1}=x_t-\frac{f(x)}{f'(x)} \tag{4.2}$$

Rearrangement of Klins and Majcher's IPR equation becomes

$$\frac{0.705}{(\bar{P}_r)^n}(P_{wf})^n+\frac{0.295}{\bar{P}_r}\left(P_{wf}\right)+\frac{q_o}{q_{o,max}}-1=0$$

Given $$f\left(P_{wf}\right)=\frac{0.705}{1,370.607^{2.6056}}(P_{wf})^{2.6056}+\frac{0.295}{1,370.607}\left(P_{wf}\right)+\frac{600}{8,280.567}-1$$

and $$f'\left(P_{wf}\right)=\frac{0.705}{1,370.607^{2.6056}}(2.6056)(P_{wf})^{1.6056}+\frac{0.295}{1,370.607}$$

Now, Newton-Rapshon's formula here is

$$(P_{wf})_{t+1}=(P_{wf})_t-\frac{\frac{0.705}{1,370.607^{2.6056}}(P_{wf})^{2.6056}+\frac{0.295}{1,370.607}\left(P_{wf}\right)+\frac{600}{8,280.567}-1}{\frac{0.705}{1,370.607^{2.6056}}(2.6056)(P_{wf})^{1.6056}+\frac{0.295}{1,370.607}}$$

Let us make an initial guess $(P_{wf})_0$=1,350 psia. So, with our value of $(P_{wf})_0$=1,350 psia, our approximation for $(P_{wf})_1$ is given by

$$(P_{wf})_1=1,350-\frac{\frac{0.705}{1,370.607^{2.6056}}\left(P_{wf}\right)^{2.6056}+\frac{0.295}{1,370.607}\left(P_{wf}\right)+\frac{600}{8,280.567}-1}{\frac{0.705}{1,370.607^{2.6056}}\left(2.6056\right)\left(P_{wf}\right)^{1.6056}+\frac{0.295}{1,370.607}}$$

$$\approx 1,323.25682 \text{ psia}$$

Using a scientific calculator, it is possible to finish the sum. Take the value of $(P_{wf})_1$ and repeat the above calculations using this as the initial guess. The resulting answer will be $(P_{wf})_2$. Again, repeat the procedure until the 5th decimal places remain unchanged. Therefore, $P_{wf}=1,322.883$ psia correctly rounded to 5 decimal places. Table 4.15 shows the result of calculation well bottomhole flowing pressure at $q_o=600\ STB/D$ using Newton-Raphson method.

Later, all oil production rates are calculated for corresponding well bottomhole flowing pressure and the calculated results are demonstrated in Table 4.16. Afterward plot the IPR curve as represented in Figure 5.16. Then, MAPE is determined for case R001 as shown in Table 4.17.

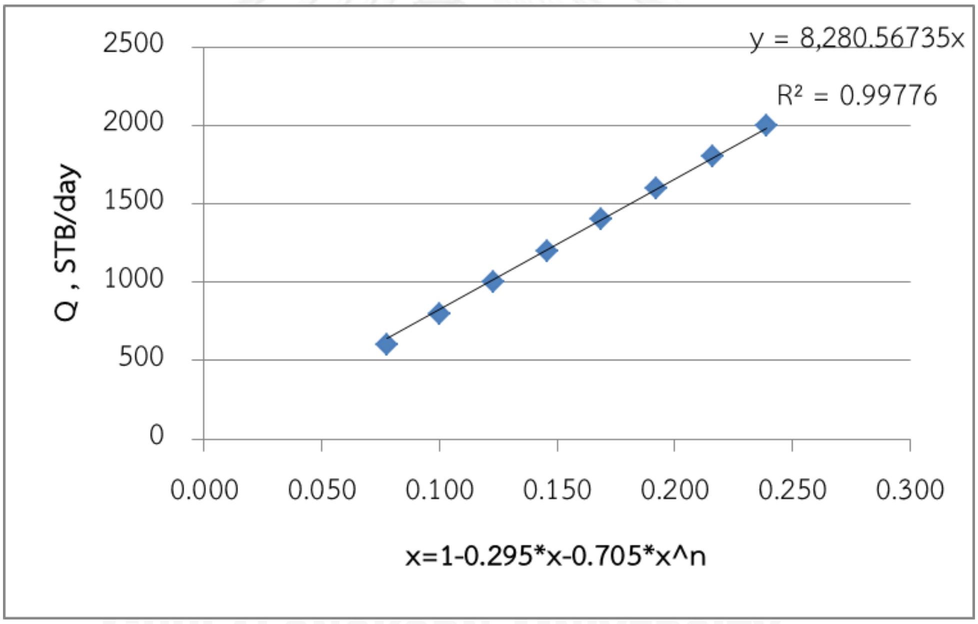

Figure 4.15 A plot to determine $(q_o)_{max}$ for Klins and Majcher's IPR (case R001)

Table 4.15 Newton-Raphson result for Klins and Majcher's IPR at q_o*=600 STB/D* (case R001)

t	$(P_{wf})_t$	$f((P_{wf})_t)$
0	1350.00000…	0.040737203…
1	1323.25682…	0.000554089…
2	1322.88292…	0.000000107…
3	1322.88285…	0.000000000…
4	1322.88285…	0.000000000…

Table 4.16 Well bottomhole flowing pressure predictions by Klins and Majcher's correlation (case R001)

Oil production rate (STB/D)	*Well bottomhole flowing pressure (psia)*
600.000	1322.883
800.000	1306.438
1000.000	1289.705
1200.000	1272.671
1400.000	1255.321
1600.000	1327.639
1800.000	1219.610
2000.000	1201.216
4968.000	866.558
8280.567	0.000

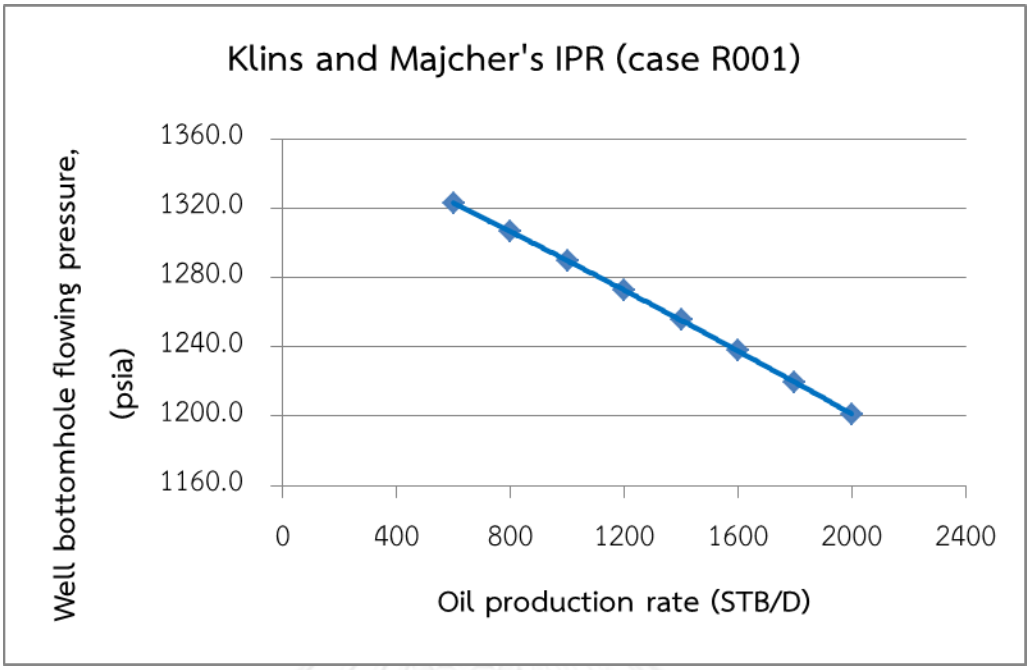

Figure 4.16 Klins and Majcher’s IPR curve (case R001)

Table 4.17 Calculation of the mean absolute percentage error of Klins and Majcher’s IPR (case R001).

q_o (STB/D)	A_t P_{wf} (ECLIPSE)	F_t P_{wf}(Klins and Majcher)	$Abs(\frac{A_t-F_t}{A_t})$	MAPE (%)
600	1319.3362	1322.883	0.00269	**0.11715**
800	1303.9633	1306.438	0.00190	
1000	1288.2430	1289.705	0.00114	
1200	1272.1156	1272.671	0.00044	
1400	1255.5183	1255.321	0.00016	
1600	1238.3712	1327.639	0.00059	
1800	1220.6233	1219.610	0.00083	
2000	1203.1838	1201.216	0.00164	

Finally repeat each step to solve for other cases and calculate the average MAPE and standard deviation for Klins and Majcher’s IPR.

4.2.5 Jones et al.'s IPR

In this correlation, IPR can be constructed similar to Vogel methodology for the first three steps. Then, a set of oil production rates corresponding to well bottomhole flowing pressures are plotted to find the two coefficients in which *A* is in the laminar flow condition and *B* is in the turbulent flow. Then, the well bottomhole flowing pressure at any given oil production rate can be calculated by the equation

$$\frac{p_r - p_{wf}}{q_o} = A + Bq_o$$

The calculated well bottomhole flowing pressures are shown in Table 4.18. Figure 4.17 displays the plot to determine coefficients *A* and *B* for case R001. The calculation yields $A=0.0819$ and $B=0.0000007$.

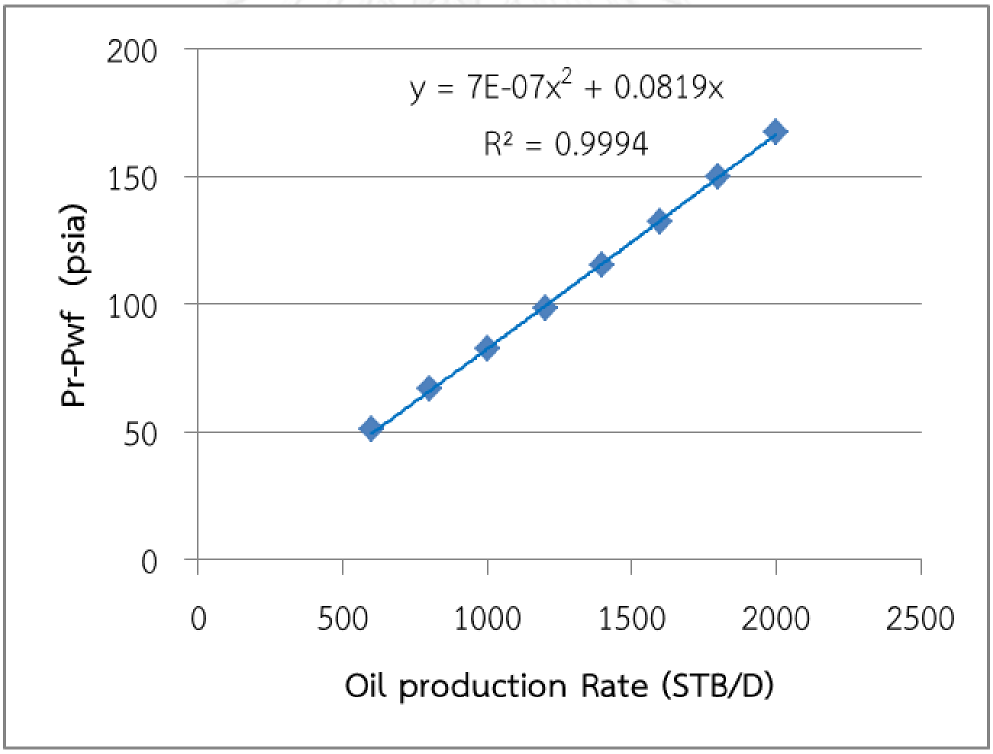

Figure 4.17 A plot to determine coefficients *A* and *B* for Jones et al.'s IPR (case R001)

Example calculation of case R001, at q_o=600 STB/D and $\overline{P}_r$*=1,370.607 psia*

Substitute the coefficients *A* and *B,* q_o=600 STB/D and $\overline{P}_r$*=1,370.607 psia* into Equation (8),

So that $$\frac{1{,}370.607\ psia - P_{wf}}{600\ STB/D} = 0.0819+0.0000007(600\ STB/D)$$

$$P_{wf}=1{,}321.215\ psia$$

Next, we repeat each step to solve for other oil production rates and then plot IPR curve as shown in Figure 4.18. After that, we average MAPE and calculate standard deviation for Jones, Blount and Glaze's IPR as illustrated in Table 4.19.

Table 4.18 Well bottomhole flowing pressure predictions by Jones et al.'s correlation (Case R001)

Oil production rate (STB/D)	*Well bottomhole flowing pressure (psia)*
600.000	1321.315
800.000	1304.639
1000.000	1288.007
1200.000	1271.319
1400.000	1254.575
1600.000	1237.775
1800.000	1220.919
2000.000	1204.007
8910.154	585.291
14850.257	0.000

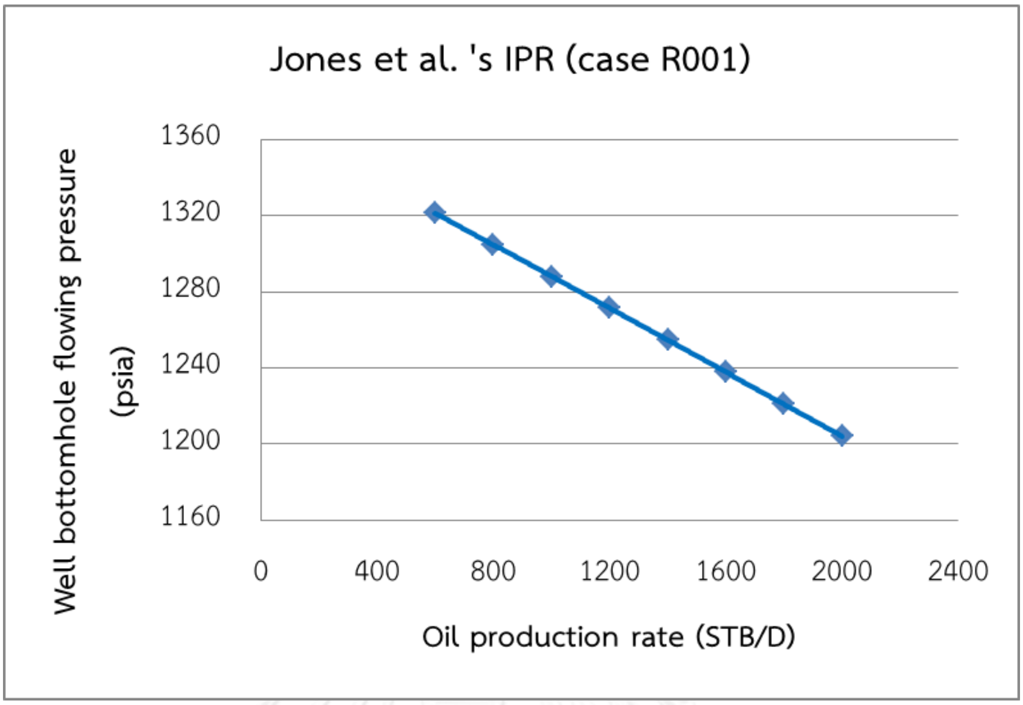

Figure 4.18 Jones et al.'s IPR curve (case R001)

Table 4.19 Calculation of the mean absolute percentage error of Jones et al.'s IPR (case R001).

q_o (STB/D)	A_t P_{wf} (ECLIPSE)	F_t P_{wf}(Jones et al.)	$Abs(\frac{A_t-F_t}{A_t})$	MAPE (%)
600	1319.3362	1321.315	0.00142	**0.06139**
800	1303.9633	1304.639	0.00052	
1000	1288.2430	1288.007	0.00018	
1200	1272.1156	1271.319	0.00063	
1400	1255.5183	1254.575	0.00075	
1600	1238.3712	1237.775	0.00048	
1800	1220.6233	1220.919	0.00024	
2000	1203.1838	1204.007	0.00068	

CHAPTER V
RESULTS AND DISCUSSIONS

In this chapter, the results of all studied about IPR correlations and their limitations are illustrated and discussed in order to evaluate the accuracy and reliability of each IPR correlations.

5.1 Evaluation of IPR correlations

In this study, 150 cases were initially generated by trial version of JMP software as discussed in Section 4.2. Eight test points for flow rate varying from 600 to 2000 STB/D were simulated for each case. However, there are 45 cases that cannot be completed by ECLIPSE100 simulation software because of non-linear equation convergence failure. As a result, only 105 cases that were successfully run from ECLIPSE100 are used to analyze for the performance of five IPR correlations. The evaluated results of five IPR correlations in term of Mean Absolute Percentage Error (MAPE) and standard deviation of MAPE are determined and analyzed. In addition, the limitation and finding from each IPR correlation will be discussed.

The result of evaluation of five correlations in term of Mean Absolute Percentage Error (MAPE) is based on eight designed test points tabulated in Table 5.1. It is important to note that Jones et al. correlation has the limitation that it does not guarantee a negative value of the coefficient *B*, the turbulent flow condition. Thus, only 56 cases can be analyzed for Jones et al. while 105 cases can be used in the other four correlations.

Table 5.1 Summary of MAPE for all cases of five IPRs.

RUN ID.	Mean Absolute Percentage Errors (%)				
	Vogel	Fetkovich	Sukarno and Wisnogroho	Klins and Majcher	Jones et al.
R001	0.074352	0.062632	0.592036	0.117145	0.061385
R002	0.164661	0.04032	0.783312	0.307753	0.061175
R003	0.073508	0.068446	0.678352	0.204653	0.077425

Table 5.1 Summary of MAPE for all cases of five IPRs (continued)

RUN ID.	Mean Absolute Percentage Errors (%)				
	Vogel	Fetkovich	Sukarno and Wisnogroho	Klins and Majcher	Jones et al.
R004	0.160638	0.038859	0.710018	0.229584	0.057188
R005	0.101523	0.05621	0.612158	0.1363	0.060367
R006	0.187143	0.040089	0.78708	0.310687	0.070926
R007	0.103282	0.056133	0.616943	0.140202	0.077774
R008	0.343752	0.011375	1.070753	0.615988	0.079102
R009	1.14296	0.220884	2.378083	2.19535	0.1118
R010	1.14296	0.220884	2.378083	2.19535	0.1118
R011	0.086183	0.063454	0.596529	0.122287	0.063958
R012	0.136235	0.03505	0.617983	0.149902	
R013	0.189102	0.031482	0.736549	0.255942	
R026	0.225544	0.049238	0.855068	0.390156	0.052696
R027	1.378214	0.465667	2.752036	2.490851	0.133417
R028	1.377789	0.634034	2.770635	2.601094	1.007595
R029	1.129377	0.444089	2.57236	2.351825	0.193665
R030	0.256544	0.067775	0.910813	0.441147	0.055363
R031	0.256544	0.677749	0.910813	0.441147	0.055363
R032	0.116731	0.043288	0.65401	0.174467	0.051723
R033	0.071298	0.562819	0.602164	0.122983	0.053142
R034	0.066731	0.05641	0.597562	0.118356	0.060873

Table 5.1 Summary of MAPE for all cases of five IPRs (continued)

RUN ID.	Mean Absolute Percentage Errors (%)				
	Vogel	Fetkovich	Sukarno and Wisnogroho	Klins and Majcher	Jones et al.
R035	0.120047	0.04555	0.653842	0.169611	0.055427
R036	0.733194	0.386471	1.754907	1.422409	0.302022
R037	2.017524	0.812618	4.114235	3.976598	0.203966
R038	1.082772	0.392511	2.50398	2.248734	0.620144
R039	1.206057	0.28741	2.578002	2.302746	0.371701
R040	0.103281	0.010125	0.634334	0.295033	0.025219
R041	0.063496	0.012473	0.527858	0.069945	
R042	0.075775	3.88583	0.555655	0.122825	
R043	0.062335	2.129307	0.527664	0.076707	
R044	0.070824	0.014796	0.559613	0.138367	
R045	0.060869	4.945416	0.55275	0.136531	0.029934
R046	0.064868	0.027637	0.511241	0.070293	
R047	0.063826	0.028044	0.509717	0.068557	
R048	0.065387	0.029032	0.511993	0.070293	
R049	0.071368	0.013524	0.552125	0.120411	
R050	0.653184	0.208845	1.688717	3.529585	0.049794
R051	0.226579	0.173075	1.53897	5.117441	0.254109
R052	0.1145	0.046252	0.788443	0.744014	0.049859
R053	0.365891	0.261761	1.370865	3.04994	0.159725

Table 5.1 Summary of MAPE for all cases of five IPRs (continued)

RUN ID.	Mean Absolute Percentage Errors (%)				
	Vogel	Fetkovich	Sukarno and Wisnogroho	Klins and Majcher	Jones et al.
R054	4.552801	2.902554	11.57443	22.01135	0.728665
R056	0.106751	0.043823	0.700386	0.571404	0.025508
R057	0.37104	0.264176	1.18231	2.099486	0.153889
R060	7.958771	5.29924	16.94128	25.35941	0.891737
R061	0.03302	0.030659	0.548304	0.191615	0.032483
R062	0.113237	0.008758	0.678842	0.431902	0.028517
R063	0.068449	0.015608	0.561675	0.147126	0.268473
R064	0.267403	0.027885	0.972573	1.223729	0.049201
R065	0.058699	3.909159	0.538529	0.10603	
R066	0.059642	0.015069	0.526067	0.007745	
R067	0.115206	0.008966	0.674853	0.41063	0.036834
R068	0.203282	0.149172	0.885818	1.375632	0.248047
R069	0.067839	0.04032	0.544921	0.109222	
R070	0.118878	0.015639	0.677272	0.409798	0.019475
R071	0.077616	0.013195	0.570535	0.155279	
R072	0.092125	0.002922	0.557432	0.121404	
R073	0.086122	0.001276	0.56048	0.139275	
R074	0.123156	0.007143	0.605246	0.199116	
R075	0.10898	0.003983	0.588878	0.178295	

Table 5.1 Summary of MAPE for all cases of five IPRs (continued)

RUN ID.	Mean Absolute Percentage Errors (%)				
	Vogel	Fetkovich	Sukarno and Wisnogroho	Klins and Majcher	Jones et al.
R076	0.112519	0.006544	0.581222	0.149461	
R077	0.403116	0.030974	0.893461	0.436942	
R078	0.163109	0.007102	0.652344	0.262218	
R079	0.165162	0.007505	0.647971	0.241767	
R080	0.158453	0.006234	0.644597	0.246683	
R081	0.146497	0.014842	0.661678	0.355752	
R082	0.166915	0.012577	0.667479	0.310278	
R083	0.155395	0.016232	0.675609	0.388401	
R084	0.46553	0.061127	1.266395	2.858732	0.067806
R085	0.15489	0.04946	0.715605	0.611576	0.016395
R086	0.052827	0.016663	0.585271	0.377566	0.026375
R087	0.024091	0.023166	0.512985	0.256657	0.020681
R088	0.146313	0.026126	0.793007	1.194138	0.045164
R089	0.128349	0.014651	0.660107	0.421196	0.028415
R090	0.0237	0.022973	0.567626	0.540264	0.123008
R091	1.77476	0.781808	3.396486	15.62505	0.205221
R110	4.199226	2.384955	5.089981	10.73884	
R113	6.538017	0.382042	6.163013	17.2623	
R114	8.611883	4.285322	9.24335	17.2623	

Table 5.1 Summary of MAPE for all cases of five IPRs (continued)

RUN ID.	Mean Absolute Percentage Errors (%)				
	Vogel	Fetkovich	Sukarno and Wisnogroho	Klins and Majcher	Jones et al.
R115	5.508132	4.638391	6.546769	16.71432	
R116	5.71709	1.519441	6.91067	20.06518	
R118	7.08146	0.680729	8.40635	14.70986	
R119	5.046005	1.836727	5.957796	10.05798	
R120	5.644991	4.539098	6.649953	14.70986	
R121	9.513165	2.139306	11.43951	15.75678	
R122	5.692993	4.720301	6.759852	10.97715	
R123	4.999288	4.725858	7.046852	20.6729	

Refer to cases that the absolute open flow cannot be determined.

Moreover, scope of study was expanded to check the accuracy and reliability of well performance prediction at 60% of maximum oil production rate (absolute open flow) which is not covered by the eight designed test points. It is important to note that the number of cases study depends on the correlation due to the fact that there are some cases that 60% of maximum oil production rate places within the range of designed test points as illustrated in Table 5.2.

Table 5.2 APE for all cases of five IPRs at 60% absolute open flow rate.

RUN ID.	Absolute Percentage Errors (%)				
	Vogel	Fetkovich	Sukarno and Wisnogroho	Klins and Majcher	Jones et al.
R001	2.632186384	0.691606684	6.276541837	3.72199	7.07696
R002	3.302786422	1.811020194	5.100196156	3.62414	0.80955
R003	2.608447918	1.622888777	4.532291095	3.10111	2.30265
R004	2.995703943	0.470436061	5.742847902	3.59668	35.31818
R005	3.058966974	0.156914390	6.757936811	3.94599	
R006	3.076110713	1.263361010	5.100234982	3.49545	2.4036
R007	3.076969073	0.273740789	6.759200799	3.99828	
R008	2.534535043	1.140035208	3.783324025	2.67531	0.56639
R009			1.660921973		0.27167
R010			12.3472265		19.69131
R011	5.755471454	3.506652213	8.385402259	5.92753	0.56383
R012	4.124851619	6.489806557	9.254832743	4.96532	
R013	3.623142945	0.797154551	6.227035316	4.08719	
R026	1.5744583	2.419024251	3.709409565	2.34791	6.78917
R027					0.69008
R028					2.7234
R029					1.23912
R030	2.705144965	2.339132577	4.459098945	3.15935	2.81768
R031	3.477941529	10.69872286	0.154389314	1.42608	31.82736

Table 5.2 APE for all cases of five IPRs at 60% absolute open flow rate (continued)

RUN ID.	Absolute Percentage Errors (%)				
	Vogel	Fetkovich	Sukarno and Wisnogroho	Klins and Majcher	Jones et al.
R032	2.940689485	9.523785759	6.225586779	3.86413	
R033	2.278435188	8.899284933	5.813120741	3.42885	8.67918
R034					
R035	2.947145409	9.769721461	6.279149474	3.87357	
R036	1.413459654		2.00046629	1.28768	0.44326
R037					0.35038
R038					3.90569
R039					0.37451
R040	3.242773153	1.345573634	4.552620009	3.53149	10.00067
R041	4.672441881		13.58638143	5.64826	
R042	3.699468841		9.082934748	4.61524	
R043	4.04721939		11.59801259	4.99179	
R044	2.337326559	0.858791016	7.572036792	3.82936	
R045	2.378135496		7.366016195	3.66225	
R046	5.445387908	23.39118643	13.53795894	5.76448	
R047	4.546395584		13.62436812	5.52647	
R048	4.185855524	9.330656724	11.93921103	5.09887	
R049	2.763797288	1.369440771	8.544533075	4.30217	
R050	5.452289545	0.428398535	2.044393999	14.84513	0.49168

Table 5.2 APE for all cases of five IPRs at 60% absolute open flow rate (continued)

RUN ID.	Absolute Percentage Errors (%)				
	Vogel	Fetkovich	Sukarno and Wisnogroho	Klins and Majcher	Jones et al.
R051					1.2837
R052	2.071982028		4.286670221	2.55099	5.1199
R053	0.732488823	0.376684142	1.7399728		1.9495
R054					
R056	2.273513221	1.522931009	4.641710818	2.84705	1.82295
R057	1.876847083	1.264237697	2.857228001		1.47555
R061	1.43413837	0.493062531	5.51646377		3.24556
R062	2.912551603	1.469040678	5.383972154	3.06462	1.23985
R063	2.028674148	0.745661326	7.22028164	3.76708	3.45896
R064	1.95205539	0.817900981	3.552235891	1.98392	0.48804
R065	3.61782765		8.972095779	4.43700	
R066	2.975562185	6.893420147	10.89646859	4.67080	
R067	2.51369172	0.98535532	5.269675533	3.14081	6.11915
R068	2.483165294	1.742463961	3.611212007	1.55617	4.44184
R069	2.716918725	15.42423974	8.857428077	4.17925	
R070	3.373436323	1.932816603	5.810392562	3.53717	1.58534
R071	3.619768446	0.7240661	7.939986836	4.12692	
R072	9.814644583	4.875805199	13.06777266	0.74505	
R073	7.001709107	2.676623678	11.05814727	5.23200	

Table 5.2 APE for all cases of five IPRs at 60% absolute open flow rate (continued)

RUN ID.	Absolute Percentage Errors (%)				
	Vogel	Fetkovich	Sukarno and Wisnogroho	Klins and Majcher	Jones et al.
R074	7.299086266	2.869364406	10.67329841	5.17869	
R075	7.093698939	2.826971153	10.64832462	5.09046	
R076	10.62935731	6.490241298	13.03034397	6.27880	
R077	5.653715704		10.55055977	3.82984	
R078	9.21439694	5.632436566	11.25920333	5.50785	
R079	9.979666848	5.404663087	11.97464513	5.89681	
R080	9.367449488	5.490856154	11.53907859	4.04132	
R081	4.544445469	1.481113314	7.825156222	4.84478	
R082	8.09459503	3.059456944	9.77424406	4.03636	
R083	4.973829351	1.991437763	7.887073028	0.80748	
R084	1.995335099	0.674142033	3.213763921		2.84115
R085	2.935706329	1.533733906	5.683546893	4.27226	19.2728
R086	5.744159977	4.610512018	8.03807481	2.70926	6.22014
R087	1.454616148	0.707108181	4.286351417	4.29401	7.69549
R088	4.74020842	2.448620192	7.726533467	1.73632	
R089	15.18908219	10.47066408	5.530021129	2.30466	35.75095
R090	0.177418619	0.291585358	3.769000173	2.75163	6.05766
R091					0.65313
R092	1.766603489	0.908591379	3.314278108		2.53437

Table 5.2 APE for all cases of five IPRs at 60% absolute open flow rate (continued)

RUN ID.	Absolute Percentage Errors (%)				
	Vogel	Fetkovich	Sukarno and Wisnogroho	Klins and Majcher	Jones et al.
R093			18.49007948	2.10369	
R094	0.883555194	1.015762335	4.150118084	1.91230	2.52474
R095	1.632142875	0.807801906	3.856678509	0.27086	4.20989
R096	1.407629897	0.557997897	2.537650269		2.85282
R097	5.012653205	1.148301693	9.329373408	5.54428	
R098	9.534998427	5.929254569	10.66088934	4.18785	
R099	4.138156413	1.176083785	8.251467743	4.70458	
R100	6.44229716	2.435830797	9.477772894	4.56988	
R101	5.002930048	1.120144366	9.214344335	4.93729	
R102	5.429268198	1.147787423	10.40611441	3.54012	
R103	4.096153794	2.673152637	6.912013596	5.33707	3.96089
R104	14.09191918	20.32812457	2.209231936	9.88486	
R105	16.24327515	14.59349299	16.48678215	10.22296	
R106	16.80273352	15.37962155	16.81611768	12.47264	
R107	7.421091131	3.04275366	2.732513452	8.60395	
R108	14.09831311		14.57955974	9.17685	
R109	15.02825737	13.3694597	15.30621409	19.51714	
R110	18.95431966	21.94775151	16.46062767		
R113	16.80911547		16.21517508		

Table 5.2 APE for all cases of five IPRs at 60% absolute open flow rate (continued)

RUN ID.	Absolute Percentage Errors (%)				
	Vogel	Fetkovich	Sukarno and Wisnogroho	Klins and Majcher	Jones et al.
R114					
R115	16.67318502	19.55071391	15.81744879		
R116	17.30097778	22.04237663			
R118	17.87176568	24.95062752	16.84938232		
R119	17.43796515	22.7307597	16.08524728		
R120	16.97447495		16.84938232		
R122	17.11513202	18.89302245	15.76800587		
R123					

Refer to cases that the bottom hole pressure has reached the lower limit of 14.7 psia

Refer to cases that 60% absolute open flow rate is below 2,000 STB/D

5.1.1 Vogel's IPR

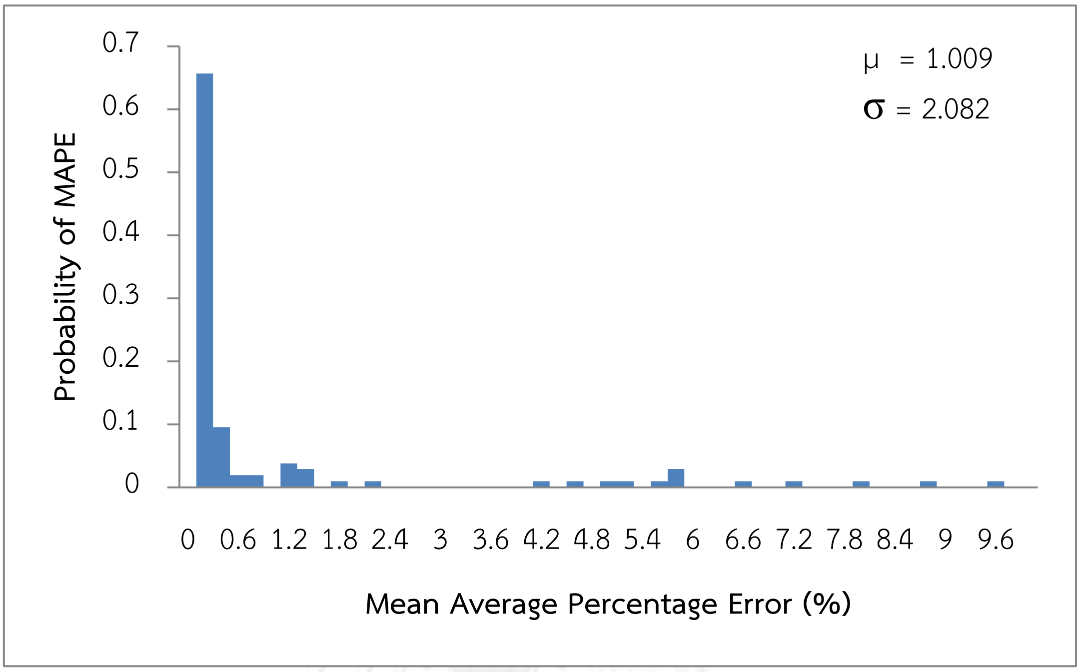

Figure 5.1 MAPE distributions for Vogel's IPR

In this study, the average MAPE of Vogel's IPR from 105 cases is 1.009 % with standard deviation of MAPE about 2.082%. Obtaining from the histogram shown in Figure 5.1, 79.048% of total cases have MAPE less than 1.0 percent.

Based on 105 cases simulation, this study has found that Vogel's IPR provides the best fit IPR when the absolute permeability is 500 mD (average MAPE=0.340%, SD=0.481%) when compared with the other two absolute permeability values (100 and 1000 mD). The average MAPE of Vogel's IPR becomes highest (1.631 %) when the absolute permeability is 1,000 mD and the value tends to be spread out with standard deviation of 2.724% as shown in Figure 5.2.

Due to ECLIPSE100 non-linear equation convergence failure, only a few cases in which the bubble point pressure is 4,712.048 psia and the absolute permeability is 1000 mD can be successfully simulated. Based on the successful cases, we found that the bubble point pressure has significant effect to the curve of IPR and the well performance prediction of Vogel's IPR correlation when the bubble point pressure is higher than 3,000 psia. When we exclude the highest bubble point pressure cases, the average MAPE is lower as the absolute permeability increases since the oil can flow better. The average MAPE becomes 0.185% with standard deviation of 0.250%

as absolute permeability is 1,000 mD. As a result, more consideration shall be taken when using Vogel's IPR correlation to predict the well inflow performance for reservoirs containing oil with bubble point pressure higher than 3,000 psia.

Further study about well inflow performance prediction found that when the prediction is made out of the test range, the accuracy and reliability decrease. In this study, the oil rate at 60% of absolute open flow is chosen for evaluation. Figure 5.3 shows that the average Absolute Percentage Error (APE) of prediction of bottomhole pressure at such rate is 5.995% with standard deviation of 5.111% in comparison with average MAPE of 1.009% and 2.082% standard deviation when the predictions are made for eight designed test points. Overall, 82.95% of total cases yield the APE less than 10.0%.

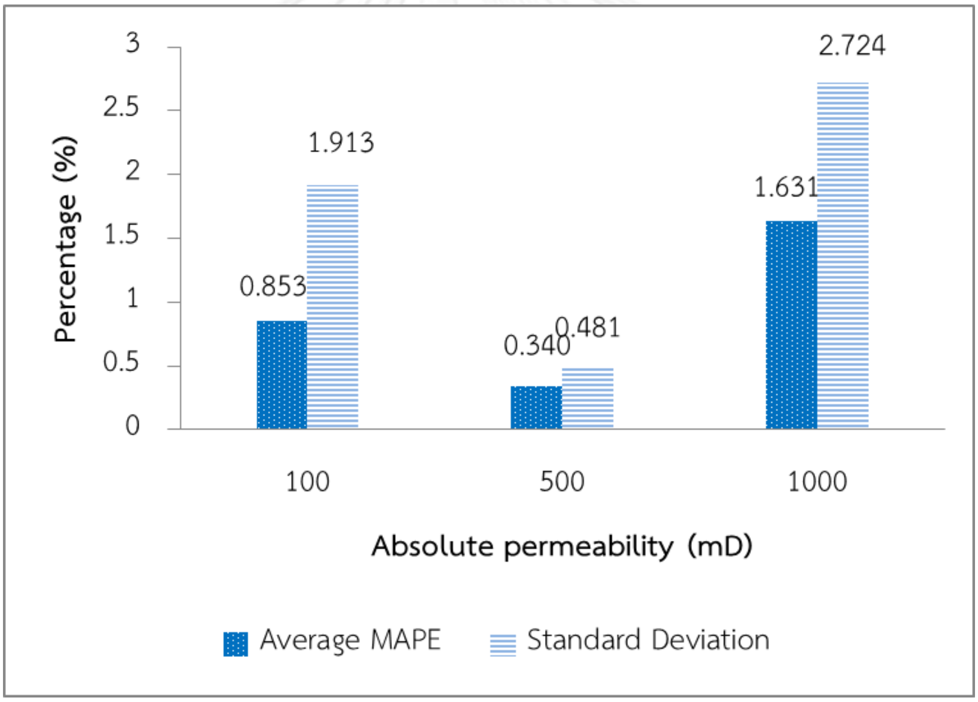

Figure 5.2 Average and standard deviation of MAPE for Vogel's IPR with absolute permeability at 100 mD, 500 mD and 1,000 mD

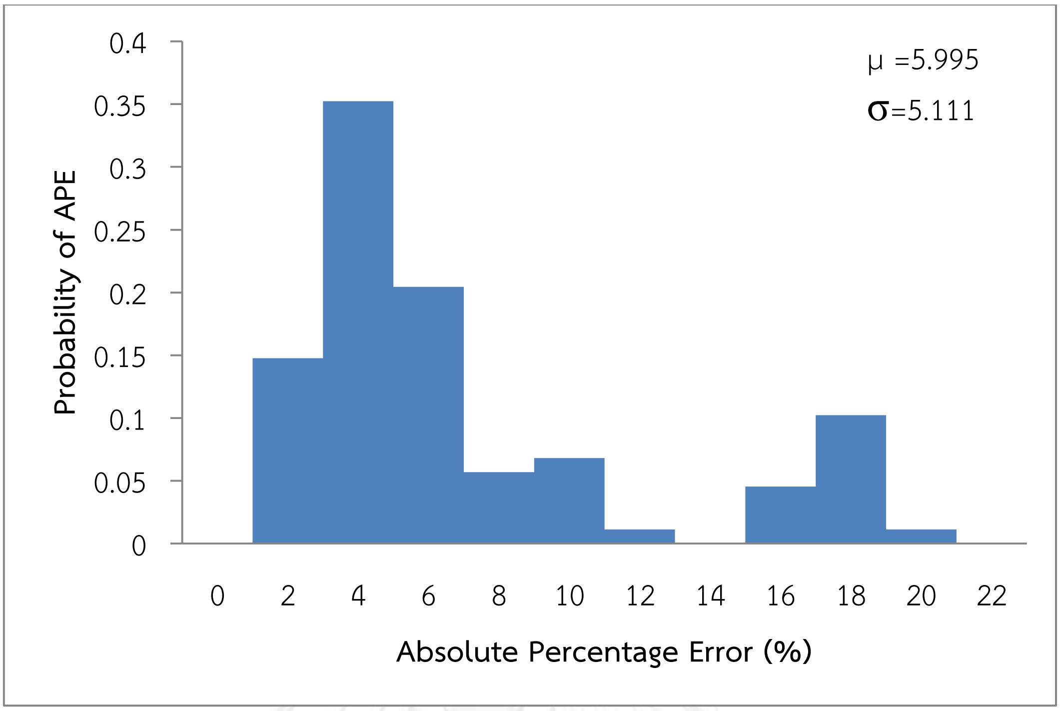

Figure 5.3 APE distributions for Vogel IPR at 60% of maximum oil production rate (absolute open flow).

5.1.2 Fetkovich's IPR

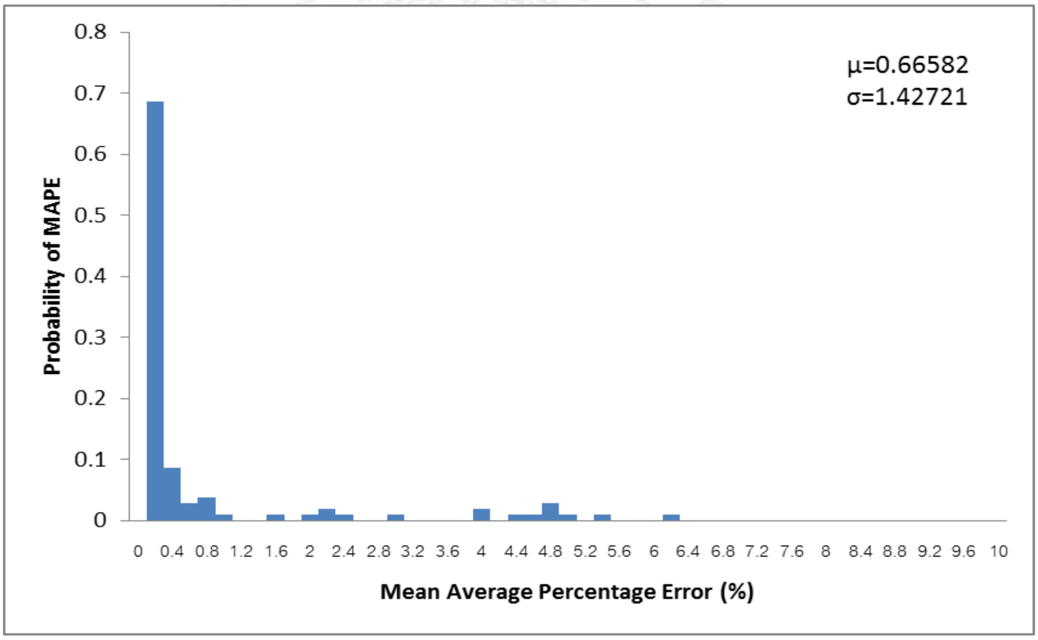

Figure 5.4 MAPE distributions for Fetkovich's IPR

Resulting from histogram (Figure 5.4), 84.762% of total cases represent MAPE less than 1.0% compared with ECLIPSE100 results. The average MAPE for reservoir with absolute permeability of 1,000 mD is the highest among the three absolute permeability values used in this study. Similar to Vogel's IPR, at absolute permeability of 500 mD, Fetkovich' IPR provides the best matching with ECLIPSE100 results with an average MAPE of 0.408% and a standard deviation of 1.149% as illustrated in Figure 5.5.

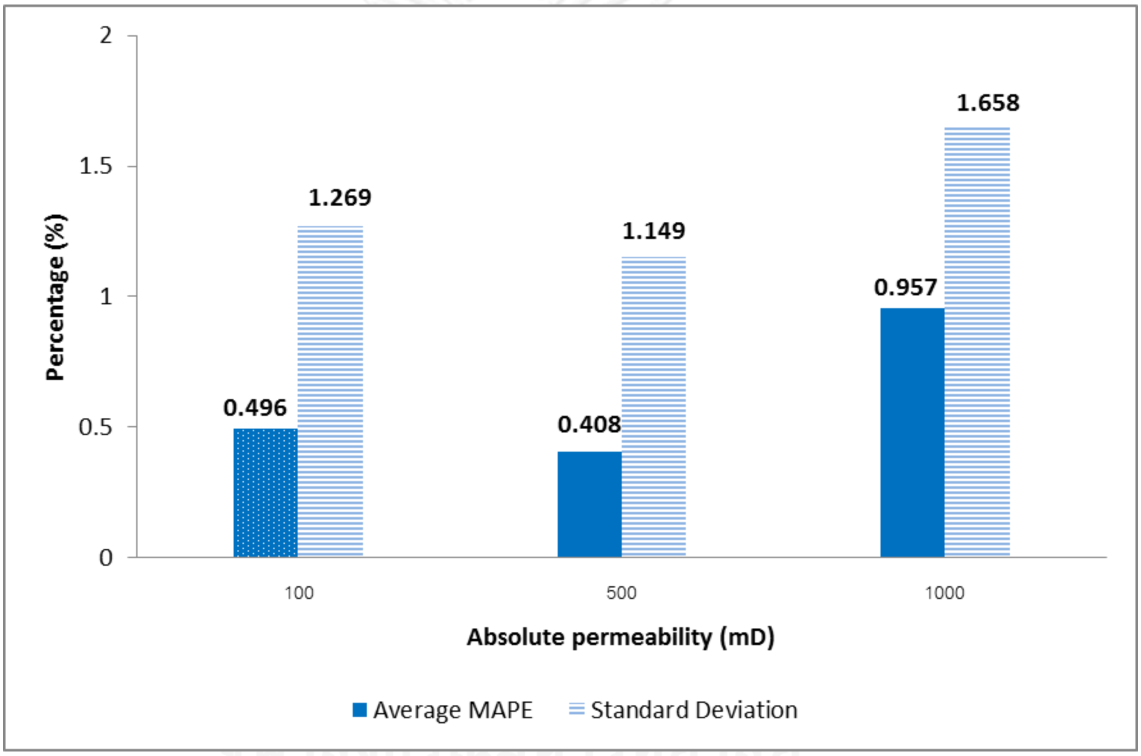

Figure 5.5 Average and standard deviation of MAPE for Fetkovich's IPR with absolute permeability at 100 mD, 500 mD and 1,000 mD

Moreover, when excluding the cases of bubble point pressure of 4,712.048 psia, the average MAPE is decreased to 0.347% with standard deviation of 1.085%. As a result, the higher the absolute permeability, the better the accuracy.

For the prediction point which is not covered by the eight designed test points, the APE is poorest than the one for the eight designed test points. Figure 5.6 represents the histogram of Fetkovich's MAPE when the oil production rate is out of range of test points. The results indicate that 80.52% of total cases give the APE less than 10.0%.

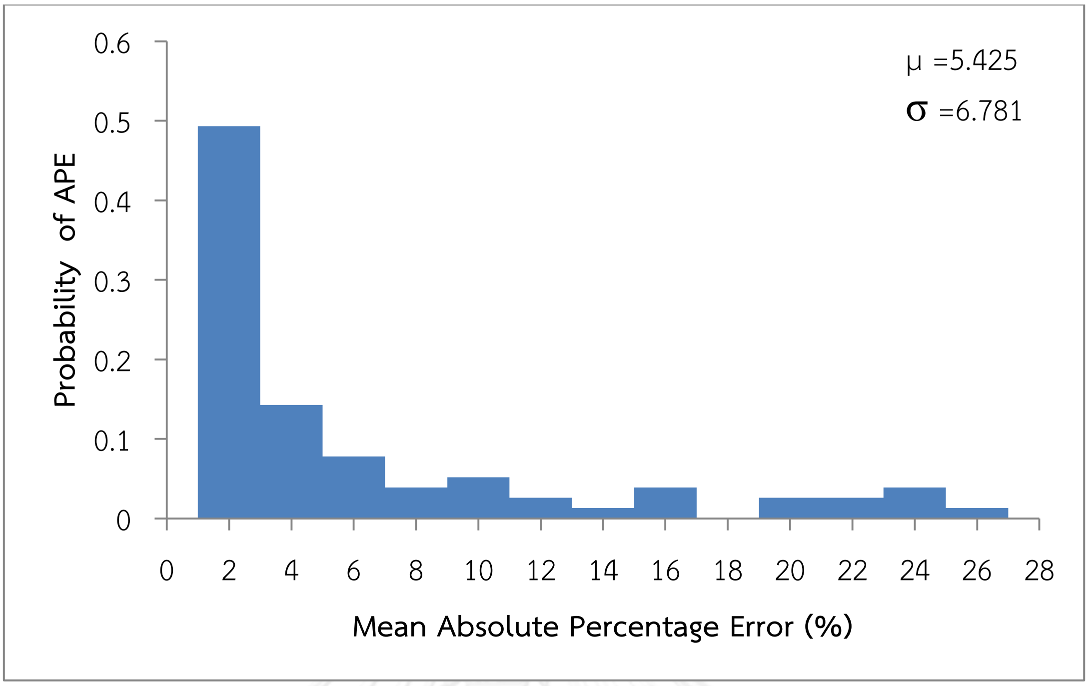

Figure 5.6 APE distributions for Fetkovich IPR at 60% of maximum oil production rate (absolute open flow)

5.1.3 Sukarno and Wisnogroho's IPR

The mean absolute percentage error proportion of Sukarno and Wisnogroho's IPR histogram is illustrated in Figure 5.7. As shown, 71.429% of total 105 cases represent MAPE ranging from 0.0 to 1.0 %. The average MAPE of Sukarno and Wisnogroho method is 1.702 % with standard deviation of 2.346%.

The prediction of well inflow performance has the smallest MAPE when the absolute permeability is 500 mD as shown in Figure 5.8. The proposed correlation by Sukarno and Wisnogroho is based on the bubble point pressure between 1,457 psia to 3,149 psia and absolute permeability between 100 mD to 625 mD. When neglecting the cases of bubble point pressure of 4,712.048 psia, the average MAPE is decreased to 0.735% with standard deviation of 0.426%. In this case, the higher the absolute permeability, the better the accuracy can be predicted by Sukarno and Wisnogroho's IPR.

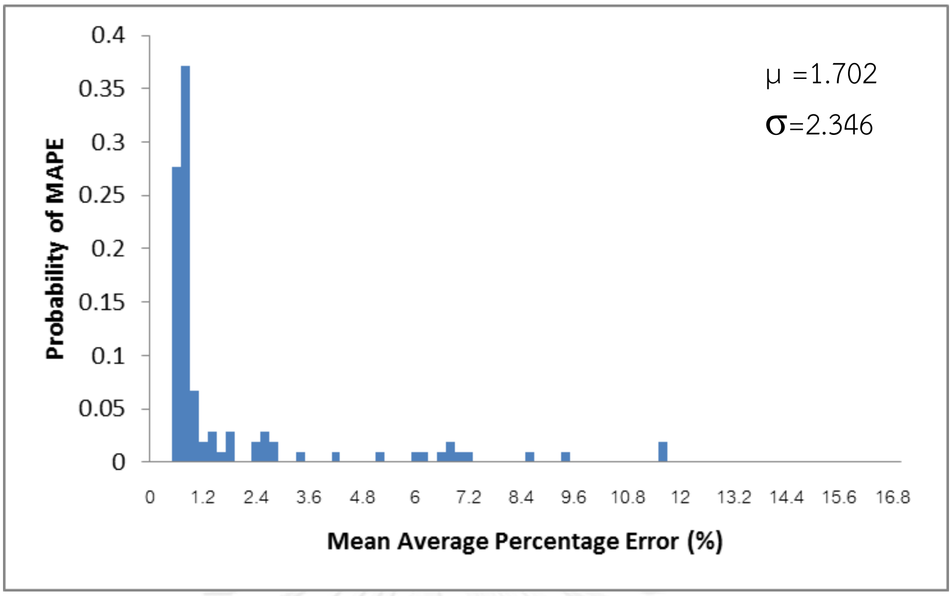

Figure 5.7 MAPE distributions for Sukarno and Wisnogroho's IPR

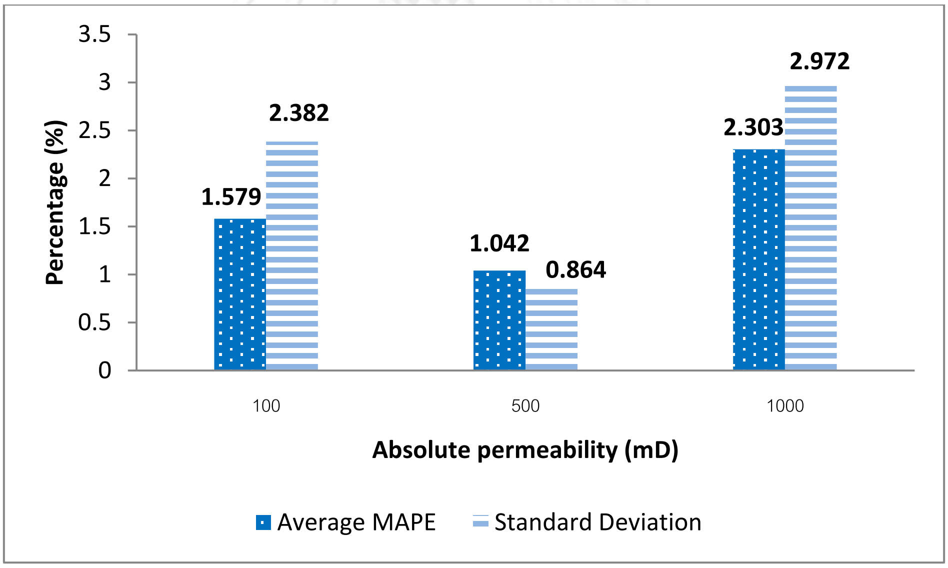

Figure 5.8 Average and standard deviation of MAPE for Sukarno and Wisnogroho's IPR with absolute permeability at 100 mD, 500 mD and 1,000 mD

In this study, when we use Sukarno and Wisnogroho's correlation to predict the well bottom-hole pressure at 60% of maximum oil rate which is not covered by the eight designed test points, 66.67% of 90 cases represent the APE less than 10.0% as shown in Figure 5.9.

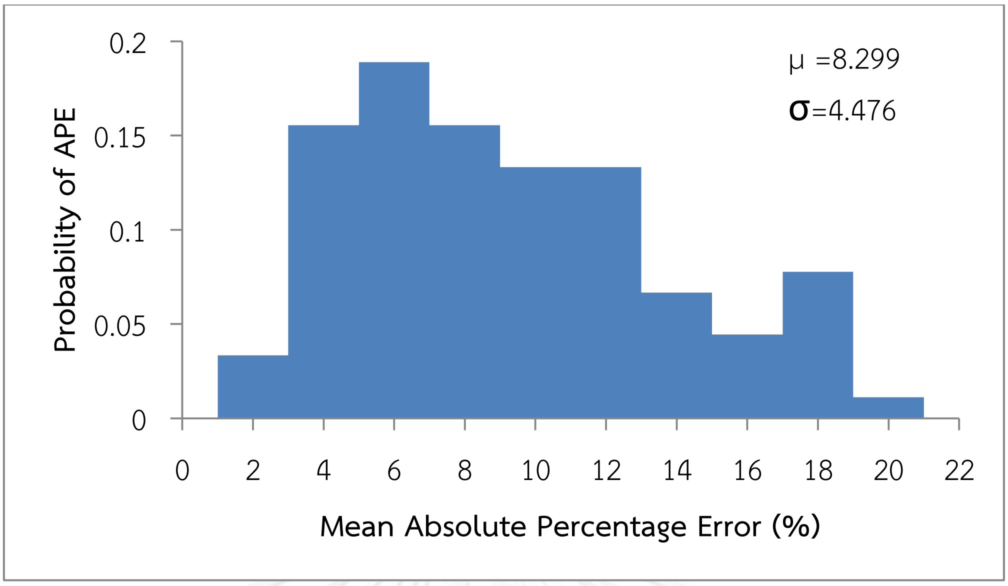

Figure 5.9 APE distribution for Sukarno and Wisnogroho's IPR at 60% of maximum oil production rate (absolute open flow)

5.1.4 Klins and Majcher's IPR

Figure 5.10 shows the distribution of mean absolute percentage error of Klins and Marcher's IPR. As displayed in the histogram, 67.619% of total cases have the MAPE less than 1.0% which is the lowest probability compared with other correlations. The average mean absolute percentage error is 2.849%, and the standard deviation is 5.708%.

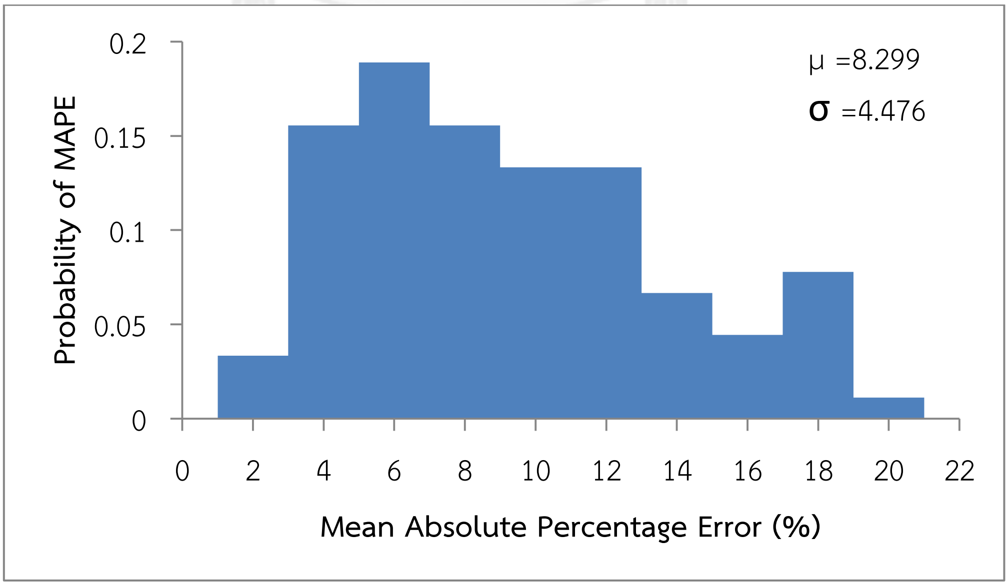

Figure 5.10 MAPE distributions for Klins and Majcher's IPR

When grouping the results based on absolute permeability, the best number of MAPE is 0.718% belonging to the representative group of 500 mD. Alike other correlations, cases of bubble point pressure of 4712.048 psia with absolute permeability of 1,000 mD have more error for erroneous of well performance prediction. As a result, MAPE and standard deviation of 1,000 mD cases are high as shown in Figure 5.11.

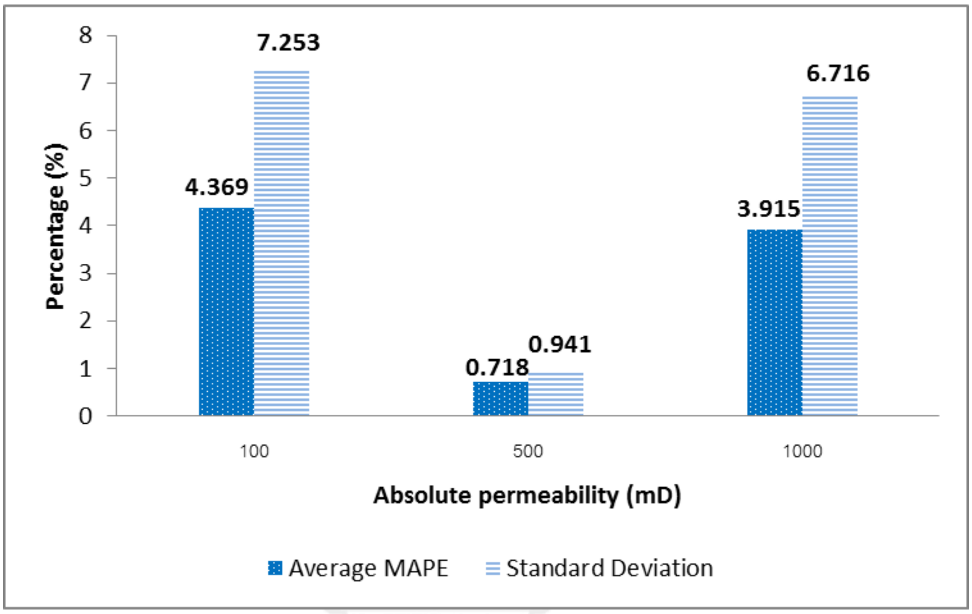

Figure 5.11 Average and standard deviation of MAPE for Klins and Majcher's IPR with absolute permeability at 100 mD, 500 mD and 1,000 mD

In fact, Klins and Majcher obtained the equation from bubble point pressure ranging between 1,000 psia to 4,000 psia. Neglecting cases with bubble point pressure of 4,712.048 psia, the value of average MAPE and standard deviation when absolute permeability is 1,000 mD becomes 0.319% and 0.484, respectively.

As shown in Figure 5.12, the prediction of well inflow performance at 60% of maximum flow rate which is not covered by the eight designed test points provides very good prediction. 94.74% of the cases have APE lower than 10.0%.

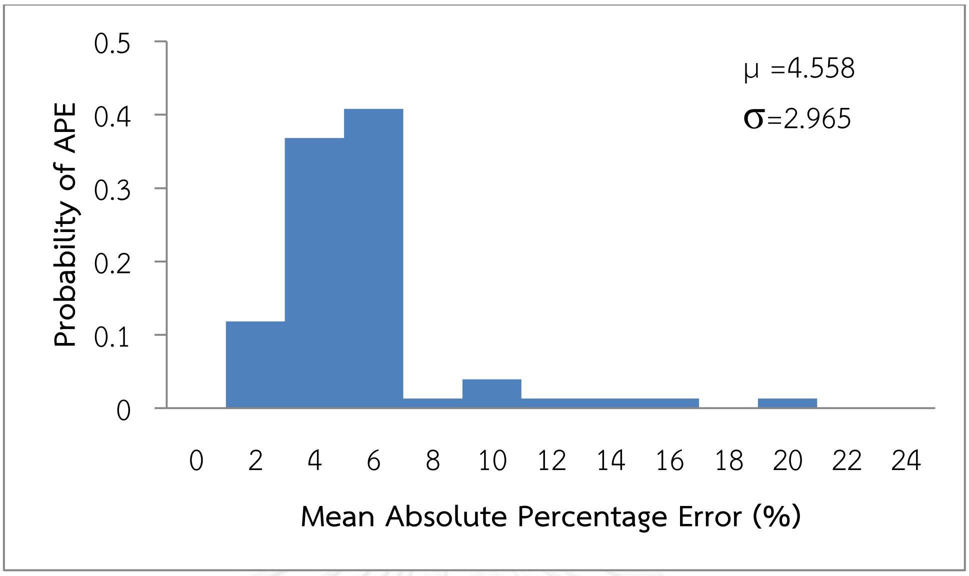

Figure 5.12 APE distributions for Klins and Majcher's IPR at 60% of maximum oil production rate (absolute open flow)

5.3.5 Jones et al.'s IPR

For Jones et al.'s IPR, we have found that it does not guarantee a negative value of the coefficient B, the turbulent flow condition. Thus, only 56 cases can be analyzed for Jones et al. From histogram (Figure 5.13), 100.00% of total cases provides MAPE less than 1%.

In addition, when the absolute permeability is higher, the better well inflow performance can be predicted as illustrated in Figure 5.14. Moreover, when the prediction is evaluated for the point which is not covered by the eight designed test points, the correlation still provides good accuracy as 86.96% of total cases have APE less than 10.0% as displayed in Figure 5.15.

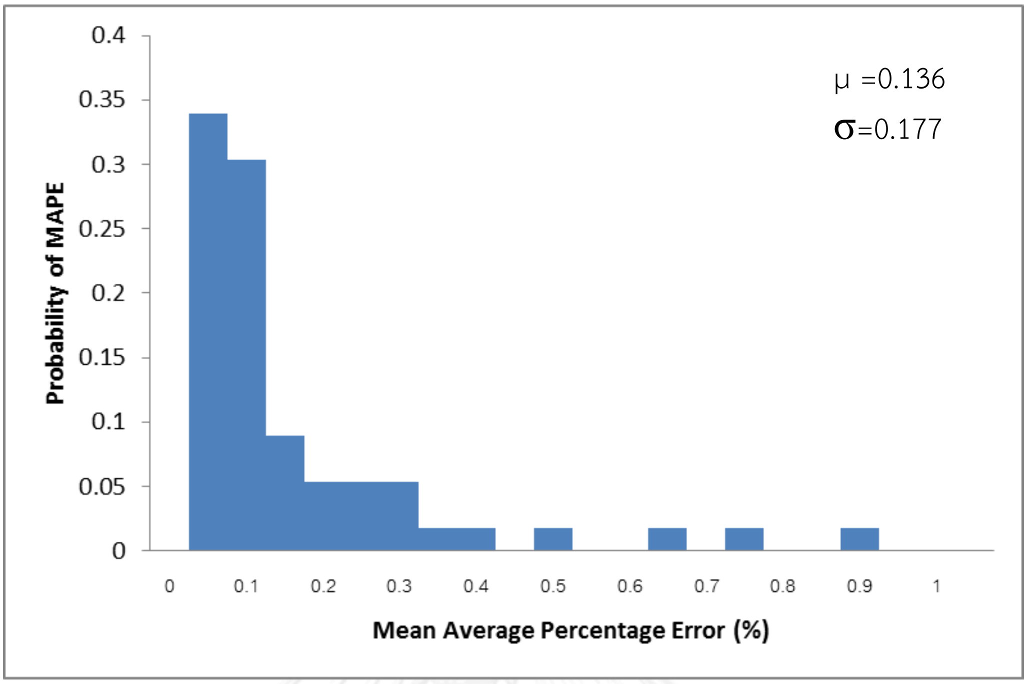

Figure 5.13 MAPE distributions for Jones et al.'s IPR

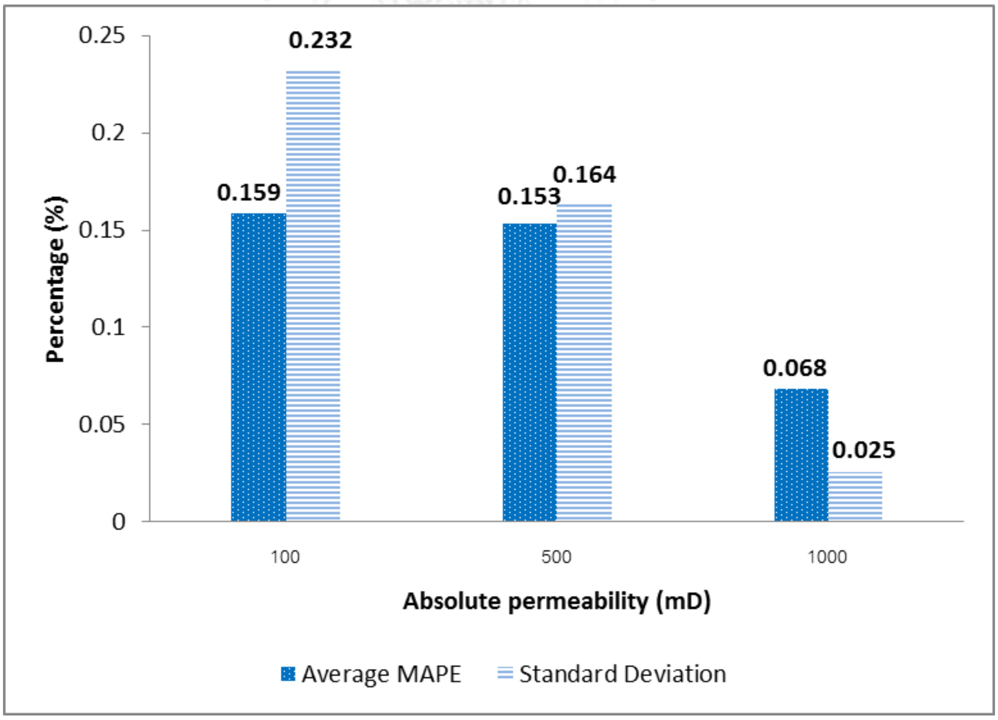

Figure 5.14 Average and standard deviation of MAPE for Jones et al.'s IPR with absolute permeability at 100 mD, 500 mD and 1,000 mD

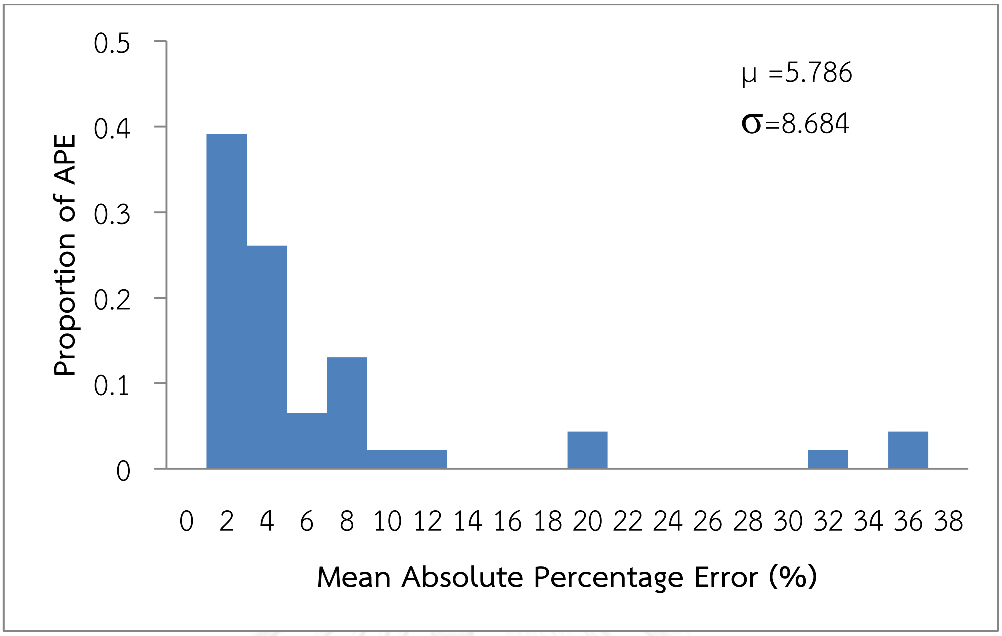

Figure 5.15 APE distributions for Jones et al.'s IPR at 60% of maximum oil production rate (absolute open flow)

5.2 Performance comparison of five IPR correlations

In this thesis, the accuracy and reliability of each IPR corrections are evaluation by comparing the between the simulated pressures (ECLIPSE100) and the calculated pressures for the five correlations. The study focuses on the accurate prediction of the eight designed test points and at a 60% maximum oil production rate which is not covered by the eight designed test points in an average for various reservoir conditions. The result of this study will help petroleum engineers to be able to choses appropriate IPR correlation to predict the well inflow performance at the starting point when there is insufficient well data.

This paper also studies the influence of absolute permeability to the accuracy of well inflow performance prediction of five correlations.

5.2.1 Overall comparison

The average and standard deviation of Mean Absolute Percentage Error (MAPE) between the simulated pressures (ECLIPSE100) and the calculated pressures for the five correlations are represented in Table 5.3. When considering only 56 cases that can be evaluated using five correlations, Jones *et. al.* gives the lowest average MAPE and standard deviation of 0.136% and 0.177%, respectively. Fetkovich is the second best while Vogel, Sukarno and Wisnogroho, and Klins and Majcher follow in less accurate order.

However, when considering 105 cases, 0.666% average MAPE and 1.427% standard deviation of Fetkovich correlation tends to do a better job of predicting well performance when compared with other IPR correlations excluding Jones *et. al.* As a matter of fact, the average MAPE of Fetkovich correlation is almost 1.5 times that of Vogel's method. Similar to the analysis for 56 cases, Fetkovich, Vogel, Sukarno and Wisnogroho, and Klins and Majcher provide the same trend from good to poor accuracy and reliability in that order. Overall, Vogel, Sukarno and Wisnogroho and Klins and Majcher provide average MAPE below 3% in the cases examined.

Table 5.4 shows that Klins and Majcher correlation provides the best prediction of well inflow performance when the evaluation point is at 60% of maximum oil production rate. While Fetkovich, Jones et al., Vogel, and Sukarno and Wisnogroho correlations provide the Absolute Percentage Error (APE) and standard deviation of APE in the range of 5.5% to 8.3% and 4.4% to 8.6%, respectively.

Table 5.3 Summary performance prediction on eight designed test points.

	Vogel		Fetkovich		Sukarno and Wisnogroho		Klins and Majcher		Jones et al.	
	Number of Cases Study									
	105	56	105	56	105	56	105	56	105	56
Average MAPE (%)	1.009	0.584	0.666	0.383	1.847	1.346	2.849	2.189	-	0.136
STD	2.082	1.243	1.427	1.013	2.777	1.618	5.708	4.761	-	0.177

Table 5.4 Summary of performance prediction at 60% absolute open flow rate

	Vogel	Fetkovich	Sukarno and Wisnogroho	Klins and Majcher	Jones et al.
	Number of Cases Study				
	88	76	90	76	46
Average APE (%)	5.995	5.425	8.299	4.558	5.786
STD	5.111	6.781	4.476	2.965	8.684

5.2.2 Comparison based absolute permeability

In this thesis, the cases studied include variation in absolute permeability in addition to other fluid and rock properties as discussed in Chapter IV. The permeability is categorized as low, medium, and high permeability which are 100 mD, 500 mD and 1,000 mD, respectively.

Considering low permeability condition of 100 mD, there are a total of 21 cases. Jones et al. provides the best fit to ECLIPSE100 result with 0.159% average MAPE and standard deviation of 0.232%. The second best is Fetkovich correlation with average MAPE of 0.496% while Vogel, Sukarno and Wisnogroho, and Klins and Majcher correlations are in less accurate as illustrated in Figure 5.16.

When the absolute permeability increases to 500 mD, Jones et al. still gives the best well inflow performance prediction with the average MAPE of 0.159% based on 22 cases in total. For the other four correlations, the total number of cases is 38. As mentioned before, we cannot find Jones et al.'s IPR for all cases as the coefficient B is nonnegative. Comparing among the four correlations, Figure 5.17 shows that Vogel's IPR correlation yields the most accurate and prediction with 0.34% MAPE and 0.481% standard deviation. Fetkovich, Klins and Majcher, and Sukarno and Wisnogroho provide less accurate well performance prediction as shown in Figure 5.17.

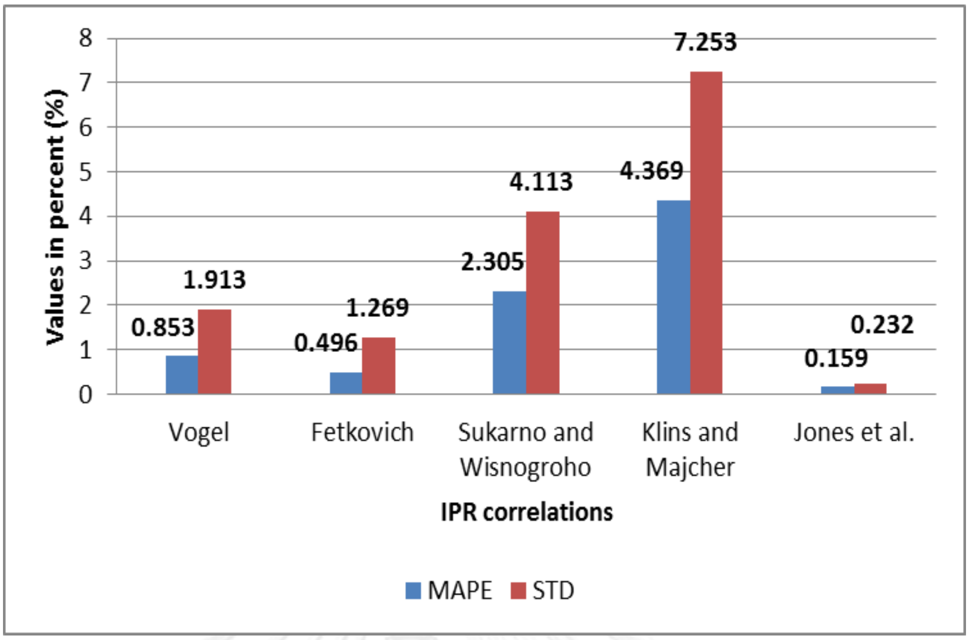

Figure 5.16 Average and standard deviation of MAPE for five's IPR with absolute permeability at 100 mD.

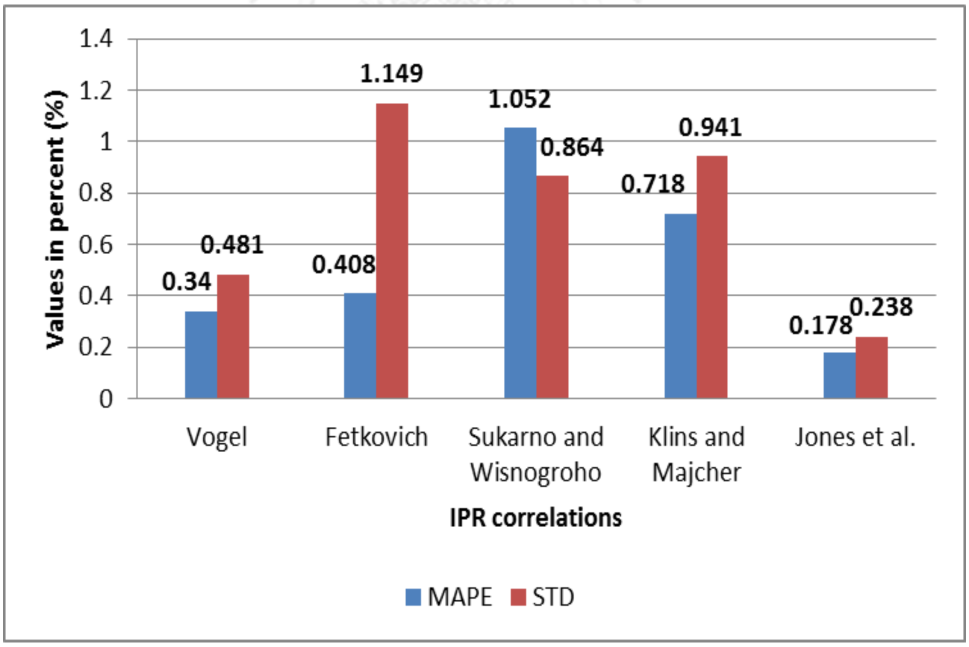

Figure 5.17 Average and standard deviation of MAPE for five's IPR with absolute permeability at 500 mD.

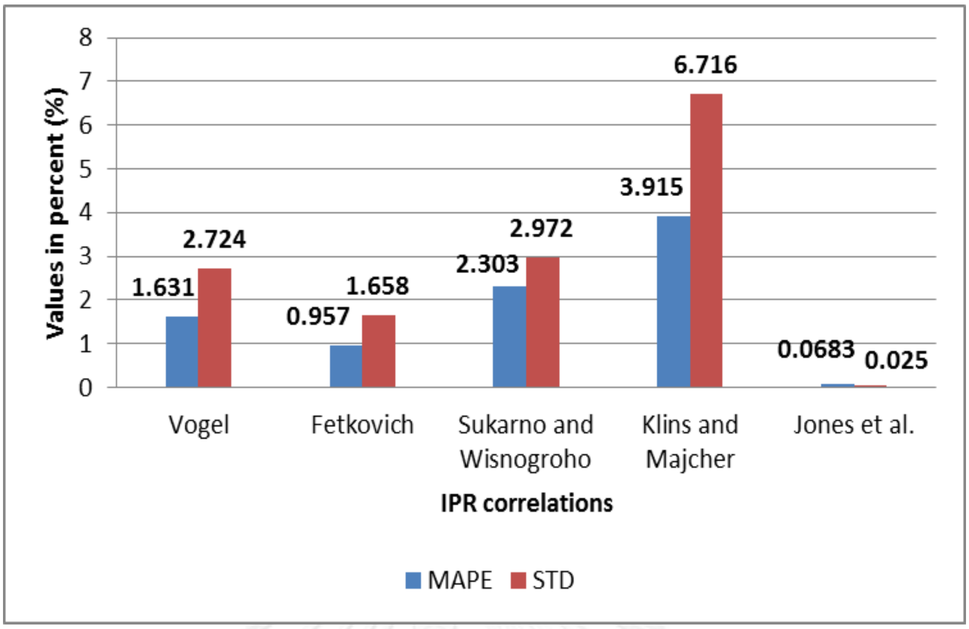

Figure 5.18 Average and standard deviation of MAPE for five's IPR with absolute permeability at 1000 mD.

As the absolute permeability is increased to 1,000 mD, there is significant impact to the well inflow performance prediction. From Figure 5.18, although Jones et al. provides the least MAPE and standard deviation of MAPE but these values from 13 cases while average and standard deviation of MAPE for other correlations come from 46 cases. It is important to note that Klins and Majcher correlation provides the least accurate when the absolute permeability is equal to 1,000 mD. Fetkovich gives the best prediction and yields average MAPE of 0.957% with standard deviation of 1.658%.

When neglecting the cases with bubble point pressure equal to 4,712 psia, 11 cases of high absolute permeability are excluded. Table 5.5 shows that the four correlations which are Vogel, Fetkovich, Sukarno and Wisnogroho, and Klins and Majcher correlations have a significant improvement of well inflow performance prediction. Comparing to previous analysis of 46 cases, Klins and Majcher correlation provides the best improvement at about 8.8 times less for average MAPE and 13.8 times less for standard deviation. Vogel correlation is the second in term of improvement of well inflow prediction while Fetkovich and Sukarno and Wisnogroho and also significantly improved.

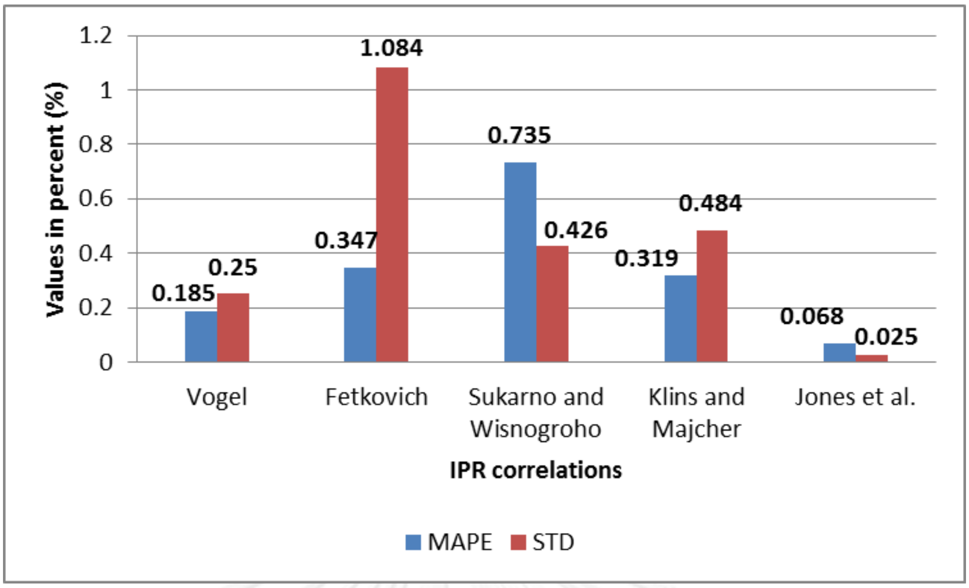

Figure 5.19 Average and standard deviation of MAPE for five's IPR with absolute permeability at 1000 mD when excluding cases with the bubble point pressure of 4,712 psia.

Table 5.5 Comparison of performance prediction for high absolute permeability.

	All cases of 1,000 mD		Neglecting the cases with Pb of 4,712 psia	
	46 cases		35 cases	
IPR correlations	MAPE %	STD %	MAPE %	STD %
Vogel	1.631	2.724	0.1854	0.25
Fetkovich	0.957	1.658	0.347	1.084
Sukarno and Wisnogroho	2.303	2.972	0.735	0.426
Klins and Majcher	3.915	6.716	0.319	0.484
Jones et al.	0.0683	0.025	0.068	0.025

In addition to MAPE analysis for eight designed test points, we evaluate the absolute percentage error (APE) at a flow rate that is 60% of absolute open flow. Considering low permeability condition of 100 mD, Jones et al. provides the least fit to ECLIPSE100 result with 6.045% average APE and standard deviation of 8.830% while Fetkovich correlation gives the best fit with average APE of 1.841% and standard deviation of 2.625%. The second best is Vogel, followed by Klins and Majcher and Sukarno and Wisnogroho correlations in less accurate order as illustrated in Table 5.6.

Table 5.6 Comparison of performance prediction for low absolute permeability (60% absolute open flow rate)

IPR correlations	Average APE (%)	STD (%)	Number of cases Studied (Cases)
Vogel	3.146	3.599	16
Fetkovich	1.841	2.625	15
Sukarno and Wisnogroho	5.069	3.873	17
Klins and Majcher	3.549	3.716	12
Jones et al.	6.045	8.830	17

When the absolute permeability increases to 500 mD, Jones et al correlation gives the best well inflow performance prediction with the average APE of 4.441% based on 19 cases in total. Although it gives the best average APE, this correlation gives the highest standard deviation of 7.041%. For the other four correlations, the total number of cases is quite similar. As mentioned before, we cannot find Jones et al.'s IPR for all cases as the coefficient *B* is nonnegative. Comparing among the four correlations except Jones et al., Table 5.7 shows that Klins and Majcher's IPR correlation yields the most accurate prediction with 5.074% APE and 3.853% standard deviation. Vogel, Fetkovich, and Sukarno and Wisnogroho provide less accurate well performance prediction as shown in Table 5.7.

Table 5.7 Comparison of performance prediction for medium absolute permeability (60% absolute open flow rate)

IPR correlations	Average APE (%)	STD (%)	Number of cases Studied (Cases)
Vogel	5.494	4.7115	31
Fetkovich	5.615	5.805	28
Sukarno and Wisnogroho	7.550	4.224	31
Klins and Majcher	5.074	3.853	31
Jones et al.	4.441	7.041	19

As the absolute permeability is increased to 1,000 mD, there is significant impact to the well inflow performance prediction. From Table 5.8, it is important to note that Klins and Majcher correlation is the most accurate when the absolute permeability is equal to 1,000 mD. Fetkovich gives the second best prediction and yields average APE of 6.892% with standard deviation of 8.249%. Sukarno and Wisnogroho correlation provides the least accurate when the absolute permeability is equal to 1,000 mD. In fact, all correlations except Klins and Majcher tend to provide less accurate when the absolute permeability is 1,000 mD compared to those when the absolute permeability is 500 mD.

Table 5.8 Comparison of performance prediction for high absolute permeability (60% absolute open flow rate)

IPR correlations	Average APE (%)	STD (%)	Number of cases Studied (Cases)
Vogel	7.486	5.44	41
Fetkovich	6.892	8.249	33
Sukarno and Wisnogroho	10.159	4.035	41
Klins and Majcher	4.439	1.139	33
Jones et al.	7.900	11.418	10

When neglecting the cases with bubble point pressure equal to 4,712 psia, the numbers of cases of high absolute permeability are not the same. Table 5.9 shows that three correlations which are Vogel, Fetkovich, and Sukarno and Wisnogroho correlations have a significant improvement of well inflow performance prediction. Comparing to previous analysis of non-neglecting cases, Fetkovich correlation provides the best improvement at about 1.9 times less for average APE and 1.8 times less for standard deviation. Sukarno and Wisnogroho correlation is the second in term of improvement of well inflow prediction while Vogel is about 47% improved. In addition, Klins and Majcher and Jones et al. provide the same values compared as the number of cases are the same.

Table 5.9 Comparison of performance prediction for high absolute permeability when neglecting the cases with Pb of 4,712.048 psia (60% absolute open flow rate)

	All cases of 1000 mD			Neglecting the cases with Pb of 4,712 psia		
IPR correlations	Average APE (%)	STD (%)	Number of cases	Average APE (%)	STD (%)	Number of cases
Vogel	7.486	5.44	41	5.084	2.529	33
Fetkovich	6.892	8.249	33	3.604	4.593	27
Sukarno and Wisnogroho	10.159	4.035	41	8.932	3.210	35
Klins and Majcher	4.439	1.139	33	4.439	1.139	33
Jones et al.	7.900	11.418	10	7.900	11.418	10

CHAPTER VI
CONCLUSIONS AND RECCOMENDATIONS

In this chapter, effect of the well inflow performance prediction for five IPR correlations and result obtained from each correlation comparison with ECLIPSE100 are concluded. Some comments and recommendations which might be benefit for future are also presented.

6.1 Conclusions

The statistical analysis on the accuracy of the well inflow performance prediction based eight designed test points show that Jones et al.'s IPR yields the highest proportion of cases that provide the Mean Absolute Percentage Error lower than 1.0%. This is followed by Fetkovich's IPR (84.76%), Vogel's IPR (79.05%), Sukarno and Wisnogroho's IPR (71.43%) and Klins and Majcher's IPR (67.62%), respectively as shown in Figure 6.1. At 60% of absolute open flow rate, Klins and Majcher's IPR gives the best fit to ECLIPSE100 results as 94.74% of total cases yield the MAPE less than 10% while Jones et al.'s IPR (86.96%) is the second best. This is followed by Vogel's IPR (82.95%), Fetkovich's IPR (80.52%) , and Sukarno and Wisnogroho's IPR which provides the poorest value of Absolute Percentage Error of 66.67% as illustrated in Figure 6.2.

However, the primary concern is the reliability evaluation of the IPR because this study result is based on cases generated by JMP Software for modeling in ECLIPSE100 simulation. In addition, the non-linear convergence error for some cases reduces the number of cases for the highest bubble point pressure at 4,712.048 psia. When excluding cases with bubble point pressure of 4712.048 psia, the most important information emerges from the analysis is that the average of mean absolute percentage error becomes smaller in the highest permeability reservoir (1000 mD). All the methods show a similar decrease in average MAPE when the absolute permeability becomes higher.

From this study, there is no single correlation which is the most suitable for every test. It has been investigated that in one particular case, one IPR correlation will provide the most accurate prediction while it may provide a poor estimate in the next case. From this observation, consideration should be given to use more than one correlation in order to predict of well inflow performance in order to gain a wide range of possible conclusions. The empirical IPR curves are dynamic curves which change with pressure-rate. Therefore, different IPR curves may be used for different pressure-rate conditions.

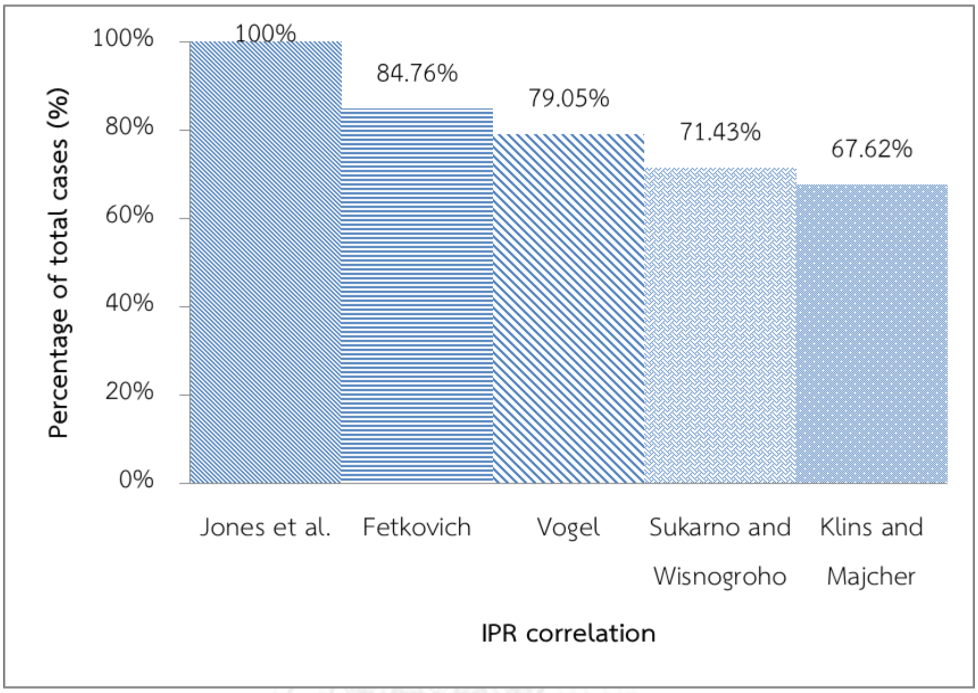

Figure 6.1 Probability for 5 IPRs of design test points yield MAPE less than 1.0 %

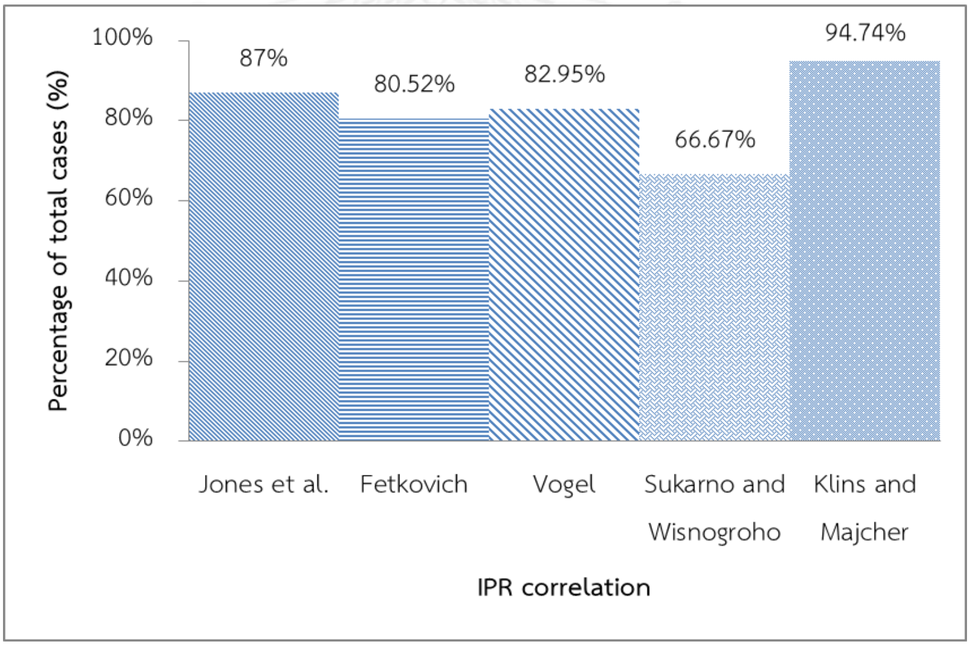

Figure 6.2 Probability for 5 IPRs as 60% of absolute open flow rate yield APE less than 10.0 %

6.2 Recommendations

1. Based on the well inflow performance evaluation method in this study and ECLIPSE100 result analysis, Jones et al. and Fetkovich method tend to be the most reliable. It has been shown that the average MAPE of these methods are less than those for others. Also, both methods provide consistent performance prediction for the entire range of interest.
2. As there is no single correlation that provides the most accurate prediction for every reservoir, evaluation should be performed using multiple correlations to estimate well inflow performance to get a rage of predicted values rather than a single value.
3. Using *Jones et. al.* correlation may cause a problem in finding the absolute open flow since this correlation does not guarantee the negative value of turbulent flow coefficient *B*.
4. Based on study result, at bubble point pressure of 4,712.048 psia, the MAPE and standard deviation are significantly higher (10 to 33 times) from the cases of 3,534 psia. Therefore, more consideration should be taken when the reservoir has the bubble point pressure above 3,534 psia for all correlation.
5. The oil production rate selection for well inflow performance testing is a significant parameter associated to the accuracy of IPR correlations. It is suggested that selected test data should be as close as operating conditions.
6. A single point at 60% of maximum oil production rate (absolute open flow) which is located beyond the range of eight designed testing points is selected for evaluation of the empirical IPRs in this study. Evaluation of multipoints where located beyond tested points should be investigated to gain more cases for assessment.

REFERENCES

[1] Vogel, J.V. Inflow Performance Relationships for Solution-Gas Drive Wells. Journal of Petroleum Technology, January 1968.

[2] Fetkovich, M.J. The Isochronal Testing of Oil Wells. Paper SPE 4529 presented at SPE Annual Fall Meeting, Las Vegas, Nevada, 30 September–3 October 1973.

[3] Ahmed T. and McKinney P. D. Advanced Reservoir Engineering. Elsevier Inc. 2005, pp 5/342-5/350.

[4] Jones, L.G., Blount, E.M., and Glaze, O.H. Use of Short Term Multiple Rate Flow Tests to Predict Performance of Wells Having Turbulence. Paper SPE 6133 presented at SPE Annual Technical Conference and Exhibition, New Orleans, 3–6 October 1976.

[5] Klins, M.A. and Majcher, M.W. Inflow Performance Relationships for Damaged or Improved Wells Producing Under Solution-Gas Drive. Journal of Petroleum Technology, December 1992.

[6] Sukarno, P. and Wisnogroho, A. Generalized Two-Phase IPR Curve Equation Under Influence of Non-linear Flow Efficiency, *Proc.*, Soc. of Indonesian Petroleum Engineers Production Optimization Intl. Symposium, Bandung, Indonesia, 1995.

[7] Beggs H. D. Production Optimization Using Nodal Analysis. OGCI and Petroskills Publication, Tulsa, Oklahoma, 2003.

[8] Somabutr S. Empirical Correlation for Future IPR Curves for Solution-Gas Drive Reservoir. Master thesis, Chulalongkorn University, Thailand, 2005.

APPENDIX

APPENDIX

Reservoir model

A reservoir model is constructed using ECLIPSE100 reservoir simulator. The model used in this study is the homogeneous rectangular reservoir. The block centered geometry type consists of Cartesian grid of 25 x 25 x 5 cells, each cell having dimension of 150 ft. x 150 ft. x 20 ft. in the x-, y- and z- directions. The following required data are input in each section of the program.

1. Case Definition

Simulator	Black oil
Model dimension	Number of cells in the x-direction 25
	Number of cells in the y-direction 25
	Number of cells in the z-direction 5
Grid type	Cartesian
Geometry type	Corner Point
Oil-Gas-Water options	Oil and dissolved gas
Solution type	Fully Implicit

2. Reservoir properties

<u>Gird</u>

Active Grid Block	X (1-25) = 1
	Y (1-25) = 1
	Z (1-5) = 1
X Permeability	100 md (case R001)
Y Permeability	100 md (case R001)
Z Permeability	100 md (case R001)
Porosity	0.18
Grid block sizes	3750 ft. x 3750 ft. x 100 ft.

3. PVT

Fluid density at surface condition	Oil density	57.11876	lb/cu.ft
	Water density	62.42803	lb/cu.ft
	Gas density	0.05306378	lb/cu.ft
Water PVT properties	Reference pressure (Pref)	4000	psia
	Water FVF at Pref	1.021734	rb/stb
	Water compressibility	3.098498E-6	/psi
	Water viscosity at Pref	0.3013227	cp
	Water viscosibility	3.387726E-6	/psi
Rock properties	Reference pressure	4000	psia
	Rock compressibility	1.942842E-6	psi-1

Live oil PVT properties (dissolved gas)

Rs (Mscf /stb)	Pbub (psia)	FVF (rb /stb)	Visc (cp)
0.020723063	200	1.0777156	4.1887659
	400	1.0702102	4.2790399
	600	1.0677203	4.419903
	800	1.0664775	4.6000688
	1000	1.0657325	4.8143558
	1200	1.0652361	5.0601077
	1367.0891	1.0649329	5.2885309
	1600	1.064616	5.6412864
	1800	1.0644094	5.9759137
	2000	1.0642441	6.3399525
	2200	1.0641089	6.7336935
	2400	1.0639962	7.1575367
	2600	1.0639009	7.6119407

	2800	1.0638192	8.0973847
	3000	1.0637484	8.6143387
	3200	1.0636865	9.1632389
	3400	1.0636318	9.7444671
	3600	1.0635832	10.358334
	3800	1.0635398	11.005062
	4000	1.0635006	11.684774
0.047767761	400	1.0898135	3.5048378
	600	1.0842586	3.5750153
	800	1.0814922	3.6728906
	1000	1.0798358	3.7938995
	1200	1.0787329	3.9354321
	1367.0891	1.0780595	4.0682377
	1600	1.0773559	4.2742921
	1800	1.0768973	4.4699832
	2000	1.0765306	4.6825706
	2200	1.0762306	4.9118092
	2400	1.0759807	5.1575545
	2600	1.0757692	5.4197247
	2800	1.0755881	5.6982738
	3000	1.0754311	5.9931712
	3200	1.0752937	6.3043857
	3400	1.0751725	6.6318731

	3600	1.0750648	6.975566
	3800	1.0749684	7.3353659
	4000	1.0748817	7.7111357
0.077855561	600	1.1034931	2.9763016
	800	1.0988582	3.0347292
	1000	1.0960873	3.110755
	1200	1.0942439	3.2020593
	1367.0891	1.0931189	3.2889556
	1600	1.0919441	3.4250254
	1800	1.0911785	3.5549932
	2000	1.0905664	3.6965623
	2200	1.0900659	3.8493768
	2400	1.089649	4.0131726
	2600	1.0892964	4.1877463
	2800	1.0889942	4.372934
	3000	1.0887323	4.5685949
	3200	1.0885033	4.7745996
	3400	1.0883012	4.99082
	3600	1.0881217	5.2171223
	3800	1.087961	5.4533612
	4000	1.0878164	5.6993746
0.11010723	800	1.1183956	2.5706397
	1000	1.1142762	2.6207458

	1200	1.1115393	2.6829744
	1367.0891	1.10987	2.743273
	1600	1.1081276	2.8388451
	1800	1.1069927	2.9308859
	2000	1.1060856	3.0316154
	2200	1.105344	3.1406611
	2400	1.1047263	3.2577331
	2600	1.104204	3.3825988
	2800	1.1037565	3.5150645
	3000	1.1033688	3.654962
	3200	1.1030296	3.802139
	3400	1.1027305	3.9564507
	3600	1.1024646	4.1177545
	3800	1.1022268	4.2859048
	4000	1.1020129	4.4607494
0.14406982	1000	1.1343367	2.2548636
	1200	1.1305335	2.2986595
	1367.0891	1.1282165	2.34204
	1600	1.1257993	2.4118318
	1800	1.1242257	2.4797416
	2000	1.1229683	2.5545239
	2200	1.1219406	2.635817
	2400	1.121085	2.723334

	2600	1.1203614	2.8168414
	2800	1.1197416	2.9161425
	3000	1.1192048	3.0210668
	3200	1.1187352	3.1314609
	3400	1.1183211	3.2471823
	3600	1.1179531	3.3680938
	3800	1.1176239	3.49406
	4000	1.1173277	3.6249441
0.14406982	1000	1.1343367	2.2548636
	1200	1.1305335	2.2986595
	1367.0891	1.1282165	2.34204
	1600	1.1257993	2.4118318
	1800	1.1242257	2.4797416
	2000	1.1229683	2.5545239
	2200	1.1219406	2.635817
	2400	1.121085	2.723334
	2600	1.1203614	2.8168414
	2800	1.1197416	2.9161425
	3000	1.1192048	3.0210668
	3200	1.1187352	3.1314609
	3400	1.1183211	3.2471823
	3600	1.1179531	3.3680938
	3800	1.1176239	3.49406

	4000	1.1173277	3.6249441
0.1794612	1200	1.1512002	2.0045063
	1367.0891	1.1481195	2.0364696
	1600	1.1449095	2.0888079
	1800	1.1428208	2.1403707
	2000	1.1411526	2.1975816
	2200	1.1397895	2.2600977
	2400	1.1386549	2.3276449
	2600	1.1376957	2.3999977
	2800	1.1368741	2.4769663
	3000	1.1361626	2.5583858
	3200	1.1355404	2.6441091
	3400	1.1349917	2.7340009
	3600	1.1345041	2.8279337
	3800	1.1340681	2.9257836
	4000	1.1336758	3.0274284
0.20998149	1367.0891	1.1659361	1.8328817
	1600	1.1619629	1.8746507
	1800	1.1593803	1.9162871
	2000	1.1573184	1.962825
	2200	1.155634	2.0139388
	2400	1.1542323	2.0693669
	2600	1.1530476	2.1288935

	2800	1.152033	2.1923363
	3000	1.1511545	2.2595376
	3200	1.1503863	2.3303569
	3400	1.1497089	2.4046664
	3600	1.1491072	2.4823466
	3800	1.148569	2.5632829
	4000	1.1480849	2.6473639

Dry gas PVT properties (no vaporized oil)

Press (psia)	FVF (rb /Mscf)	Visc (cp)
200	16.139031	0.012698614
400	7.8365288	0.012963851
600	5.0747972	0.013312025
800	3.699668	0.013742158
1000	2.8805023	0.014257622
1200	2.3405564	0.014862592
1367.0891	2.0155692	0.015438783
1600	1.6833814	0.016349297
1800	1.4737623	0.017225844
2000	1.3123598	0.018179489
2200	1.1861407	0.019195604
2400	1.086163	0.02025678
2600	1.0060375	0.021345149
2800	0.94107749	0.022444457

3000	0.88779469	0.023541338
3200	0.84357336	0.024625732
3400	0.80644333	0.025690661
3600	0.77491452	0.026731697
3800	0.74785402	0.027746356
4000	0.72439483	0.028733547

4. SCAL

Water/oil saturation functions

Sw	Krw	Kro	Pc (psia)
0.2	0	0.8	0
0.25	0.000122	0.561866	0
0.3	0.001951	0.376406	0
0.35	0.009877	0.237037	0
Sw	Krw	Kro	Pc (psia)
0.4	0.031215	0.137174	0
0.45	0.076208	0.070233	0
0.5	0.158025	0.02963	0
0.55	0.29276	0.008779	0
0.6	0.499436	0.001097	0
0.65	0.8	0	0
1	1	0	0

Gas/oil saturation functions

Sg	Krg	Kro	Pc (psia)
0	0	0.8	0
0.025	0	0.717311	0
0.109375	0.001563	0.480542	0
0.19375	0.0125	0.302615	0
0.278125	0.042188	0.175125	0
0.3625	0.1	0.089664	0
0.446875	0.195313	0.037827	0
0.53125	0.3375	0.011208	0
0.615625	0.535938	0.001401	0
0.7	0.8	0	0
0.8	0.8	0	0

5. Initialization

Equilibration data specification

Datum depth	3,034.864 ft
Pressure at datum depth	1,367.089 psia
WOC depth	5,000 ft
GOC depth	3,034.864 ft

6. Schedule

In reservoir simulation model, each well setting is described as follows:

Oil vertical production well

Well specification

Well name	TEST_1
Group	O
I location	13
J location	13
Preferred phase	OIL

Cross flow	No
Density calculation	SEG

Well connection data

K upper	4 (case R001)
K lower	5 (case R001)
Open/shut flag	OPEN
Well bore ID	0.5522083 ft.
Direction	Z

Production well control

Well	TEST_1
Open/shut flag	OPEN
Control	LRAT
Liquid rate	600 stb/day (varying from 600-2000 stb/day)
BHP target	14.7 psia

VITA

Suksan Luangwattanawilai was born in Suphanburi, Thailand on 6 April 1984. He completed his Bachelor Degree in Instrumentation Engineering from the Faculty of Engineering, King Mongkut's Institute of Technology, Ladkrabang in 2007. After graduating, he was hired as a Facilities Engineer at Chevron Thailand Exploration and Production, Ltd. He continued his study in Master's Degree of Petroleum Engineering at Department of Mining and Petroleum Engineering, Chulalongkorn University since 2011.